EXPLORING THE MOLECULAR MECHANISMS BEHIND BIOENERGETIC CHANGES AFTER NANOPLASTIC EXPOSURE

Silke Beelen
Student number: 01911970

Promotors: Prof. Dr. ir. Jana Asselman, Prof. Dr. ir. Andreja Rajkovic
Tutors: Dr. ir. Charlotte Grootaert, Dr. Maaike Vercauteren

Master's Dissertation submitted to Ghent University in partial fulfillment of the requirements for the degree of Master of Science in Bioscience Engineering: Cell and Gene Biotechnology
Academic year: 2023-2024

COPYRIGHT DECLARATION

ACKNOWLEDGEMENT

Firstly, I would like to thank my research promoters, Prof. Dr. ir. Rajkovic and Prof. Dr. ir. Asselman, for suggesting this topic and providing their expertise and guidance. Special thanks to my tutors, Dr. ir. Grooteart and Dr. Vercauteren, for their dedication, time, patienceand kindness. Thanks to their enthusiastic mentorship, readiness to always answer my questions and support whenever needed, I could grow as a researcher. I am grateful to get the chance to learn from them and will carry this knowledge with me for the rest of my professional life. I also like to thank all the members of Blue Growth Research Lab and the members of the department of food technology, safety and health. Additionally, I would like to thank my fellow students and my close friends, in particular Falke, who supported and accompanied me both in and out of the studies. At last, also my parents, Wim and Pascale, and my sisters Lisa and Helena earn a special thanks, as without their support, this achievement wouldn't have been possible.

We extend our appreciation to Ghent University's Special Research Fund for their generous support in procuring the Seahorse equipment under grant BOF.BAS.2020.0035.01 and to Research Foundation Flanders for grant G000123N that allowed procurement of Incucyte SX5. This research received partial funding from the ImpTox project, which was sponsored by the European Union's Horizon 2020 research and innovation program under grant No. 965173.

TABLE OF CONTENTS

ABBREVIATIONS

ACC	acetyl-CoA carboxylases
ACLY	ATP-citrate lyase
ACOT	acyl-CoA thioesterase
ACS	acyl-coenzyme A synthetase
ADP	adenosine diphosphate
AGPAT	acylglycerol-3-phosphate acyltransferase
AMPK	AMP-activated protein kinase
ATCC	American Type Culture Collection
ATGL	adipose triglyceride lipase
ATP	adenosine triphosphate
ChREBP	carbohydrate response element-binding protein
CoA	coenzyme A
CPT	carnitine palmitoyltransferase
DAMP	damage associated molecular pattern
DGAT	diacylglycerol O-acyltransferase
DNEM	Dulbecco's modified eagle medium
DPBS	Dulbecco's Phosphate-Buffered Saline
ECAR	extracellular acidification rate
EDTA	ethylenediaminetetraacetic acid
ER	endoplasmic reticulum
ETC	electron transport chain
FA	fatty acid
FABP	fatty-acid binding protein
$FADH_2$	flavin adenine dinucleotide
FASN	fatty acid synthase
FATP	fatty acid transport protein
FBS	fetal bovine serum
FCCP	cyanide-p-trifluoromethoxyphenyl-hydrazone
FDR	false discovery rate
GO	gene ontology
GPAT	glycerol-3-phosphate acyltransferase
GSEA	gene set enrichment analysis
HSL	hormone-sensitive lipase
IL	interleukin
IMM	inner mitochondrial membrane
LPA	lysophosphatidic acid
LXRs	liver X receptors
MAG	monoacylglycerol
MAPK	mitogen-activated protein kinase
MGL	monoglyceride lipase
MNP	micro- and nanoplastic
MPC	mitochondrial pyruvate carrier
mTOR	mammalian target of rapamycin
NADH	nicotinamide adenine dinucleotide

NEAA	nonessential amino acids
NF-κB	nuclear factor kappa-light-chain-enhancer of activated B cells
NP	nanoplastic
OCR	oxygen consumption rate
OCU	optical calibration units
OD	optical density
PA	phosphatidic acid
PCR	polymerase chain reaction
PPAR	peroxisome proliferator-activated receptors
PS	polystyrene
ROS	reactive oxygen species
ROT/AA	mixture of rotenone and antimycin A
RXR	retinoid X receptor
SB	silica bead
SCD	stearoyl-CoA desaturase
SREBP	sterol regulatory element binding transcription factor
TAG	triacylglycerol
TCA-cycle	tricarboxylic acid cycle
TII	total integrated intensity
TLR	toll-like receptor
UMI	unique molecular identifier
UPR	unfolded protein response
XBP1	X-box binding protein 1

ABSTRACT (ENGLISH)

Recently, the impact of micro- and nanoplastics (MNPs) on the environment has received increasing attention. However, studies on the impact of MNPs on human health are still limited, and a lot of uncertainties persist. As specific effects are still under research, the severity of the impact of MNPs on the health of human cells and tissues is not yet known. Studies indicate that MNPs affect different cell organelles, including the mitochondria, endoplasmic reticulum (ER) and lysozymes. Since these cell organelles play an important role in the cellular energy metabolism, MNPs disrupt these metabolisms as well.

This study aims at describing the effect of MNPs on cellular metabolism. The experimental setup involved repeated-dose, long-term treatment of Caco-2 cells with 100 nm polystyrene nanoplastics (PS-NPs) at environmentally relevant concentrations. Additionally, treatment with silica beads (SBs) was performed to distinguish the physical and the chemical effects of the MNPs. The results showed that chronic exposure to an environmentally relevant dose of nanoplastics (NPs) influences cellular metabolism, leading to increased oxygen consumption rates (OCRs), lipid accumulation, and altered responses to stress. It indicates a shift towards a more stressed cellular phenotype, which could ultimately be linked to chronic inflammatory diseases such as obesity. Similar results upon treatment with SBs and NPs indicate that the observed effects arise primarily from the physical presence of the particles, rather than from chemical interactions between elements bound to the particle and the cells.

ABSTRACT (NEDERLANDS)

Recentelijk wordt meer aandacht besteed aan de impact van micro- en nanoplastic (MNP) op het milieu. Onderzoek naar de impact op de menselijke gezondheid is nog steeds beperkt en er blijven veel onzekerheden bestaan. De ernst van de impact van MNP op de gezondheid van menselijke cellen en weefsels is nog niet bekend. Studies tonen aan dat MNP verschillende celorganellen beïnvloeden, waaronder de mitochondriën, het endoplasmatisch reticulum (ER) en lysozymen. Omdat deze celorganellen een belangrijke rol spelen in het cellulaire energiemetabolisme, verstoren MNP ook dit metabolisme.

Deze studie biedt inzicht in de veranderingen in het cellulaire metabolisme die worden veroorzaakt door behandelingen met MNP. Er werd gebruik gemaakt van een experimentele opstelling waarbij Caco-2-cellen langdurig behandeld werden met herhaalde dosissen van 100 nm polystyreen nanoplastic (PS-NP). Hierbij werden concentraties gebruikt die de werkelijkheid nabootsen. Bovendien werd een behandeling met silica partikels uitgevoerd om het fysische en chemische effect van de MNP te onderscheiden. De resultaten toonden aan dat chronische blootstelling aan een voor het milieu relevante dosis nanoplastic (NP) het cellulaire metabolisme beïnvloedt, wat leidt tot een verhoogd zuurstofverbruik, ophoping van lipiden en veranderde reacties op stress. Het duidt op een verschuiving naar een meer gestresseerd cellulair fenotype, dat uiteindelijk in verband kan worden gebracht met chronische ontstekingsziekten zoals obesitas. Vergelijkbare resultaten bij behandeling met silica partikels en NP geven aan dat de waargenomen effecten voornamelijk voortkomen uit de fysieke aanwezigheid van deze deeltjes en niet uit chemische interacties tussen elementen die aan het deeltje zijn gebonden en de cellen.

1 INTRODUCTION

Plastics are lightweight and chemically stable synthetic macromolecules, making them valuable in diverse industries, such as packaging, construction and the automotive industry (Lechthaler et al., 2020). Because of this wide applicability, many plastics are produced worldwide, but unfortunately, they often end up in waste streams after use. According to the OECD, the amount of global plastics waste in 2019 was around 460 million tonnes, and this is still increasing, with an estimated waste of 1231 million tonnes in 2060 (OECD, 2022). Only 9% of the used plastics are appropriately recycled (Woldemar D'ambrières, 2019). Because of the low biodegradability of these plastics and due to waste mismanagement, plastics accumulate in the environment (Lechthaler et al., 2020). These plastics will not only disrupt marine ecosystems, they can also clog urban drainage infrastructures, increasing the flood risk. Additionally, they have a negative effect on the tourism industry (Hall, 2000).

Different groups of plastics are classified according to their monomer type. Figure 1 shows the chemical structures of the most widely produced plastic types. Polyethylene constitutes 30.3% of the plastic production, followed by polypropene (17.8%), polyvinyl chloride (9.9%), polyethylene terephthalate (8.6%) and polystyrene (PS; 6.5%) (Geyer et al., 2017; Kazemi et al., 2021). This master's dissertation addresses PS, a plastic that is widely employed in disposable drinking cups, packaging, electronics and personal care products (Tanvir et al., 2014).

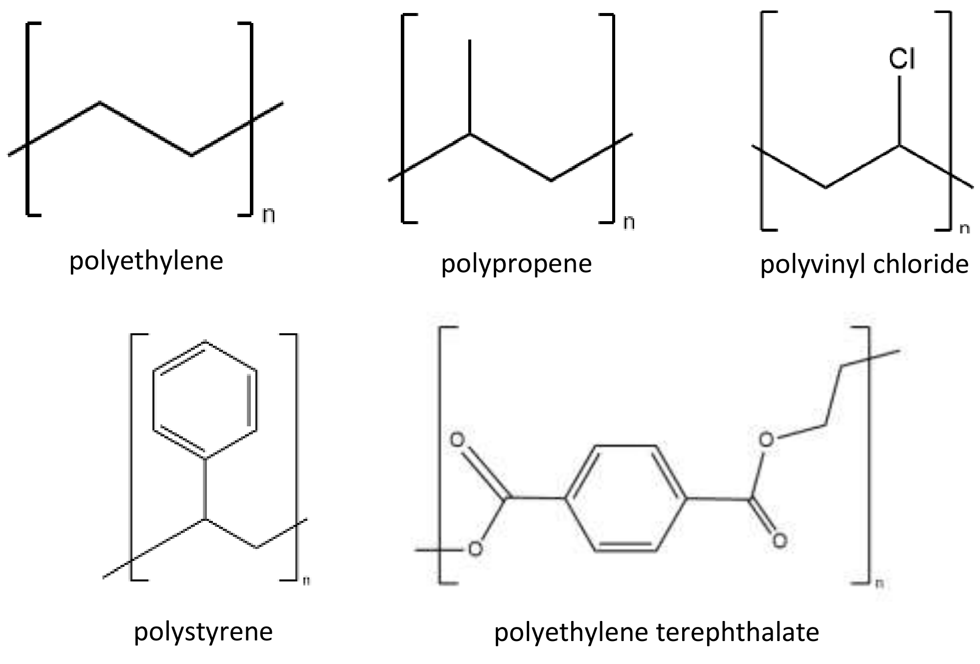

Figure 1. Monomer structures of polyethylene, polypropene, polyvinyl chloride, polystyrene and polyethylene terephthalate.

Plastics can also be categorized into three distinct size classes. This classification is crucial, as the interaction between plastics and organisms is significantly influenced by their size (Mitrano et al., 2021). Macroplastics have a diameter exceeding 5 mm and are released into the environment via either land-based or ocean-based pathways (Boucher & Billard, 2019). Microplastics (MPs) fall within the range of 5 mm to 1 µm. Production of MPs, for instance, for skin care products (Hernandez et al., 2017), can lead to accidental release into the environment, which is assigned as the primary source. Secondly, MPs can be generated through the wear and degradation of macroplastics, particularly from tire wear and clothes in laundry wastewater, which is called the secondary source of MPs due to the indirect release (Lai et al., 2022). MPs are found in seawater, freshwater, sediment, soil, air and even food such as beer, sea salt and tap water (Prata et al., 2020). At last, nanoplastics (NPs) have a diameter smaller than 1 µm. Like MPs, NPs can be released during production (primary source) or from larger plastic particles due to physical, chemical and biological forces (secondary source) (Lai et al., 2022). This master's dissertation focuses on micro- and nanoplastics (MNPs), as their prevalence is an escalating concern and their potential impact on human health remains a subject of ongoing investigation with many uncertainties and data gaps.

In a broader context, MNPs are part of the exposome, which refers to the totality of exposures from various external and internal sources. These include factors such as food, smoking, air pollution and aging. Additionally, the exposome accounts for psychosocial components, acknowledging the impact of social relations and socio-economic position on health. Exposome models highlight the concept that an individual's disease is shaped by their unique history of exposures and underlying genetic susceptibilities. Understanding the exposome holds significant importance, particularly in unravelling the risk factors associated with non-communicable diseases (Vineis et al., 2020). These chronic diseases, such as cardiovascular diseases, cancers, respiratory diseases and diabetes, pose a substantial burden on individuals, communities and economic resources. They have prolonged durations, slow progressions and are rarely completely curable (Calcaterra & Zuccotti, 2022). The onset of non-communicable diseases likely involves complex interactions between various external and internal stimuli. Therefore, research on the exposome, particularly focusing on the factors that play pivotal roles and their interactions with human health, may prove instrumental in comprehending and developing therapeutics for these diseases.

As MNPs are widely present in the environment, they may be considered one of those pivotal factors. Due to their small size, they can be internalized in the body, interfering with cells via different pathways. This interference can result in dysfunctional cells, tissues and even organs, ultimately affecting overall health in the long term. While the European Commission's Science Advice for Policy currently states the absence of direct adverse effects of MNPs on human health (Koelmans et al., 2019), emerging research indicates their potential association with health complications. For instance, existing explanations of the obesity pandemic's spread, including the genetic background and changes in lifestyle such as diet, exercise, sleep deficiency and aging, are proven to be insufficient (Brown et al., 2016). In parallel, the obesogen hypothesis states that environmental chemicals (obesogens) can affect individual susceptibility to obesity and thus help explain the recent large increases in obesity (Egusquiza & Blumberg, 2020). Völker and his team observed plastic household items and revealed that one-third of the items contained chemicals that, after extraction, caused the growth and proliferation of mouse fat cells in the lab. Examples of such chemicals are bisphenols and phthalates, which are used in the production of plastics as plasticizers, but many of the chemicals are unknown (Völker et al., 2022). As MNPs and their associated chemicals can interact with energy and lipid metabolism in several different ways, they are considered an obesogen type (Kannan & Vimalkumar, 2021). Therefore, the literature review will first discuss the 'interactomics' of MNPs with the human body, upon which the focus will switch towards the possible impact of MNPs on energy and lipid metabolism at the cellular level.

2 LITERATURE REVIEW

2.1 Human exposure routes

The human body is designed to prevent the intrusion of foreign particles. Except for the teeth, the surface of the human body is covered by epithelial cells, which form a rigid barrier to large particles. Nevertheless, the miniscule size of MNPs enables them to cross these barriers. The three primary routes of exposure are inhalation, ingestion and dermal contact (Prata et al., 2020).

Skin contact occurs with MNPs in cosmetic products like facial and body scrubs, as well as in water (Hernandez et al., 2017; Mortensen et al., 2021). The dermal barrier is very rigid and consists of various cell layers, of which the striatum corneum typically restricts the passage of substances. However, nanoparticles, including NPs, smaller than 40 nm can still cross this dermal barrier (Vogt et al., 2006). A second possible internalization pathway via the skin involves the accumulation of MNPs in follicular openings, where lower barrier integrity allows increased translocation compared to the skin surface. Further research is needed to support this internalization hypothesis (Alvarez-Román et al., 2004). At last, MNPs can also enter the skin via wounds (Schneider et al., 2009).

Despite the presence of nasal hair, mucus, macrophages and the sputum, inhalation of plastics present in the air leads to MNP accumulation in the lungs (Amato-Lourenço et al., 2021). It is estimated that up to 100,000 MPs per year are taken up through inhalation (Vianello et al., 2019). Unlike the dermal barrier, alveoli are designed to exchange oxygen and carbon dioxide, which makes this barrier less rigid and hence enables particles to cross the air-blood barrier. At this site, MNP uptake is largely determined by particle size, as smaller particles can penetrate deeper into the lungs than larger particles. Particles smaller than 200 nm can cross the air-blood barrier either through migration between endothelial cells or through endocytosis (Kreyling et al., 2014). Particles with an intermediate size are cleared by phagocytosis. In contrast, fibers ranging from 15 to 20 µm are hard to clear and tend to accumulate in the lungs (Feng et al., 2023; Llorca & Farré, 2021; Prata et al., 2020).

In this study, we especially focused on events at the level of the gastrointestinal tract, the major barrier for MNPs after ingestion via food and drinking water. Mortensen et al. (2021) reviewed the available information about MNP concentrations in drinking water and found a wide range of measured MNPs starting from 11 MPs/mL (5-50 µm), up to 1.1 x 10^8 MNPs/mL (1-10 µm). However, most researchers measured a concentration between 400 and 3,000 MNPs/mL in drinking water. In addition, seafood and several crops like rice, lettuce and peanuts can contain MNPs absorbed from polluted oceans and the soil, respectively (Jiang et al., 2022; Luo et al., 2022; Santillo et al., 2017). Moreover, several studies showed the trophic transfer of MNPs in the marine food web (McMahon et al., 1999; Santana et al., 2017). MNPs also end up in food during packaging, such as in plastic food containers (Du et al., 2020; He et al., 2021). Consequently, the tissues of the human gastrointestinal tract are currently considered among the most exposed tissues of all, with an estimated intake rate between 46,000 and 193,000 MNPs/year, however, accurate intake rates are hard to obtain as validation of in vitro cell experiments with the human intestine is not yet fully established (Llorca & Farré, 2021; Mohamed Nor et al., 2021; Senathirajah et al., 2021). Schwabl et al. (2019) indicated that 80% of ingested MNPs are believed to be excreted by the body and showed that nine different types of MNPs, including PS, are present in faeces.

Nevertheless, MNPs also accumulate in the human intestine, where they can translocate in several ways into the circulatory system (Figure 2). Transcytosis is a specialized transport mechanism in the gastrointestinal tract, mainly conducted by microfold cells situated in the Peyer's patches of the ileum. These microfold cells have the ability to endocytose extracellular cargo, transport it across the cytoplasm in membrane-bound vesicles, and release it at a distinct plasma membrane surface of the underlying tissue (Serra & Sundaram, 2021). Research has demonstrated a significant increase in MNP uptake when microfold-like cells were cocultured with gut epithelial cells, as opposed to conditions with only gut epithelial cells. Moreover, this increased MNP uptake has also been demonstrated in vivo, further supporting the observed absorption pathway. Hence, transcytosis via microfold cells is often considered the primary mode of MNP uptake in the gastrointestinal tract (Rieux et al., 2005). However, in vivo findings indicate that uptake via this mechanism may be overestimated, possibly due to the low prevalence of microfold cells on the epithelial surface and disparities between microfold-like cells and authentic microfold cells in in vitro experiments (Smyth et al., 2008). Therefore, uptake via other mechanisms, for instance, transcellular transport by enterocytes as shown by Walczak et al. (2015), is put forward. Another alternative uptake mechanism involves paracellular transport, wherein particles move between cells, driven by a concentration gradient. Only very small particles can migrate through intact epithelium, while larger particles can only pass epithelium with decreased integrity of tight junctions (Edelblum & Turner, 2015). In addition, paracellular transport can take place via the persorption process, in which pores are generated in the desquamation zone of the epithelium that allow particles to pass through (Hillyer & Albrecht, 2001). At last, uptake by migratory macrophages and dendritic cells may play a role in particle uptake, however, no direct evidence of this mechanism has been observed this far (Delon et al., 2022).

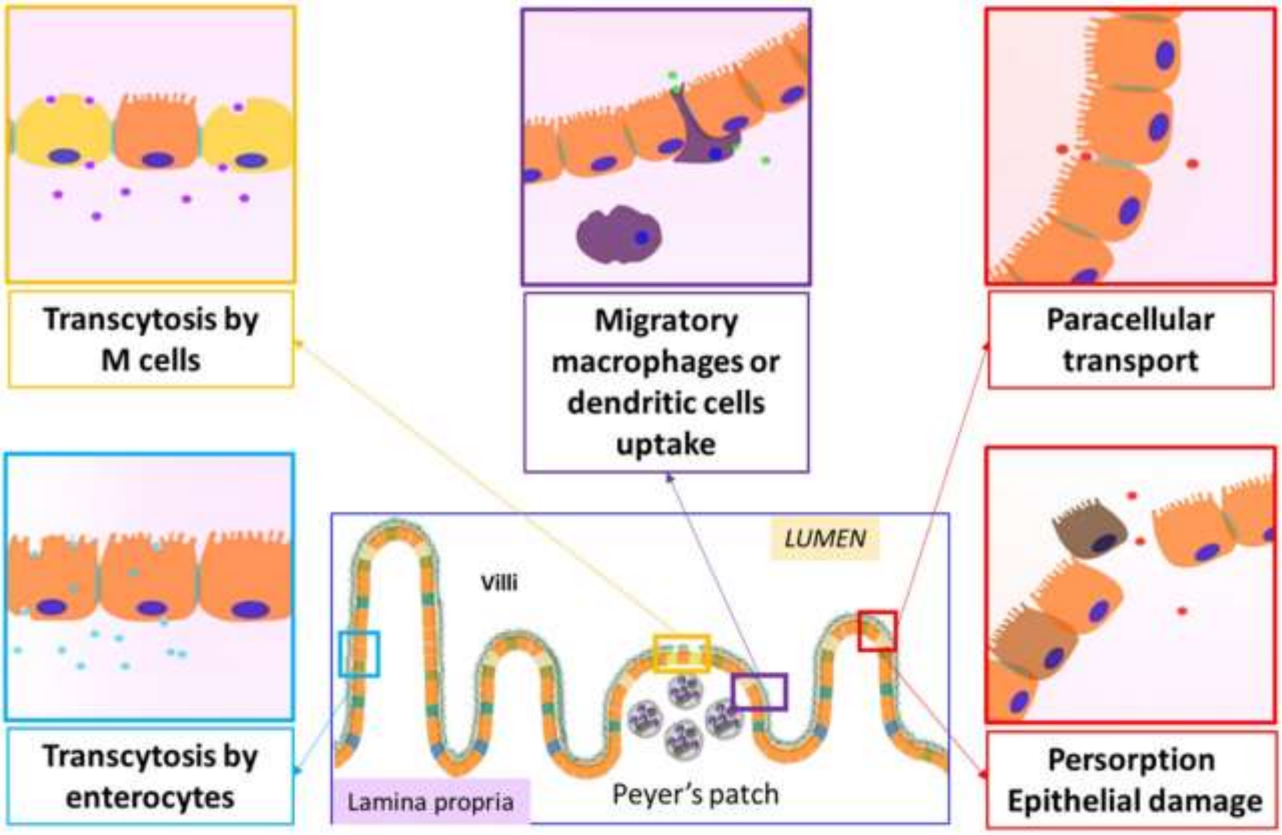

Figure 2. Uptake mechanisms of MNPs in the small intestine (Delon et al., 2022).

Once MNPs breach these initial defences, translocation within the body can occur either via passive membrane penetration or via endocytosis. Endocytosis of smaller particles tends to be mediated through clathrin- and caveolae-mediated endocytosis, while larger particles are more prone to macropinocytosis. The internalized PS particles mainly exist in lysosomes, but some particles are released again through the lysosomal pathway and passive penetration (L. Liu, Xu, et al., 2021).

2.2 Effect of MNPs on human health

As MNPs can be internalized, cells, tissues and organs may be damaged directly or indirectly. First, a description about the interaction of the MNPs at the molecular and cellular level is given. Thereafter, interactions between cellular changes and changes on higher levels including tissues and organ systems are discussed.

2.2.1 Cellular impacts of MNPs

MNPs exhibit both physical and chemical toxicity. The physical toxicity refers to the ability of the particles themselves to cause harm. The chemical toxicity refers to the interaction of MNPs with contaminants such as heavy metals (Liao & Yang, 2020) and viruses (G. Zhang et al., 2022), which may lead to the co-uptake of these pathogenic components with the MNPs. Next to contaminants, MNPs also interact with surrounding proteins, leading to a protein layer around the particle, called the protein corona, which may alter MNP properties and facilitate MNP internalization (Ramsperger et al., 2020).

While interacting with cells, MNPs may induce oxidative stress, an important mediator of downstream cellular processes in general (Hu & Palić, 2020). This oxidative stress can be induced via two different pathways. First, free radicals can be formed on the MNP surface. These free radicals react with atmospheric oxygen and produce polymer peroxy radicals, which can further react and form a cascade of reactive oxygen species (ROS) production (Duan et al., 2022). The smaller the MNPs, the larger the surface area-to-mass ratio, and hence the ability to absorb free radicals. This, together with the fact that small particles can be easier internalized, may explain the more toxic properties of smaller particles. Secondly, ROS may be induced after interaction of the MNPs with human cells, as shown in human cells of the liver, kidney and intestine (Domenech et al., 2021; Goodman et al., 2022; Peng et al., 2023; Y. L. Wang et al., 2021). These cells tend to produce ROS in the form of superoxide (O_2) and hydrogen peroxide (H_2O_2) in an attempt to neutralize the plastic particle (Hu & Palić, 2020; Regoli & Winston, 1999). Both O_2 and H_2O_2 play a role in signal transduction and serve as key mediators driving oxidative stress cascades (Reth, 2002; Y. Yang et al., 2013). Either the formed ROS or the direct interaction of the MNPs with the cells can lead to cell damage (**Error! Reference source not found.**).

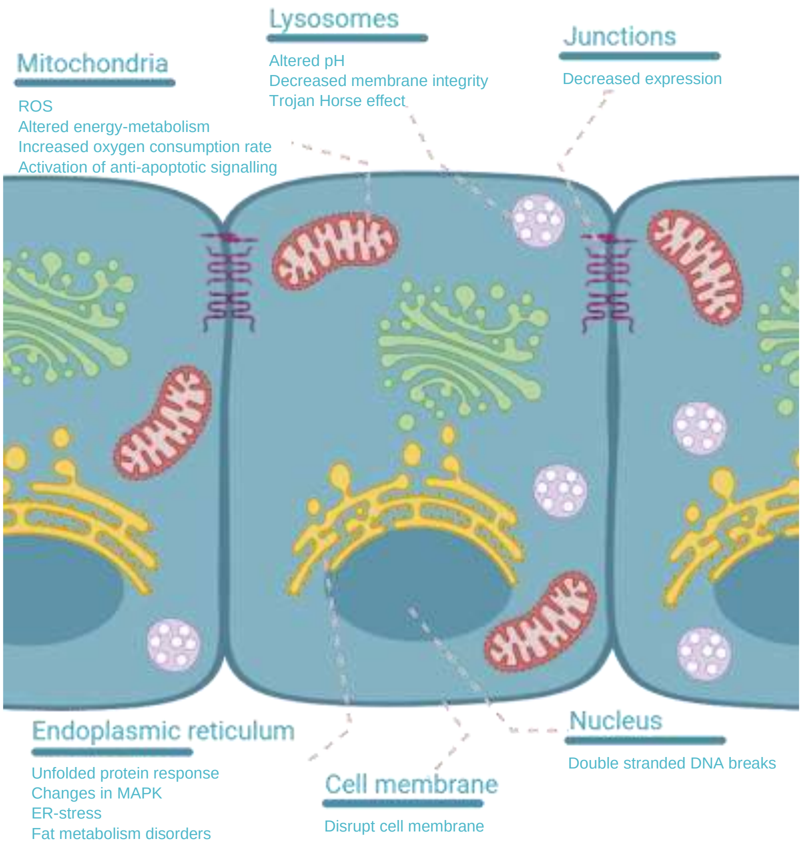

Figure 3. Effects of MNPs on cellular level. Created with BioRender.com.

MNP interactions may lead to increased acetylcholinesterase activity in liver cells, one of the most important biomarkers of neurotoxicity (Y. Deng et al., 2017). Additionally, MNPs can induce double-stranded breaks in DNA (Avio et al., 2015; Ribeiro et al., 2017), lower junction protein expression (Jia et al., 2023; Z. Zhang et al., 2023) and disrupt cell membranes, leading to cell permeability and even cell death (Hollóczki & Gehrke, 2020). These effects are often accompanied by cellular inflammation (Jia et al., 2023; Marana et al., 2022; Woo et al., 2023). Additionally, upregulation of carcinogens like Klf4 and Oct3/4 is found upon a six month exposure of Caco-2 cells to NPs (Barguilla et al., 2022). Finally, MNP exposure can also cause several problems related to the structure and function of mitochondria, the endoplasmic reticulum (ER) and the lysosomes.

Mitochondria are responsible for energy production in eukaryotes, phospholipid synthesis, calcium homeostasis, apoptotic activation and cell death. Mitochondria are affected by MNPs in several ways. First, higher cytosolic ROS levels can open mitochondrial ion channels, leading to a collapse of the mitochondrial membrane potential and extra release of ROS (Zorov et al., 2006). To counteract this ROS overload, the enzymes superoxide dismutase and catalase can be activated, which neutralise superoxide radicals and hydrogen peroxide, respectively. As further proof that ROS play a key role in MNP toxicity, alterations in superoxide dismutase are found after MNP exposure (Y. Deng et al., 2017). MNPs can also alter the energy metabolism by increasing the oxygen consumption rate, inducing proton leak (Halimu et al., 2022) and activating anti-apoptotic signalling (Bergami et al., 2019) in mitochondria as a defence against NP toxicity.

Also, the endoplasmic reticulum (ER) is affected by the MNPs. The ER is a vital organelle with key roles in protein and lipid synthesis and is crucial for intracellular signal transduction involved in cell survival and apoptosis. Disruption in the ER homeostasis may result in the accumulation of unfolded or misfolded proteins and alterations in Ca^{2+}-concentration within the ER lumen, which ultimately triggers unfolded protein responses (UPR) (Schwarz & Blower, 2016; Tang et al., 2020). Evidence of disrupted ER homeostasis, together with UPR and lipid metabolism disorders, is found in the intestinal cells of *C. elegans* after long-term exposure to NPs at low doses. These effects are mediated by intracellular mitogen-activated protein kinase (MAPK) (Qu et al., 2019; Y. Yang et al., 2020). There is a link between ROS formation and MAPK activation, which again confirms that ROS might play a key role in the reaction upon MNP exposure (McCubrey et al., 2006). Activation and phosphorylation of MAPK result in the upregulation of X-box binding protein 1 (XBP1), which induces the UPR. In addition, MAPK activation may lead to dysregulation of SBP-1 in *C. elegans*, which is equivalent to sterol regulatory element binding transcription factor (SREBP) in humans and regulates inflammation and lipid metabolism (Qu et al., 2019; Y. Yang et al., 2020). UPR after NP exposure is also associated with the accumulation of autophagosomes. This indicates a potential autophagy regulation mechanism through the ER stress caused by misfolded protein aggregation (Lim et al., 2019).

Finally, lysosomal function is impacted by exposure to MNPs (Avio et al., 2015). The lysosome is an intracellular digestive organelle that uses enzymes to actively eliminate pathological cellular waste. D. Xu et al. (2021) discovered the presence of NPs in early endosomes in Caco-2 cells, which subsequently fused with lysosomes with the intention to break down the foreign substances. MNP accumulation in lysosomes may decrease membrane integrity. Moreover, charged MNPs can dysregulate lysosomal pH and hence lead to dysfunction. In a later stage, such endolysosomes may fuse with autophagosomes, an interaction induced by NP accumulation in the cell, to form autophagolysosomes. Lysosomal proteases are present in autophagolysosomes and can degrade the engulfed components. Due to the severe damage to lysosomes, the autophagic flux can be blocked, which can ultimately result in cell death (W. Song et al., 2015). An additional factor that makes the MNPs toxic for the lysosomes is the protein corona, which can be degraded in the lysosomes, releasing ions and toxic compounds bound to the MNP surface. These free chemicals and the free MNPs themselves can cause extra damage to lysosomal membranes. The active uptake of MNPs by the cells, in combination with the release of toxic compounds in the lysosomes in an attempt to neutralise the particles, is sometimes called the Trojan horse effect (F. Wang et al., 2013).

2.2.2 Effect of MNPs on tissues and organs

The potential health effects of MNP exposure are shown in Figure 4. An important note is that, the European Commission's Science Advice for Policy states that, currently, no evidence exists for direct adverse effects of MNPs in human health (Koelmans et al., 2019). This figure is constructed based on outcomes upon acute treatment with a high MNP concentration dose, which is not fully comparable to the real-life situation where animals and humans are exposed for a long term to low MNP concentrations. Yet, even though effects may not be as severe or as directly noticeable as described below, further research is required to evaluate the severity of possible long-term exposure.

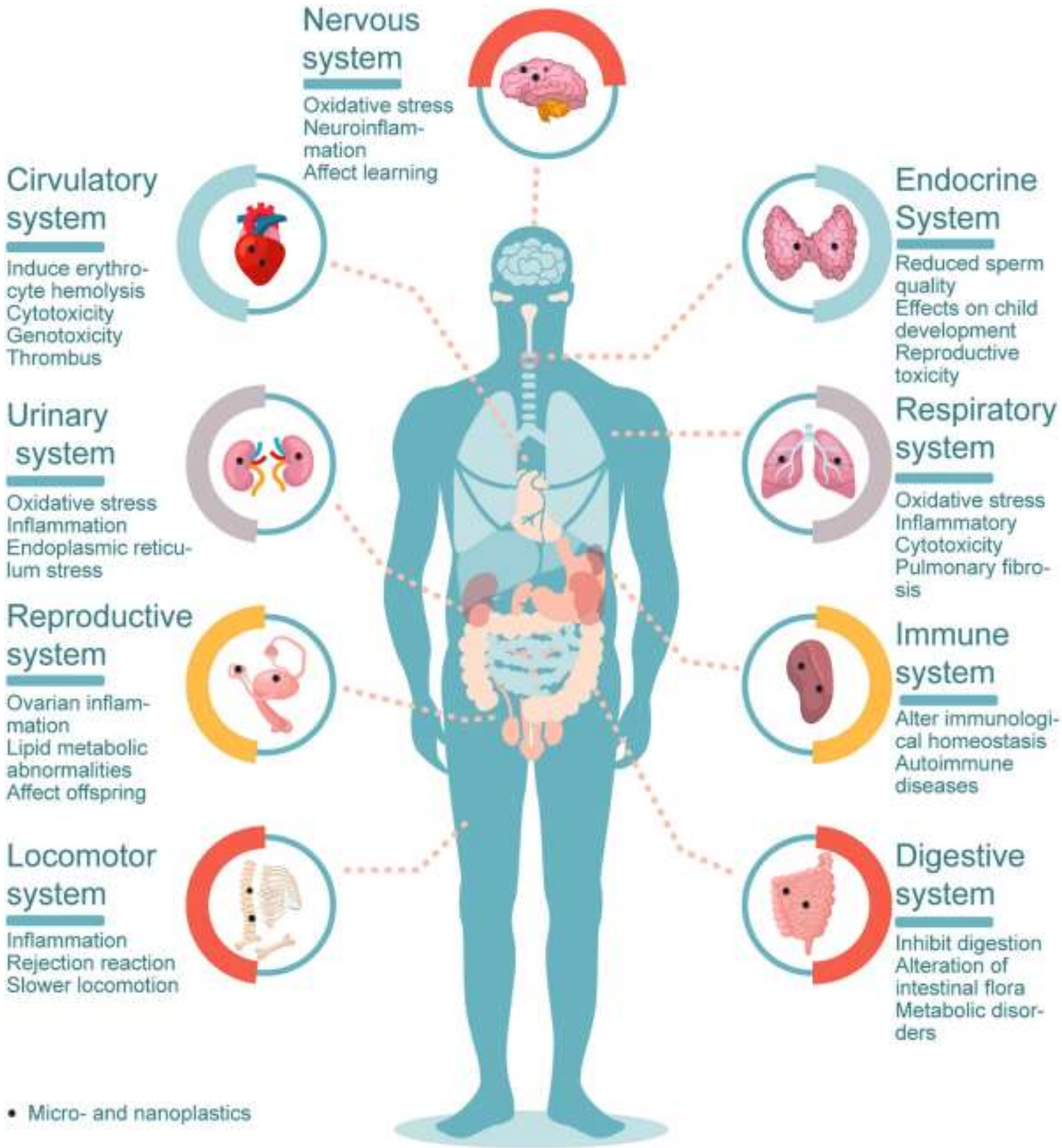

Figure 4. Potential health risks of MNPs to human organ systems (Feng et al. 2023).

In lung cells, MNPs can block the cell cycle, induce ROS formation, promote apoptosis and upregulate the expression of inflammation-related genes. This leads to cytotoxic and inflammatory effects and disrupted epithelial barriers (Woo et al., 2023; M. Xu et al., 2019). In high concentrations, plastics can activate immune defensive responses in the lungs, thereby increasing the risk of chronic obstructive pulmonary diseases (Dong et al., 2020). Plastics can also alter the endogenous lung surfactants by altering their phase behaviour, surface tension and membrane structure. In addition, MNPs can cause ROS increase in ROS in these surfactants, which may cause the collapse of alveoli and induce decreased protection of the epithelial lung cells by the surfactant, ultimately leading to lung damage (Shi et al., 2022).

In the digestive system, MNPs can cause a weakened immunological barrier, which can lead to an increased chance for intestinal pathogen infection. This was demonstrated in a long-term experiment in mice, where exposure to PS-NPs led to the disruption of the intestinal epithelium, shorter and disorganised intestinal villi and intestinal crypt dysplasia upon 14 days of exposure. 28 days after exposure, a thinner basal lamina was observed, together with decreased mucus production and downregulation of the tight junction protein Claudin-1 (Z. Zhang et al., 2023). Furthermore, MNPs induce oxidative stress, mitochondrial dysfunction and the release of cytokines in the intestinal cells, leading to inflammation. This inflammation can promote obesity and inflammatory bowel disease and can lead to dysbiosis in the gut microbiota (Frank et al., 2007; Y. Jin et al., 2018; Ley et al., 2006). Feeding mice with polyethylene increased *Staphylococcus* levels along with a decrease in *Parabacteroides* (B. Li et al., 2020), whereas PS MPs decreased *Actinobacteria* abundance (Y. Jin et al., 2019). In addition, small particles may interact with nutrients and enzymes in the intestinal lumen, thereby affecting their bioavailability or activity, respectively, leading to nutritional imbalances and altered intestinal microbiota (Deloid et al., 2018, 2022). Dysbiosis can result in an altered short-chain fatty acid composition in the intestinal lumen, causing more dysbiosis and nutritional imbalances (Z. Zhang et al., 2023).

After absorption, the MNPs end up in the circulatory system. MNPs are present in high concentrations of around 1.6 µg/mL in the human blood, which equals approximately 7.245×10^4 particles/mL if 5 µm PS particles, the mean diameter of the measurement interval, were implemented in the conversion (Leslie et al., 2022). Plastics may interact with various blood components, including erythrocytes, leading to their lysis. The resulting cell debris can cause aggregation, raising the risk of thrombosis formation (E. H. Kim et al., 2022). MNPs may also affect endothelial cells, leading to inhibition of angiogenesis and deprived wound healing (H. S. Lee et al., 2021). Furthermore, a protein corona is formed around plastics in the blood. This protein corona can decrease the toxicologic impact of MPs but can also facilitate the internalization, not only into endothelial cells, but in almost every organ, leading to MNP accumulation in different tissues (W. Yang et al., 2022).

It was shown that MPs can aggregate in the brain, leading to neuroinflammation and thereby affecting the memory (C. W. Lee et al., 2022). In addition, as previously mentioned, MNPs are found to induce oxidative stress and reduce acetylcholine, which can lead to broad systemic neurotoxicity (S. Wang et al., 2022). Moreover, studies in zebrafish showed a reduced locomotor ability after NP exposure, which can be linked to neurotoxicity (Q. Chen et al., 2017). Since no reduced locomotor function is found in humans, MNPs exclusively affect human locomotor function in scenarios where a prosthesis is required. This prosthesis can lead to MNP release, thereby inducing inflammation and rejection reactions (Sternschuss et al., 2012). In addition, MNPs can carry endocrine-disrupting chemicals such as bisphenol A, phthalates, or steroid hormones, which may affect hormone signalling, leading to reduced sperm quality and child development, as well as a higher risks for type 2 diabetes and obesity (Guedes-Alonso et al., 2021; Matsumoto et al., 2008; Rochester, 2013). MNPs are also found in the human placenta (Ragusa et al., 2021), where they may cause inflammation, oxidative stress and lipid metabolic abnormalities. This was shown in mice exposed to high concentrations of MNPs, and ultimately led to reproductive toxicity (H. Jin et al., 2021; Z. Liu et al., 2022). In addition, exposure to long-term, low-dose MNPs in mice is found to affect metabolic homeostasis and lipid metabolism in the offspring, even when these mice were not fed with MNPs during pregnancy (Y. Deng et al., 2022).

MNPs also interact with the immune system by initiating inflammatory cytokine release, amongst which interleukin (IL)-1α and IL-1β, as shown in the zebrafish gut (Y. Jin et al., 2018). In addition, research on fathead minnow found that MNPs recruit and activate neutrophils, leading to neutrophil degranulation, the release of neutrophil extracellular traps and phagocytosis (Greven et al., 2016). In addition, oxidative stress due to MNPs can induce damage associated molecular pattern (DAMP) formation. DAMPs can then activate the immune system via toll-like receptor (TLR) activation (W. Yang et al., 2022). This can lead to disrupted immune homeostasis and initiate immune system overreactions, ultimately leading to immune system disorders like autoimmune diseases. Systemic lupus erythematosus and rheumatoid arthritis were already linked to exposure to particulate matter and may also be induced by MNPs (Bernatsky et al., 2011; Chang et al., 2016). In addition, the MNPs in the body can be surrounded by a protein corona, which can complicate MNP recognition. Since the corona structure is dynamic, it provides the MNPs with new properties, further complicating their recognition. This may extend the half-life of the MNPs and lead to the escape of immunosurveillance, giving the MNPs the chance to interfere with cellular and molecular mechanisms. This ultimately enhances the development of auto-immune diseases (W. Yang et al., 2022). At last, MNPs can interact with the differentiation of T-cells in lymph nodes, leading to a significant decrease in T-cells in the blood (Z. Zhang et al., 2023). Also, a decrease in dendritic cells is observed (Park et al., 2020).

MNP clearance is performed by both the urinary system and the liver. Accumulation of MNPs in the liver is found in mice and rats, where they are involved in inflammation and liver fibrosis (Babaei et al., 2022; Shen et al., 2022). Additionally, MPs are found in human urine (Pironti et al., 2023). There, they may affect the urinary tract through accumulation in the kidneys and bladder, where they can cause oxidative stress, mitochondrial dysfunction, ER stress, inflammation and autophagy. On a higher scale, this may lead to decreased kidney and bladder quality and local inflammation (Goodman et al., 2022; Meng et al., 2022; Y. Wang et al., 2022; Y. L. Wang et al., 2021).

2.3 Cellular metabolism

Since there have been no reports of acute cell or organ dysfunction following MNP exposure in humans thus far, we might infer that their actual impact on human health is more nuanced. As such, shifts in cell and tissue metabolism are an early indicator of a persistent stress condition in general, which may ultimately lead to chronic diseases upon long-term exposure. Therefore, in the following paragraphs, the impact of MNPs on several aspects of cell metabolism is discussed, including interference with fatty acid (FA) uptake, fat metabolism and energy production.

2.3.1 FA uptake

FA uptake mechanisms are shown in Figure 5. In the intestinal lumen, lipids appearing as triglycerides (TAG) form lipid droplets, which cannot, as such, enter the unstirred water layer close to the intestinal cells and are hence not absorbed in this form. Instead, lipid droplets are enzymatically degraded by luminal lipases associated with mixed micelles surrounded by bile salts. In these micelles, FAs and monoacylglycerol (MAG) are present. Micelles can enter the unstirred water layer, leading to a closer contact between the MAGs and FAs, and the cells (Deloid et al., 2022).

When lipids are in close contact with the enterocytes, they may be absorbed in various ways. First, FAs penetrate the cell membrane, undergo flip-flop, and finally enter the cell (Massey et al., 1997). Next to flip-flop, proteins may facilitate lipid transport. Fatty acid transport protein (FATP) is a transmembrane protein that binds, transports, and activates FAs in one step (Schaffer' & Lodisht, 1994). This process involves the conversion of FAs into acyl-coenzyme A (CoA), which can then be utilized for cellular functions. At last, FAs can cross the plasma membrane via the CD36 protein, where a plasma membrane fatty-acid binding protein (FABP) recognizes FAs and guides them to CD36, a transmembrane glycoprotein facilitating the transport of various molecules, including FAs, phospholipids and lipoproteins (Abumradsb et al., 1993). Following internalization, activated FAs are transported through the cell via Acyl-CoA-binding protein (ACBP), while free FAs bind to cytosolic FABP (Deloid et al., 2022).

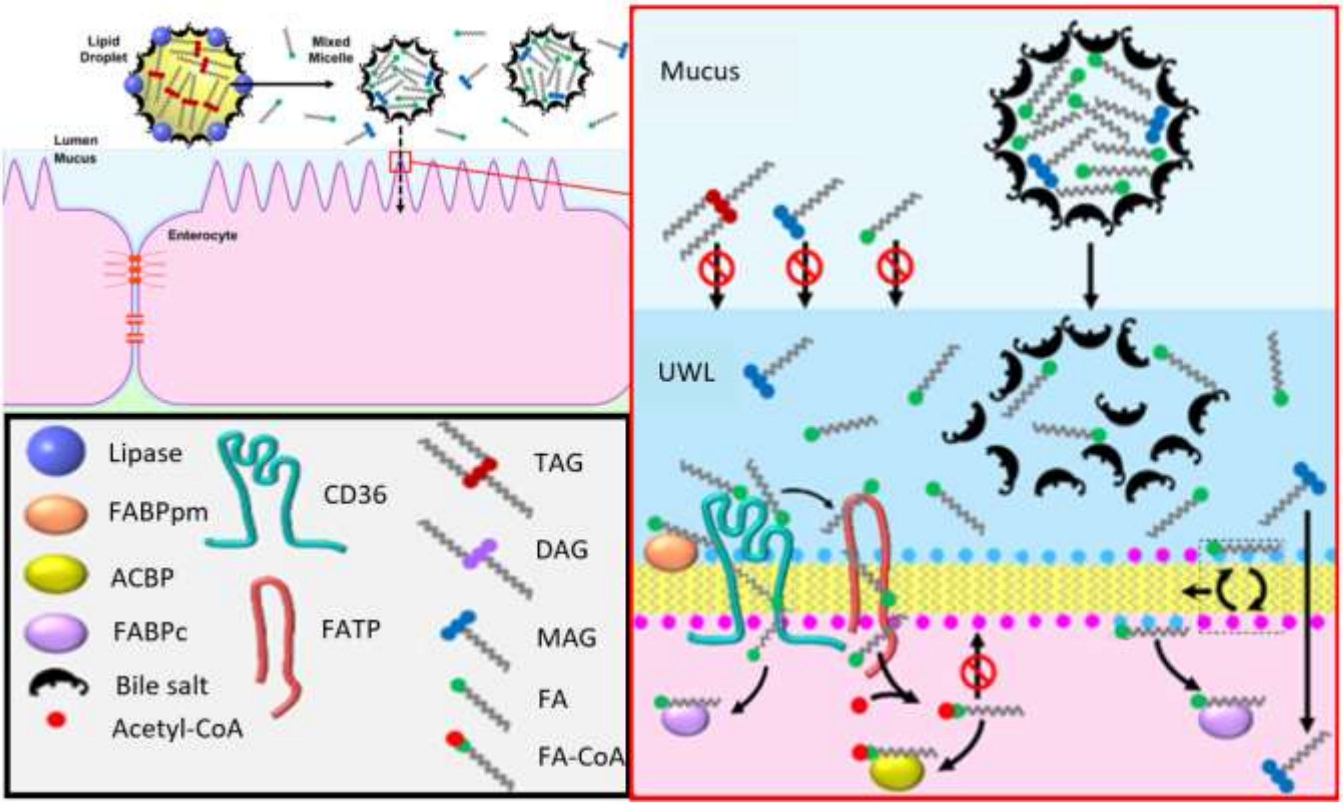

Figure 5. Mechanism of fatty acid transport across the lipid raft. UWL: unstirred water layer; FABPpm: plasma membrane fatty-acid binding protein; ACBP: Acyl-CoA-binding protein; FABPc: cytosolic fatty-acid binding protein; CoA: coenzyme A; FATP: fatty acid transport protein; TAG: triglyceride; DAG: diacylglycerol; MAG: monoacylglycerol; FA: fatty acid. Modified from (Deloid et al., 2022).

FAs must be activated upon use in cellular mechanisms. Acyl-coenzyme A synthetase (ACS) catalyses the esterification of FAs and free CoA, leading to the formation of acyl-CoA. The activated FAs, in the form of acyl-CoA, can enter the subsequent metabolic pathways to produce energy or synthesize diverse complex lipids. Alternatively, the acyl-CoA can be deactivated by acyl-CoA thioesterase (ACOT), which catalyses the inverse reaction of ACS. Consequently, the ratio of ACOTs and ASCs is of considerable importance as it regulates the equilibrium between activated and deactivated FAs (Ma et al., 2021).

MNPs present in the intestinal lumen may absorb fat due to their hydrophobic nature, thereby providing additional area for lipase binding and digestion. This was demonstrated by Deloid et al. (2022), who investigated the changes in food digest composition when MPs were introduced. Using an in vitro simulated digestion approach, it was found that both TAG and triacylglycerol lipase were present on the MNP surface, thereby catalysing the release of FAs and MAGs from TAGs. Since FAs and MAGs can be taken up in intestinal cells, in contrast to TAGs, this may lead to a higher lipid uptake in cells when food digest was first supplemented with MNPs compared to normal food digest. Interestingly, this increased lipid uptake was higher than expected, meaning that cellular lipid metabolism may also be altered due to the presence of MNPs.

Most research involving lipid metabolism upon MNP exposure has focused on marine species. Alterations in the FA transport-related genes, including FATP, FABP and ACBP, are found in the hepatopancreas of Pacific whiteleg shrimp (*Litopenaeus vannamei*) exposed to 80 nm NPs for 28 days. These alterations initially manifested as an increase, followed by a decrease, and were accompanied by increased lipid droplets and hepatopancreatic tissue structure damage (Y. Li et al., 2024). In marine clams, upregulation of FABP expression in the peroxisome proliferator-activated receptors (PPAR) α signalling pathway was noted after 7 days of exposure. This upregulation was associated with fatty acid transport, lipogenesis and cholesterol metabolism and suggested that NP exposure promoted lipid metabolism for synthesizing proteins, reserving energy and maintaining serum lipid levels (L. Liu, Zheng, et al., 2021). In liver organoids, generated from human pluripotent stem cells, CD36 is found to be increased after 48 hours of treatment with 1 µm MPs (Cheng et al., 2022). These findings collectively suggest that exposure to MNPs initially upregulates fatty acid transport, resulting in increased lipid uptake. However, with chronic treatment, the transporters are subsequently downregulated, leading to a stabilization of lipid uptake.

2.3.2 Cellular lipid metabolism

As cellular lipid metabolism is influenced by MNPs, it is important to understand the main pathways involved in lipid synthesis and lipid storage. In de novo lipogenesis, the cells synthesize lipids from non-lipid sources, such as carbohydrates. The pathway of de novo lipogenesis is illustrated in Figure 6. De novo lipogenesis often starts with the conversion of citrate from the Krebs cycle to acetyl-CoA by ATP-citrate lyase (ACLY). Then acetyl-CoA interacts with acetyl-CoA carboxylase (ACC) to form malonyl-CoA. This is followed by the reaction in which malonyl-CoA and acetyl-CoA form fatty acyl-CoA, catalysed by fatty acid synthase (FASN). Subsequently, FASN catalyses palmitoyl-CoA, which is synthesized via the stepwise addition of malonyl-CoA to the previously formed fatty acyl-CoA. This palmitoyl-CoA is an activated FA and can be used in cellular functions, including triglyceride formation. On the other hand, palmitoyl-CoA may undergo further elongation and finally desaturation with stearoyl-CoA desaturase (SCD) 1 to form complex fatty acids, including stearic acid, oleic acid and palmitoleic acid. In principle, de novo lipogenesis takes place in all cells, but it is more active in metabolic tissues such as the liver and skeletal muscle (Z. Song et al., 2018).

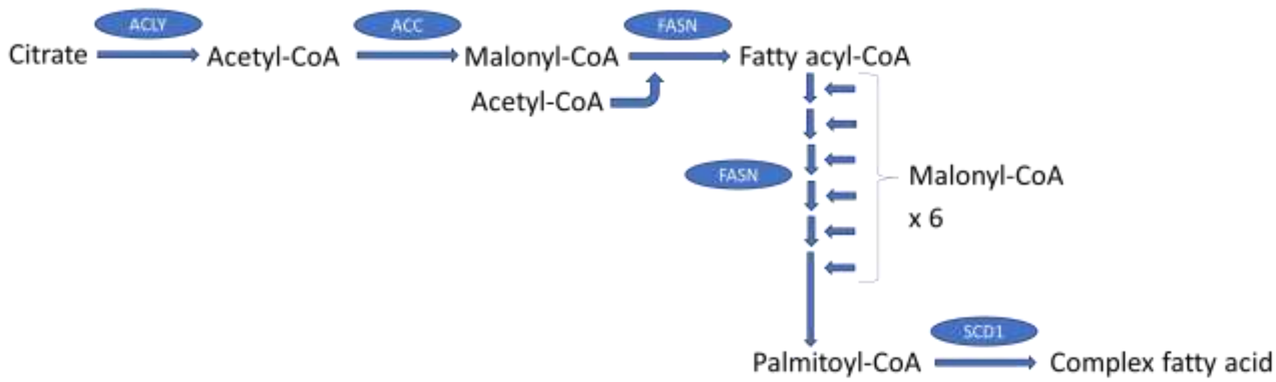

Figure 6. De novo lipogenesis pathway. ACLY: ATP-citrate lyase; ACC: Acetyl-CoA carboxylase; CoA: coenzyme A; FASN: fatty acid synthase; SCD1: Stearoyl-CoA desaturase 1.

Lipids are stored in the form of TAGs. Triglyceride formation starting from FAs, as visualised in Figure 7, also known as lipogenesis, takes place in the endoplasmic reticulum. Glycerol-3-phosphate acyltransferase (GPAT) initiates the reaction by attaching a first fatty acid to glycerol-3-phosphate, in which lysophosphatidic acid (LPA) and CoA are formed. LPA then reacts with acylglycerol-3-phosphate acyltransferase (AGPAT), which adds the second fatty acid, forming phosphatidic acid. Subsequently, phosphatic acid (PA) is converted to diacylglycerol with lipin as a catalyst. In the end, diacylglycerol acyltransferase (DGAT) catalyzes the addition of the third fatty acid, thereby completing the synthesis of the triglyceride molecule (Takeuchi & Reue, 2009).

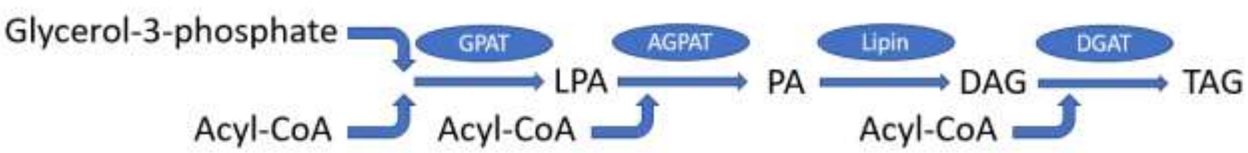

Figure 7. Triglyceride formation pathway. CoA: coenzyme A; GPAT: Glycerol-3-phosphate acyltransferase; LPA: lysophosphatidic acid; AGPAT: acylglycerol-3-phosphate acyltransferase; PA: phosphatidic acid; DAG: diacylglycerol; DGAT: diacylglycerol acyltransferase; TAG: triglyceride.

The opposite pathway of lipogenesis is lipolysis, as visualised in Figure 8. During periods of energy demand, adipocytes mobilize stored fat and use it for lipolysis. Adipose Triglyceride Lipase (ATGL) initiates lipolysis by hydrolyzing the first fatty acid from triglycerides, forming diacylglycerol. Hormone-Sensitive Lipase (HSL) further catalyses the hydrolysis of diacylglycerol, releasing a second fatty acid and leaving monoglycerides. Monoglyceride lipase (MGL) completes the process by hydrolyzing the last fatty acid, yielding glycerol and individual FAs (Bolsoni-Lopes & Alonso-Vale, 2015; Z. Song et al., 2018).

Figure 8. Lipolysis pathway. TAG: triglyceride; FA: fatty acid; ATGL: adipose triglyceride lipase; DAG: diacylglycerol; HSL: Hormone-Sensitive Lipase; MAG: monoacylglycerol; MGL: Monoglyceride Lipase.

Although our understanding of the effects of MNPs on these pathways is limited, some studies have shown that exposure to MNPs may lead to alterations in these pathways. Exposure of marine clams to 100 nm NPs for 7 days resulted in an upregulation of SCD1, indicating increased de novo lipogenesis (L. Liu, Zheng, et al., 2021). Furthermore, long-term exposure of *Siniperca chuatsi* juveniles to 80 nm NPs induced triglyceride synthesis. Thereby, it was pointed out that the increased concentration of TAG could form a potential trigger for nonalcoholic fatty liver disease and hepatitis (Chen et al., 2024). Additionally, research on the Pacific whiteleg shrimp (*Litopenaeus vannamei*) also indicated an increased content of triglycerides in hepatopancreatic tissue upon 80 nm NP exposure. However, FASN and ACC activities decreased with increasing NP concentrations, indicating an inverted relationship between MNP concentration and lipid formation. They concluded that overall, low NP concentrations appears to activate fat synthesis, whereas high concentrations are toxic and can damage lipid metabolism (Y. Li et al., 2024). Cheng et al. (2022) exposed liver organoids, deduced from human pluripotent stem cells, to 1 µm PS MPs. Also in these cells, increased FASN and SCD1 expression was found, indicating an increase in de novo lipogenesis. Moreover, decrease in DGAT was found in organoids originating from human stem cells, while organoids with mouse-origin showed an increase in DGAT, highlighting a contrasting response between mouse and human organoids.

2.3.3 Cellular energy metabolism

Cellular energy metabolism refers to metabolic pathways involved in adenosine triphosphate (ATP) synthesis, the universal energy carrier with fundamental roles in cell functioning and biosynthesis. Different molecules can serve as substrates for ATP production. An overview of the cellular metabolism is given in Figure 9. The most commonly used substrate is glucose, which can undergo glycolysis after internalization, resulting in ATP formation via substrate-level phosphorylation. In addition, during glycolysis, nicotinamide-adenine-dinucleotide is reduced from NAD^+ to form NADH. This cofactor can subsequently be used in the electron transport chain. At the end of the glycolysis, glucose is transformed into pyruvate, which may either react further, resulting in the formation of lactate, or be transported through the mitochondrial membrane using a mitochondrial pyruvate carrier (MPC). In the mitochondria, it can subsequently react in several pathways, including the Krebs cycle (Bender & Martinou, 2016; Chaudhry R & Varacallo M., 2023).

Lipids, once activated, can be used as a second energy source. FAs undergo β-oxidation, leading to the formation of the cofactor flavine-adenine-dinucleotide ($FADH_2$) and acetyl-CoA. This cofactor can supply energy to the electron transport chain, while Acetyl-CoA can be utilized in the Krebs cycle. As β-oxidation takes place within the mitochondria, the lipids must initially traverse the mitochondrial membrane. However, this membrane acts as an impermeable barrier for these acyl-CoAs. Hence, the FAs must first interact with carnitine palmitoyltransferase (CPT) 1a, an enzyme that converts acyl-CoAs to acyl carnitines. The acyl carnitines can cross the membrane and enter the β-oxidation pathway (Yoon et al., 2021).

Proteins can be used as the last energy resource. Although there is no universal pathway for ATP synthesis using proteins as substrate, it is known that the proteins are broken down to amino acids, which are used in different reactions to produce ATP. In addition, amino acids themselves, under which glutamine, can also be taken up and used for energy production (Alberts, 2002).

To study changes in substrate usage for energy production, research often uses pathway-specific inhibitors. In a study on cellular metabolic effects in obesity by Topete et al. (2023), the inhibitors UK5099, etomoxir and BPTES were used to block the use of glucose, FAs and glutamine for energy production, respectively. Similarly, the research of Han et al. (2023) employed these inhibitors in their study on mitochondrial networks and bioenergetics in lung cancer. These inhibitors, indicated in red in Figure 9, are commonly used in respirometry studies.

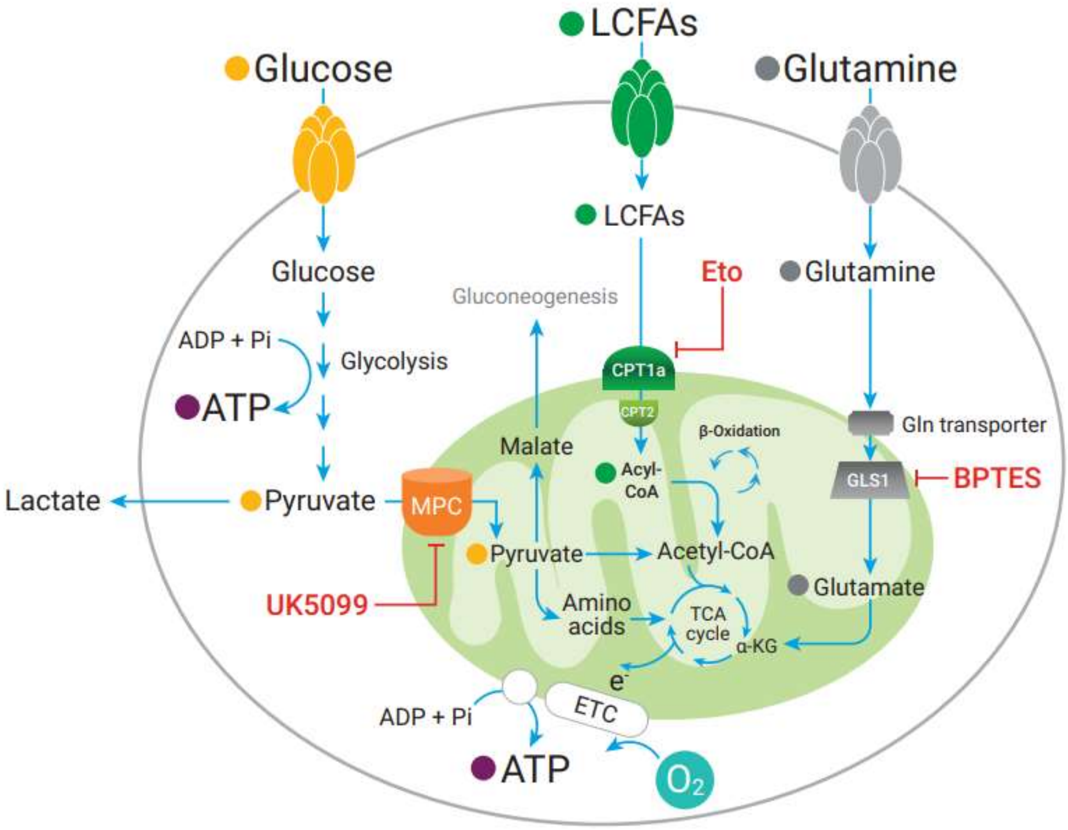

Figure 9. Primary metabolic pathways involved in energy metabolism. Glucose, FAs and glutamine are highlighted as substrates. Red text denotes relevant inhibitors. LCFA: long chain fatty acid; Eto: etomoxir; CoA: coenzyme A; TCA cycle: tricarboxylic acid cycle; ETC: electron transport chain; CPT: carnitine palmitoyltransferase; Gln: glutamine; MPC: mitochondrial pyruvate carrier; GLS: glutaminase (Agilent Technologies, 2020).

Acetyl-CoA in the mitochondria may enter the Krebs cycle, also known as the citric acid cycle or tricarboxylic acid (TCA) cycle, in which NADH is produced. The reduced cofactors NADH and $FADH_2$ contain a lot of energy and transport high-energy electrons to the inner mitochondrial membrane (IMM). As visible in Figure 10, those electrons will be carried via the electron transport chain, starting with coenzyme Q, which shuttles electrons from complex I to complex II and further to complex III. Subsequently, the electrons will be transferred to cytochrome C, which shuttles the electrons from complex III to complex IV. At each complex, the electrons will lose part of their energy, which is used to transport protons across the IMM. In complex IV, the electrons will be used to reduce molecular oxygen into water. The oxidised cofactors can return to the TCA cycle to undergo reduction again, while their energy is now captured in a proton gradient. The protons will flow back to the matrix via complex V, and the energy will be captured by the formation of ATP out of adenosine diphosphate (ADP) and Pi. Some protons can bypass complex V and traverse the inner mitochondrial membrane through other means, which is known as the proton leak (Nicholls, 2021). The oxidative phosphorylation is the main mechanism to produce ATP and thereby plays an essential role in the energy metabolism of cells (Yin & O'Neill, 2021).

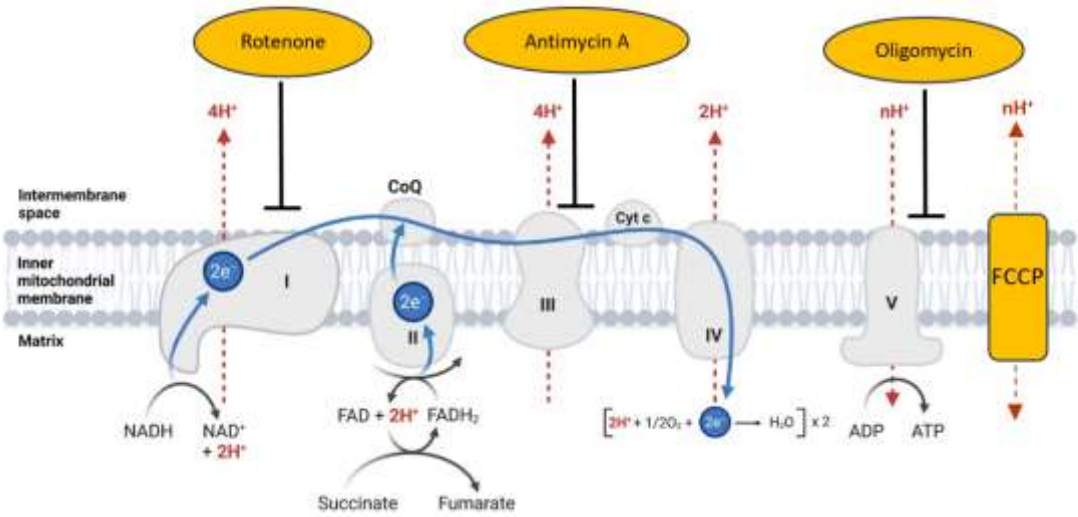

Figure 10. Oxidative phosphorylation. NADH: nicotinamide adenine dinucleotide; CoQ: coenzyme Q; FADH2: flavin adenine dinucleotide; Cyt C: cytochrome C. Modified from M. Yin & O'Neill (2021).

The flow of electrons through the ETC directly influences the OCR of cells. To perform research about the energy metabolism, the OCR can be measured after selective inhibition of specific proteins involved in the electron transport chain. Inhibitors that are often used in research are given in both Figure 10 and Figure 11. Before addition of any modulators, baseline cellular OCR is measured, from which basal respiration is derived by subtracting non-mitochondrial respiration. Oligomycin blocks complex V, trapping electrons in the intermembrane space. However, some electrons may still traverse the IMM, causing proton leak. Therefore, OCR will decrease upon oligomycin addition, revealing the ATP-linked respiration and proton leak. Another mediator is cyanide-p-trifluoromethoxyphenyl-hydrazone (FCCP), which induces full uncoupling, allowing protons to flow over the IMM and subsequently resulting in the electron transport chain functioning at maximal rate. Consequently, upon the addition of FCCP following oligomycin, the oxygen consumption rate will increase, and maximal respiration will be reached. The difference between the maximal respiration and the basal respiration is called the respiratory capacity. At last, rotenone is found to block complex I, while antimycin A is found to block complex III. Blocking these complexes will result in total inhibition of the electron transport chain, thereby revealing non-mitochondrial respiration rates (Rose et al., 2014).

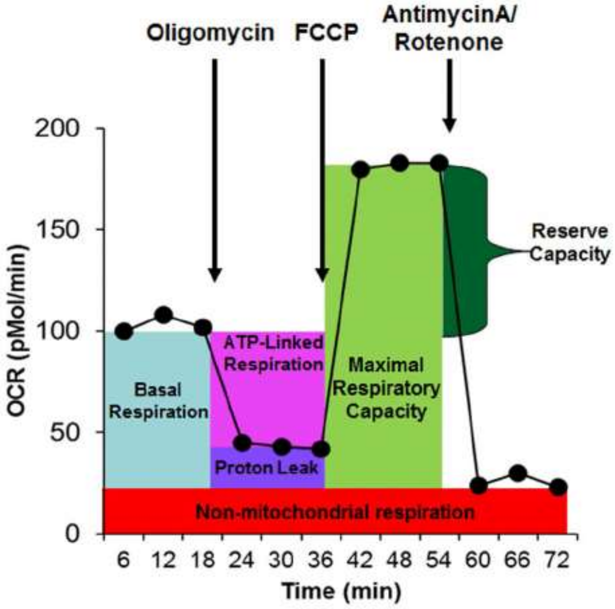

Figure 11. Alterations of OCR upon subsequent use of oligomycin, FCCP and a mix of Antimicyn A and Rotenone (Rose et al., 2014).

Several studies indicate the effect of MNPs on the cellular energy metabolism. Downregulation of CPT1a is observed in human liver organoids exposed to 1 µm MPs, suggesting a decreased β-oxidation, which ultimately results in a decreased use of lipids for energy metabolism (Cheng et al., 2022). A reduction in lipid breakdown, together with increased lipid uptake and de novo lipogenesis, ultimately induces lipid accumulation. S. J. Kim et al. (2021) further confirmed lipid accumulation in a long-term experiment involving low-level exposure of Caco-2 cells to 50 nm NPs. Bonanomi et al. (2022) exposed fibroblast-like cells to 0.5 µm and 2 µm MNPs at low doses (3.6×10^7 NPs/mL and 2.32×10^6 MPs/mL) in both acute (48 hour) and chronic (28 days) setups. They observed an increased glutamine metabolism following MNP treatments. In addition, a decrease in basal respiration was found, along with an increased glycolysis, indicating a shift from mitochondrial respiration towards glycolysis. This effect was present in both acute and chronic treatments but was more pronounced after longer exposure. Contrary to this, Peng et al. (2023) exposed Caco-2 cells to a single-dose exposure of 48 hours with low NP concentrations (1.14×10^2 - 5.68×10^5 NPs/mL) and found significantly elevated OCRs 12 days after exposure without subculturing. Halimu et al. (2022) treated A549 cells with 20 nm and 50 nm NPs for 24 hours. An increased basal respiration, together with an increase in spare respiratory capacity, proton leak and ATP production was noted at the lowest dosages (10 µg/mL for 20 nm PS and 40 µg/mL for 50 nm PS). However, these dosages were still five orders of magnitude higher than those used by Bonanomi et al., and even seven orders of magnitude higher than those of Peng et al. Higher concentrations of NPs led to decreased OCRs, suggesting that low concentrations of NPs appear to activate cellular energy metabolism, whereas high concentrations are toxic, leading to decreased energy metabolism. H. Wang et al. (2022) also reported decreases in both basal and maximal respiration and glycolysis in human liver cells subjected to acute treatment with a high concentration of 80 nm PS-NPs (100 µg/mL), further confirming the toxicity of high concentrations during acute exposure.

2.4 Lipid regulation

Lipid metabolism is regulated via several transcription factors, including sterol regulatory element-binding protein (SREBP), carbohydrate response element-binding protein (ChREBP), liver X receptors (LXR) and peroxisome proliferator activated receptors (PPAR) (Z. Song et al., 2018). Different studies already showed alterations in some of these regulators upon MNP exposure. Research in zebrafish indicated decreased levels of PPARγ and SREBP-1a mRNA and in liver cells upon long-term exposure to NPs (Zhao et al., 2020). In contrast, Caco-2 cells showed a significant increase in SREBP levels and PPARα levels upon PS exposure (S. J. Kim et al., 2021). Among all the transcription factors, SREBP and PPAR are thought to be the most influenced by MNP exposure (Figure 12).

The first important player in the disruption of lipid homeostasis upon MNP exposure is SREBP, of which three different isoforms exist. SREBP-1a activates both fatty acid and cholesterol synthesis, whereas SREBP-1c induces fatty acid synthesis, and SREBP-2 is primarily responsible for cholesterol synthesis and FA uptake (Z. Song et al., 2018). The activity of SREBP is highly regulated, and MNP exposure might disrupt these regulatory mechanisms. The first possible pathway by which MNP exposure can dysregulate SREBP and consequently disrupt lipid homeostasis is via ROS formation. ROS can induce ER-stress, subsequently affecting SREBP processing and lipid metabolism (Fang et al., 2013). In addition, elevated ROS levels due to MNP exposure can result in activation of the p38 MAPK pathway (McCubrey et al., 2006). According to Y. Yang et al. (2020), p38 MAPK signalling upon PS NP exposure can dysregulate SBP-1 in *C. elegans*, which is equivalent to SREBP in mammals. SBP-1 activation led to UPR activation and decreased susceptibility to PS NP toxicity. Additionally, research indicated that MNP exposure may activate a pro-inflammatory state via NF-κB activation (Cao et al., 2023). Increased NF-κB is found to induce SREBP-activation in macrophages, leading to foam cell formation (L.-C. Li et al., 2013). It is plausible that NF-κB activation due to MNP exposure can also induce SREBP-2 activation, leading to lipid accumulation. The activation of SREBP can also be initiated by the mammalian target of rapamycin (mTOR), a process influenced by various regulators, including AKT and the ERK/MAPK pathway. ROS production upon MNP exposure may also affect these regulatory pathways (Laplante & Sabatini, 2009; Sui et al., 2023).

Next to ROS formation, SREBP may be influenced via the activation of receptors. (Y. Yang et al., 2021) noted an upregulation of PAQR-2 in *C. elegans* upon PS NP exposure. This G protein-coupled receptor (GPCR) is equivalent to Adipo2 in humans and is found to influence AMPK. Subsequently, AMPK can inhibit SREBP via activation of mTOR. In contrast, acute treatment of human kidney and human liver cells with PS-NPs revealed a decrease in mTOR, which should normally be accompanied by lower SREBP and thus lower lipid content (H. Wang et al., 2022). Activation of TLRs, under which TLR4 and TLR2, upon exposure to NPs, lead to a pro-inflammatory state via NF-κB and p38 activation, which can be linked to increased lipid content (Antunes et al., 2023; L.-C. Li et al., 2013; Y. Yang et al., 2020).

The second transcription factor that plays an important role in lipid homeostasis is PPAR, which dimerizes with the retinoid X receptor (RXR), thereby altering gene expression involved in glucose and lipid metabolism. PPARα and PPARβ play a crucial role in lipid catabolism and upregulation of β-oxidation, whereas PPARγ induces lipid biosynthesis and upregulation of CD36, followed by higher lipid uptake (Varga et al., 2011). Natural ligands of PPAR include poly- and monounsaturated fatty acids, eicosanoids and lipophilic hormones (Maradonna & Carnevali, 2018). In addition, some xenobiotics like tributyltin and phthalates, commonly used in the production of plastics, may bind to PPARγ and RXR at nanomolaire concentrations, promoting adipogensis and lipid accumulation. However, these plastic additives also possess the potential to activate PPARα, creating ambiguity in their effects on lipid metabolism by influencing both anabolic and catabolic processes (Chamorro-Garcia et al., 2017; Hurst & Waxman, 2003). Next to direct activation, upregulation of PAQR-2 in *C. elegans*, an equivalent to human AdipoR2, influences lipid metabolism, not only via AMPK, but also via PPARα (Y. Yang et al., 2021). Furthermore, PPARs can crosstalk with other regulators, under which SREBP-1c, NF-κB and mTOR, which can indirectly alter the metabolic state of the cell (Dayn es & Jones, 2002; Laplante & Sabatini, 2009; W. Zhang et al., 2021).

At last, TLRs are activated after MNP exposure in different animal cells under which lung cells of mice, intestinal cells of gilthead seabream and intestinal cells of the zebrafish (Cao et al., 2023; Del Piano et al., 2023; Marana et al., 2022). These TLRs are correlated with altered FA uptake and triglyceride formation, mediated via NF-κB. Other unknown mechanisms may play a role in lipid accumulation after TLR activation. Murine macrophages showed a significant increase in CD36 activation via TLR2 and TLR4, indicating an increased lipid uptake (Feingold et al., 2012). In contrast, in the research of Huang et al. (2014), which focussed on thioglycolate-elicited peritoneal macrophages, no significant increase in CD36 was noticed. However, the results showed a decrease in CPT1a, indicating a decreased use of lipids for energy production. Additionally, research indicated that the conversion of FA to triglycerides may be elevated after TLR activation, due to increased ACSL1 and DGAT, and decreased ATGL (Feingold et al., 2012; Huang et al., 2014). It is possible that similar reactions occur after TLR activation due to MNP exposure as well.

The common thread in this regulatory mechanism is that most regulatory factors do not only influence lipid accumulation but are also closely linked to inflammation. NF-κB activation via TLRs is known to induce inflammation, while PPAR plays an anti-inflammatory role. SREBP regulates the expression of Nlrp1a, a subunit of the inflammasome complex, thereby increasing the production of the pro-inflammatory cytokines IL-1β and IL-18 (Im et al., 2011). However, SREBP-1a leads to FA production, of which some are anti-inflammatory and play an important role in the resolution phase of the inflammatory response. The resolution phase is the phase wherein the inflammatory process is actively terminated, and tissue homeostasis is restored (Oishi et al., 2017). In addition, intermediate regulators altered by MNP exposure, including NF-κB and MAPK signaling, are closely linked to inflammation (Wu et al., 2020).

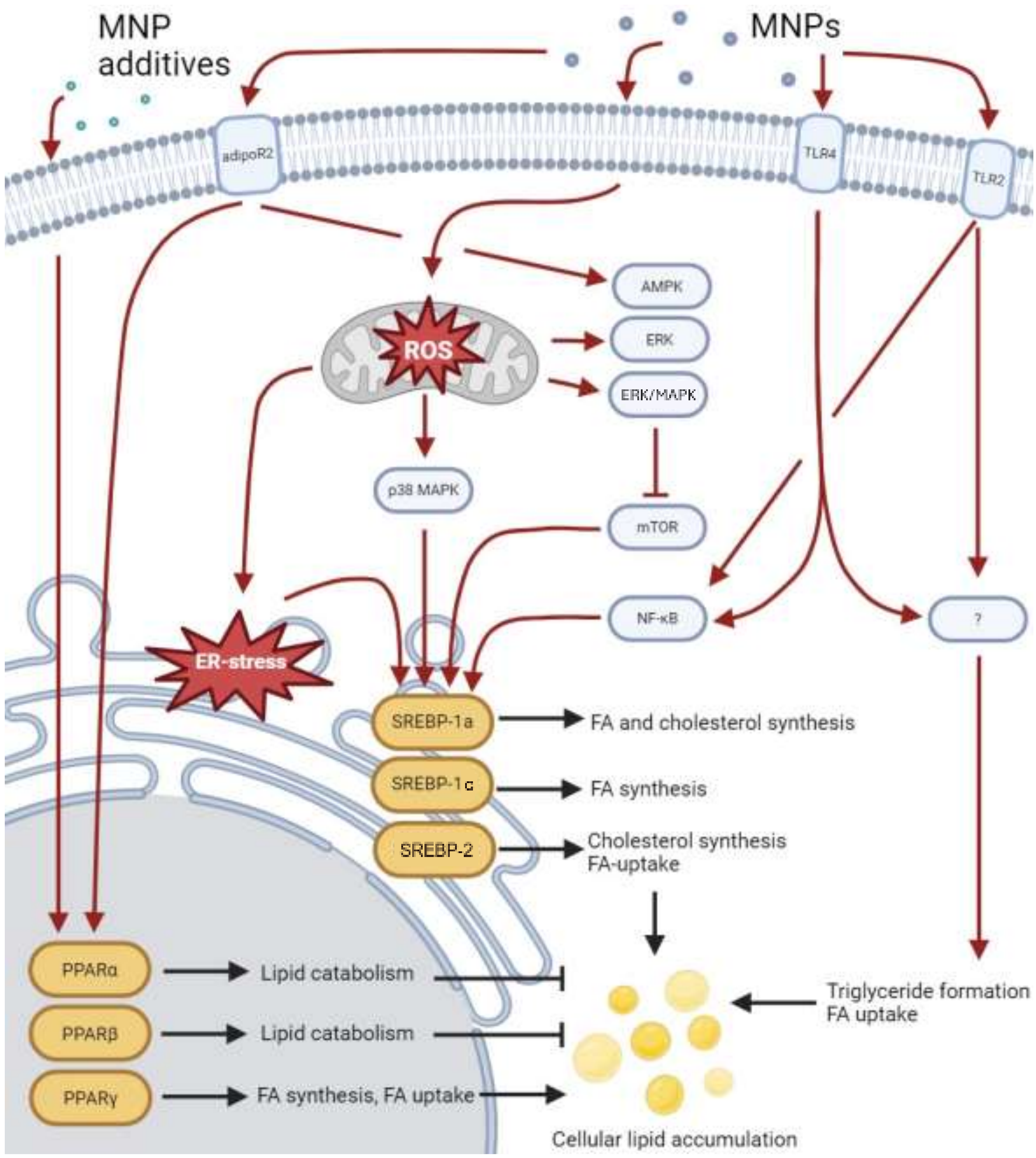

Figure 12. Overview of alterations in lipid regulation upon MNP exposure. Created with BioRender.com.

3 OBJECTIVES

The impact of NPs on human health is a growing concern. While NPs can influence cellular metabolism, their effect on lipid metabolism remains poorly understood. In addition, there is uncertainty about whether these effects are due to the physical presence of nanoparticles or result from the specific properties of specific plastic types. Previous studies often used acute treatments with high NP concentrations, which may not reflect real-life exposure.

Therefore, the major objective of this research is to study lipid metabolism upon intestinal exposure to NPs at physiologically relevant concentrations and in different repeated dose exposure scenarios. To this end, a Caco-2 intestinal cell culture was treated with a low dose of plastics and glass particles to study the effect of **particle type and concentration**.

Next, we aimed to investigate **two physiological states** of the intestinal epithelium. In a first scenario, growing and differentiating enterocytes along the villus axis were mimicked by a 12-day repeated exposure of cells cultured in the same vessel. In a second scenario, the continuously dividing cells at the bottom of the intestinal crypt were modelled by subculturing the same cell line in the presence of the NPs and glass beads before reaching confluency, and hence differentiation, for more than 40 days.

Finally, we aimed to investigate how **cells respond to a nutritional stress**, and whether the stored lipids were used for cell survival. To this end, cells were exposed to a nutrient-depleted medium without glucose and pyruvate for an additional 4 hours after a repeated exposure to NPs and SBs.

Using these scenarios, we studied **lipid metabolism** in three ways, i.e. (i) microscopic evaluation of lipid droplet storage using fluorescence microscopy, (ii) live-cell respirometry either or not in combination with an inhibitor of fatty acid transport in the mitochondria and (iii) transcriptomics in collaboration with the NXTGNT sequencing facility.

4 METHODS

4.1 Basic cell culture procedures

For all the experiments, the human colorectal adenocarcinoma cell line (Caco-2) purchased from the American Type Culture Collection (ATCC; USA) and deposited under Biobank number BB190156 was used. Culture medium containing phenol red Dulbecco's modified eagle medium (DMEM; refnr. 61965-026/059, Thermo Fisher Scientific, USA) enriched with 10% fetal bovine serum (FBS; refnr. 10082-147, Thermo Fisher Scientific, USA), a mix of 100 units/mL penicillin and 100 µg/mL streptomycin (refnr. 15070-063, Thermo Fisher Scientific, USA) and 2% nonessential amino acids (NEAA; refnr. 11140-068, Thermo Fisher Scientific, USA) was used. The cells were incubated in a CO_2 incubator at 37 °C with 5% or 10% CO_2, depending on the experiment and >95% relative humidity. Cells were subcultured according to standard procedures and were trypsinized and detached by sequentially adding excess Dulbecco's phosphate-buffered saline without magnesium and calcium (DPBS) and 0.5% trypsin-ethylenediaminetetraacetic acid (trypsin-EDTA; refnr. 15400-054, Thermo Fisher Scientific, USA). Throughout the entire research, the passage number of the cell lines was maintained below 50.

4.2 Exposure of the cells to nanoparticles

Cells were subject to two distinct treatment scenarios, as illustrated in Figure 13. In the first scenario, cells were cultured continuously throughout the experiment, potentially undergoing slight differentiation at the final timepoint. In the second setup, subcultures were taken throughout the experiment, thereby controlling differentiation.

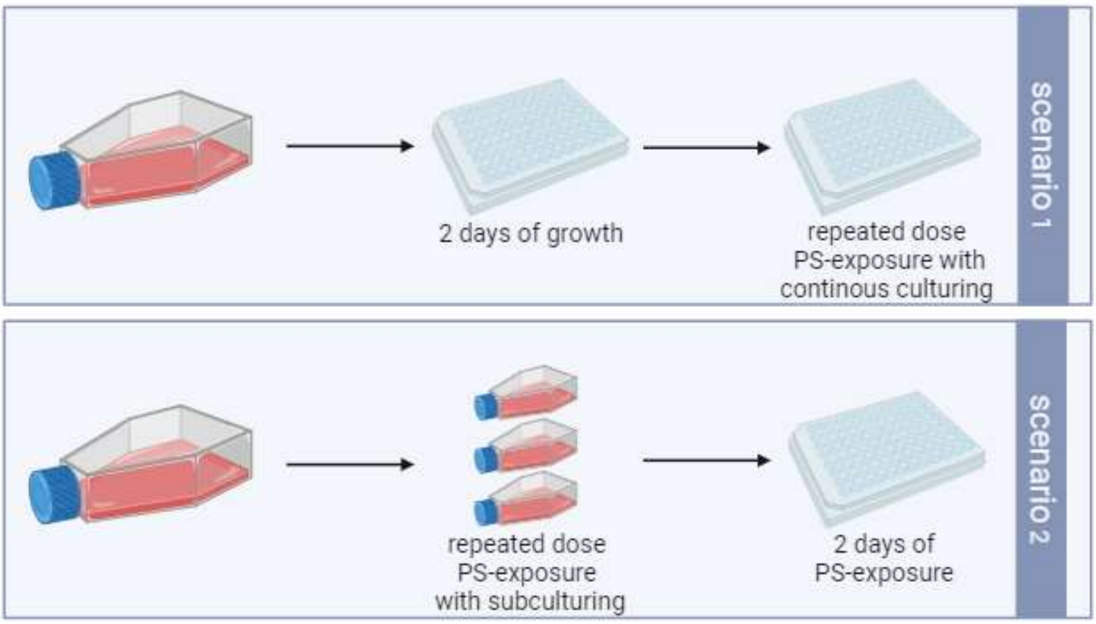

Figure 13: schematic overview of the experimental design implemented in this study. Two scenarios were used. In the first scenario, Caco-2 cells were seeded in 96-well plates, wherein they were continuously cultured. First, they were grown for two days, whereafter exposure was initiated with repeated doses of different concentrations of PS-NPs and SBs. In the second scenario, Caco-2 cells were exposed to repeated doses of SBs and NPs in culture flasks, while subculturing. After long-term exposure in the flasks, cells were seeded in 96-well plates where they were treated for two more days. After exposure, biological responses of the particles were analysed. Created with BioRender.com.

4.2.1 Scenario 1: long-term exposure of Caco-2 cells without subculturing

This scenario was used for AdipoRed staining and transcriptomics. Two tests with AdipoRed assays were performed. In test 1, Caco-2 cells were seeded in a 96-well Agilent Seahorse XF Cell Culture Microplates (Agilent Seahorse Bioscience, USA) at a cell density of 5,100 cells/well. Treatment was done using spherical polystyrene nanoplastics (PS-NPs; 100 nm, 4.55 x 10^{13} particles/mL) purchased from Polybead® (Polysciences Inc., USA). The cells were grown for 48 hours and subsequently exposed to different concentrations of NPs (4.55 x 10^{3} NPs/mL, 4.55 x 10^{6} NPs/mL and 4.55 x 10^{9} NPs/mL). The first treatment, two days after seeding, was performed using DMEM, supplemented with NEAA and streptomycin and penicillin. Thereafter, full growth medium was used. Treatment was performed every 2 or 3 days, and the last treatment of the cells was done at least 48 hours before the bioassay to be sure that there was no influence of the treatment on the results. In the end, an AdipoRed assay was performed.

In test 2 of the AdipoRed assay, the following modifications were used: cells were seeded in a normal well plate (Greiner bio-one), at a density of 12,800 cells/well. Treatment was done using full medium throughout the entire experiment. Conditions that were incorporated in this test were untreated conditions, treatment with NPs (4.55 x 10^{3} NPs/mL and 4.55 x 10^{6} NPs/mL) and treatment with SBs (900 nm, 5% w/w, purchased from Sigma-Aldrich, USA, 4.55 x 10^{3} SBs/mL and 4.55 x 10^{6} SBs/mL). In addition, controls for each treatment condition were implemented. As the NPs were suspended in distilled water, a solvent control containing filter sterilised distilled water in the same concentration as the concentration in which the solvent of the NPs was present during the treatment was used (0.1 nL water/L medium and 0.1 µL water/L medium corresponding to a NP concentration of 4.55 x 10^{3} NPs/mL and 4.55 x 10^{6} NPs/mL, respectively). As the SBs were suspended in ethanol, a control containing ethanol was needed (0.1 µL ethanol/L medium and 0.1 mL ethanol/L medium corresponding to a SBs concentration of 4.55 x 10^{3} beads/mL and 4.55 x 10^{6} beads/mL respectively).

A similar setup was used for the transcriptomics, with the following modifications: cells were seeded at 600,000 cells per well in a 12-well plate and repeatedly exposed to the NPs at the same concentrations as test 1 of the AdipoRed. In one subset of wells, cells were harvested after 12 days for RNA extraction, so they have always been exposed to full medium with 4.5 g/L glucose, 1 mM pyruvate and 2 mM glutamin. In another subset of wells, cells grown for 12 days were exposed to depleted medium for an additional 4 hours. This depleted medium consisted of Seahorse base medium, without glucose or pyruvate, but with 2 mM glutamin.

4.2.2 Scenario 2: long term exposure of Caco-2 cells with subculturing

Caco-2 cells were grown in culture medium supplemented with 5.44 x 10^{6} NPs/mL or 5.44 x 10^{6} SBs/mL, in small T25 culture flasks. A solvent control containing ethanol (0.13 µL ethanol/mL medium) was implemented. Once a week, the cells were trypsinized. After counting the cells, using the Trypan blue method with a Bürker counting chamber, a seeding density of 12,800 cells in each culture flask was always applied. This led to a culture that reached sufficient confluency the next week. After 7 days, 15 days and 41 days of treatment, a subculture was taken and used for plating in either 96-well Agilent Seahorse XF Cell Culture Microplates (Agilent Seahorse Bioscience, USA) or normal 96-well plates (Greiner Bio one), whereafter these plates were incubated for 48 hours with the same treatment conditions as before. Subsequently, respirometry was performed on the seahorse plates, while normal plates were used for cellular stainings.

4.3 Cellular assays

4.3.1 Cell confluency

The confluency of the cells per well was determined by high-throughput microscopy using the phase contrast option of the Incucyte SX5 Live cell Imager (Sartorius) using AI confluence. Four random pictures were selected, and additional cleanup and filter steps were performed. Hole fill, pixel size and minimal area were adapted to ensure consistency between the software measurements and the actual area. Then, an analysis was started using the parameters defined based on these four pictures and the phase/area/confluence (%) were measured.

4.3.2 AdipoRed assay

To perform the AdipoRed assay, the cells were fixated with 4% paraformaldehyde and stored in the fridge for a brief period if necessary. Then the fixative was removed, cells were washed with DPBS and 2.5% AdipoRed reagent was added. After at least 15 minutes of incubation, a picture was taken using the Incyte Live Cell Imager (Sartorius), with an exposure time of the orange channel of 400 ms. The pictures were analyzed with the incucyte software. A surface fit segmentation was used for background subtraction and edge splitting was turned on, with a value of minus 75. Four random pictures were selected, and additional cleanup and filter steps were performed. Threshold, hole fill, pixel size and minimal area were adapted to ensure consistency between the software measurements and the actual area. Then, an analysis was started using the parameters defined based on these four pictures and the total integrated fluorescence intensity (in optical calibration units (OCU) x μm^2 /well) was measured. This measure takes both the intensity and the area of the fluorescent pixels into account. To correct the total integrated intensity with the confluence, an extra metric was added, which normalized the total integrated fluorescence intensity by the confluence (OCU x μm^2 /well/%). The latter was used in the results.

4.3.3 SRB staining

To perform SRB, the cells were fixated with 10% trichloroacetic acid (TCA) and stored in the fridge for a brief period of time if necessary. On the day of the SRB-staining, the fixative was removed and the cells were washed five times with water before being air-dried. Thereafter, the proteins of the cells were coloured incubating them with an excess amount of 0.4% sulforhodamin B (SRB) dissolved in 1% glacial acetic acid for at least 30 minutes. The SRB-solution was removed, and the cells were washed with 1% glacial acetic acid. At last, the stained proteins were dissolved in 10 mM Tris buffer, and the absorbance at 490 nm was measured using a Spectramax plate reader (Molecular Devices).

4.3.4 Respirometry analysis with the Seahorse XF96 Efflux Analyzer

Hydration of the cartridge. One day prior to the assay, 180 µL of deionized water (filtered by a 0.22 µm filter) was added to each well of an empty calibration plate to hydrate the Seahorse XF Sensor Cartridge. Subsequently, the cartridge was incubated at 37 °C for 24 hours without CO_2. On the day of assay, the deionized water was removed from the hydrated cartridge, and 180 µL calibration medium (Agilent Seahorse Bioscience, USA) was added in each well. The sensor cartridge was further incubated for an hour at 37 °C, without CO_2.

Preparation of the cell culture plate. To simulate nutrient rich conditions (non-starvation), assay medium was obtained by supplementing Seahorse XF DMEM Medium, pH 7.4 (Agilent Seahorse Bioscience, USA) with glucose (10mM), pyruvate (1mM) and glutamine (2mM), all purchased from Agilent Seahorse Bioscience, USA. For the nutrient depleted condition (starvation), assay medium was obtained by supplementation of the same medium only with glutamine (2mM). The cells in the seahorse plate were washed three times with assay medium. After the third washing step, 180 µL assay medium was added and the cells were incubated at 37 °C without additional CO_2 for one hour.

Loading of inhibitors and modulators in the injection ports of the cartridge. To perform the seahorse assay with the Seahorse XF96 Efflux Analyzer (Agilent), the XF Long Chain Fatty Acid Oxidation Stress Test Kit (p/n 103672-100) was used. Etomoxir, oligomycin, FCCP and a mixture of rotenone and antimycin A (ROT/AA), all purchased from Agilent Seahorse Bioscience (USA) where suspended in the assay media at concentrations of 40 µM, 15 µM, 5 µM , respectivily 5 µM. Subsequently, for all wells of the cartridge, the ports were loaded with 20 µL of etomoxir in port A, 22 µL of oligomycin in port B, 25 µL of FCCP in port C and 27 µL of ROT/AA in port D. Thereafter, the calibration plate with the loaded sensor cartridge was placed in an Agilent Seahorse XF96 Analyzer (Agilent Seahorse Bioscience, USA) for calibration. Finally, the calibration plate was replaced with the cell culture microplate. OCR and extracellular acidification rate (ECAR) were measured by the Seahorse XF96 Efflux analyzer. The injection and measurement strategy involved repeated cycles of 10 seconds of mixing, 1 minute 30 seconds of waiting and 2 minutes 30 seconds of measuring. Initially, the baseline OCR was measured over three cycles. Subsequently, either medium or etomoxir was injected, followed by five measurement cycles. This was followed by sequentially injection of oligomycin, FCCP and Rot/AA, each followed by three measurement cycles.

4.4 Transcriptomics

Transcriptomics was not performed by the student, but a dataset was generated by Miao Peng (PhD) and Charlotte Grootaert (tutor), who prepared the cells according to the procedures described in 4.2 and extracted the RNA. The quality control, data processing and comparison with databases were performed by NXTGNT. The reported data were further interpreted by the student, with a special focus on pathways that may explain the effects on lipid and energy metabolism observed in other cellular and respirometric assays. Methods used for transcriptomics are described in Appendix 1.

4.5 Statistical analysis of non-transcriptomic data

R-studio was used for the statistical analysis of the data. The normality of the data was determined with a Shapiro test. The data did not show a normal distribution, probably due to the small number of observations. Therefore, when multiple hypotheses where simultaneously tested, a non-parametric Kruskal-Wallis test was performed, followed by a pairwise Wilcoxon rank sum test. When only two groups were compared in the test, a Wilcoxon test was used. As most of the tests were done with small sample sizes, the Benjamini-Hochberg procedure was used for correction with multiple testing. A p-value lower than 0.05 was seen as significant.

4.6 Chat GPT

For this research, ChatGPT was used as a tool to facilitate understanding of the complex interactions described in this work. Furthermore, ChatGPT was used for refining the writing style throughout the master's dissertation.

5 RESULTS

For scenario 2, three biological replicates were used. After the second week, a procedural error occurred, and two biological replicates treated with NPs were deceased. The third biological replicate was split into three new cultures, and the experiment was continued until 43 days from the start.

5.1 Cellular growth

Treatment with NPs and SBs following scenario 1 only started after 2 days of growth. A confluence of 50-80% was found on day 4, two days after the start of exposure. Thereafter, confluence stayed 100% for all conditions. No influence of the conditions on cellular growth was noticed.

In scenario 2, the number of cells were counted, and the initial number of cells (12,800 cells/culture flask) was subtracted, which enabled the measurement of the cell growth over the course of the week. This action was repeated for five to six weeks. In addition, each time deceased cells were counted. The number of counted dead cells was low throughout the entire experiment. In Figure 14, indicating cell production over time, no major differences between the different treatment conditions are noticed.

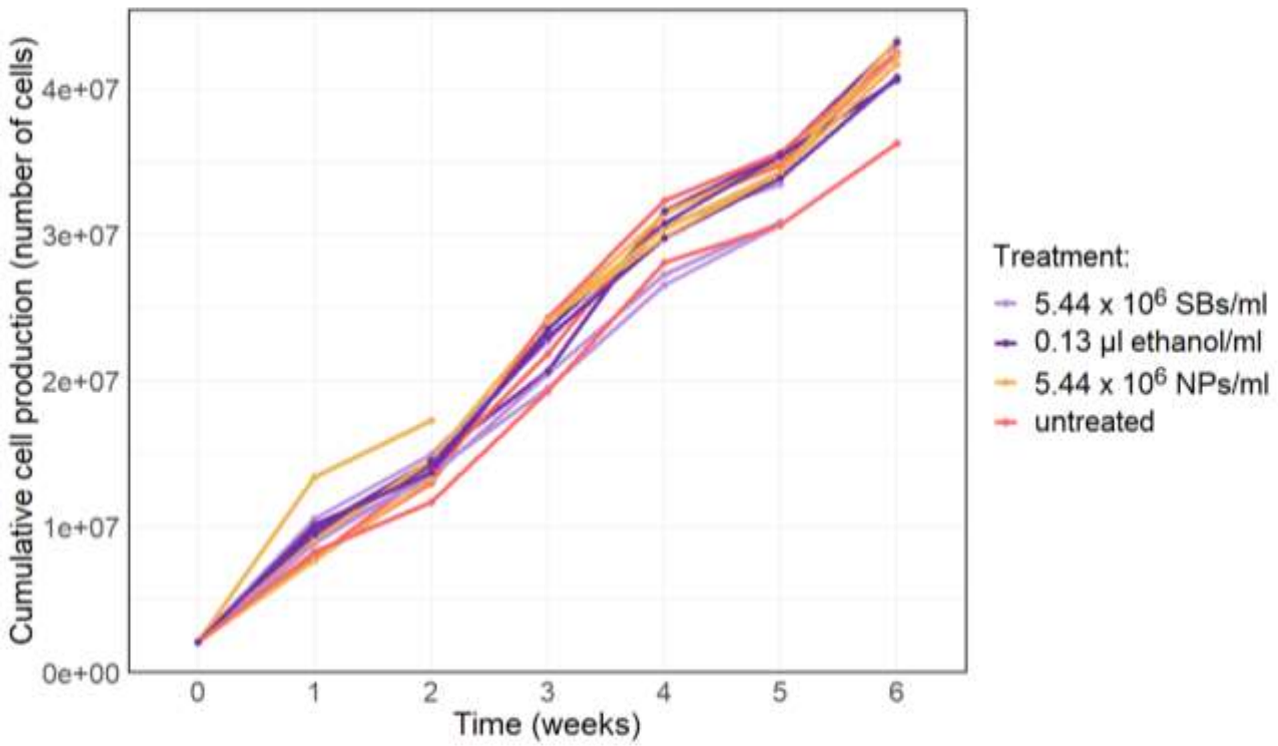

Figure 14. Cumulative cell production in a T25 culture flask for each week. Cells were either untreated or exposed to SBs, NPs, or ethanol, according to scenario 2. Three biological replicates are shown for each condition. Between the second and the third week, 2 biological replicates were diseased, therefore, their growth curve stopped at week 2.

First, the controls are looked into. Following scenario 2, a similar confluence was obtained for the ethanol control and the untreated condition after 9 and 17 days of treatment, as visible in Figure 15. However, after 43 days, ethanol increased cell growth, leading to a significantly higher confluence. Since there was a noticeable difference between the ethanol and the untreated control at day 43 of the experiment, the results from treatments were compared with their respective control.

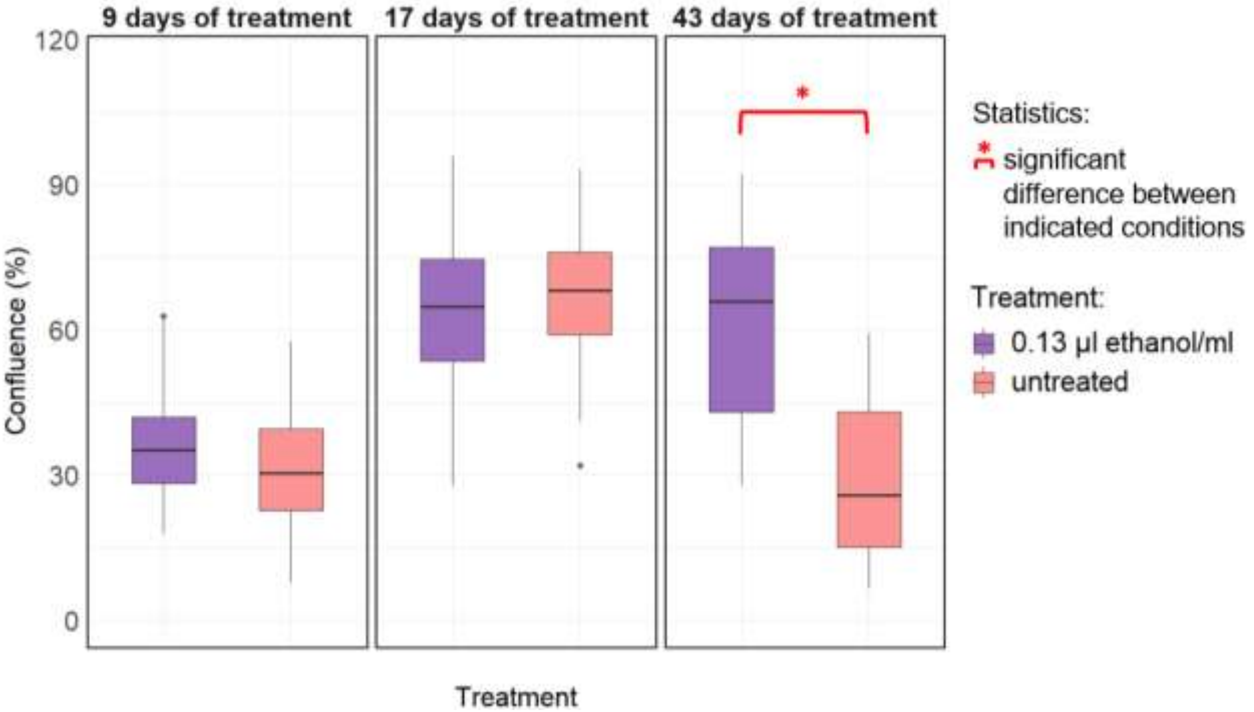

Figure 15. Confluence, expressed as a percentage of the area of the wells. Ethanol control and untreated conditions at day 9, 17 and 43 of the experiment following scenario 2 are shown. For each condition, three biological replicates were seeded in wells of a 96-well plates (19≤n≤26) and shown together in one boxplot. Statistically significant differences between two groups are indicated with a red star.

The confluence data of the treated conditions, relative to their respective controls, is given in Figure 16. The confluence was significantly lower in all the treated conditions compared to their respective controls. For the cells treated with NPs, the difference in confluence between the control and the treated condition decreased over time.

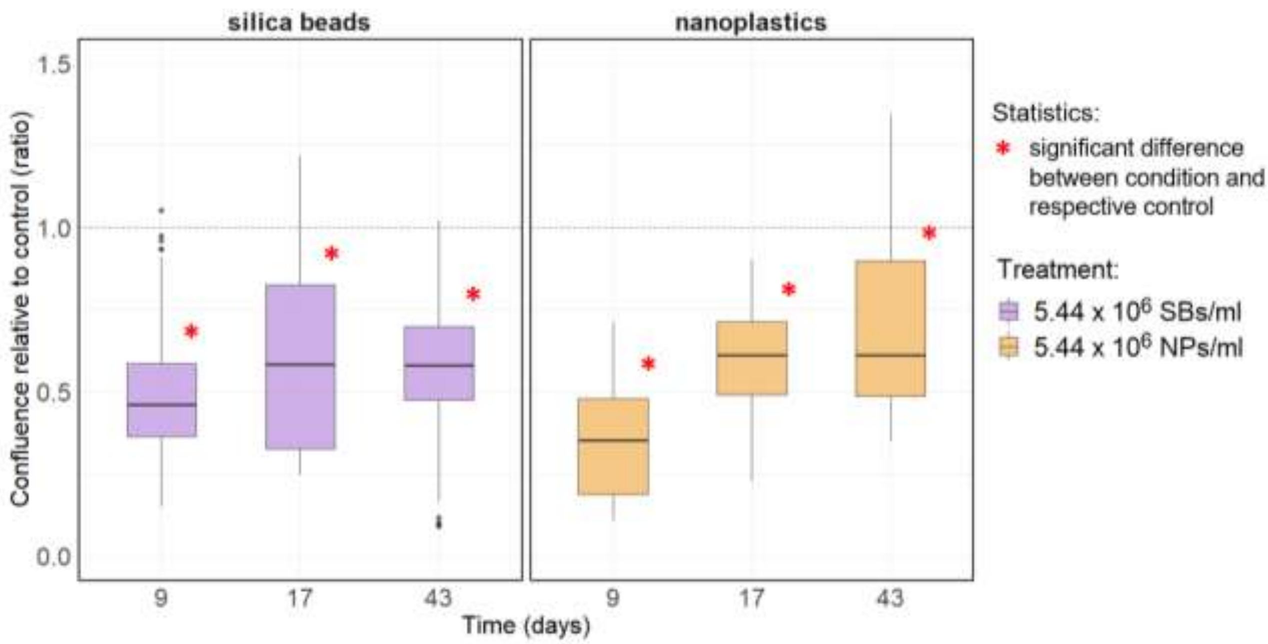

Figure 16. Ratio of the confluence of the cells treated with either SBs or NPs and the mean confluence of their respective controls, given over time. The values of the controls are indicated by 100%. Cells were treated in accordance with scenario 2 and for each condition, three biological replicates were seeded in wells of a 96-well plate (19≤n≤26). The three biological replicates are shown together in one boxplot. When the difference between the untreated condition and the treated condition is statistically significant, a red star is placed next to the boxplot.

5.2 Protein staining

Protein staining was only performed using cells treated as described in scenario 2. The results from the controls, shown in Figure 17, are first investigated. A significant difference was observed between the ethanol control and the untreated condition after 9 days and after 43 days of treatment.

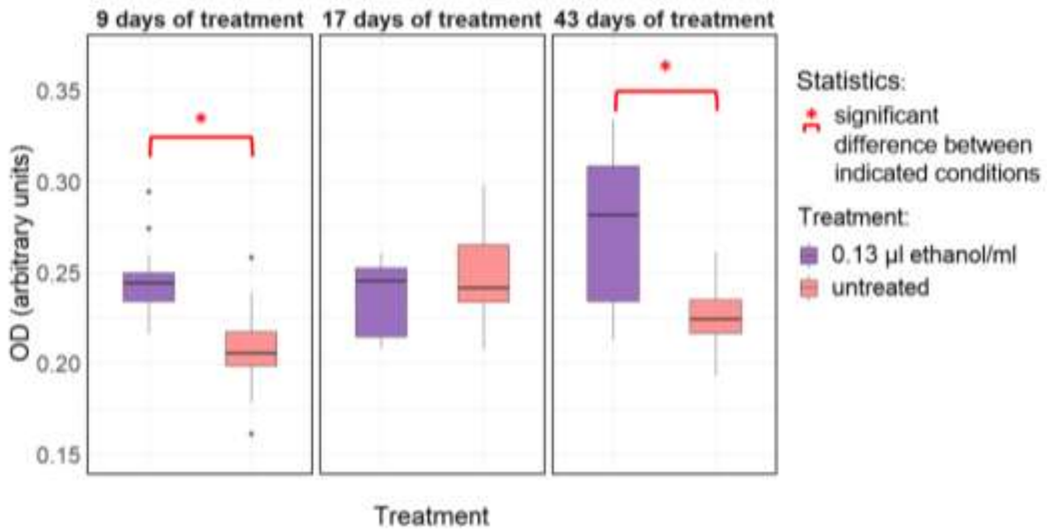

Figure 17. Optical density (OD), expressed in arbitrary units, of the ethanol control and untreated conditions after protein staining, at days 9, 17 and 43 of the experiment following scenario 2. For each condition, three biological replicates are seeded, each in five wells of a 96-well plate, and shown together in one boxplot. Statistically significant differences between two groups are indicated with a red star.

The results of the protein staining of the treated conditions, relative to their respective controls, are given in Figure 18. A similar profile between the results of the protein staining and the confluence data of the Incucyte can be noticed. For the SBs, significantly fewer proteins were present after 9 and 17 days of treatment. Moreover, this decreased protein content was most abundant after 9 days of treatment. For all the NP concentrations, the protein-content in the treated conditions was significantly lower than the protein-content in the untreated conditions. However, the difference between the treated and untreated condition also decreased over time.

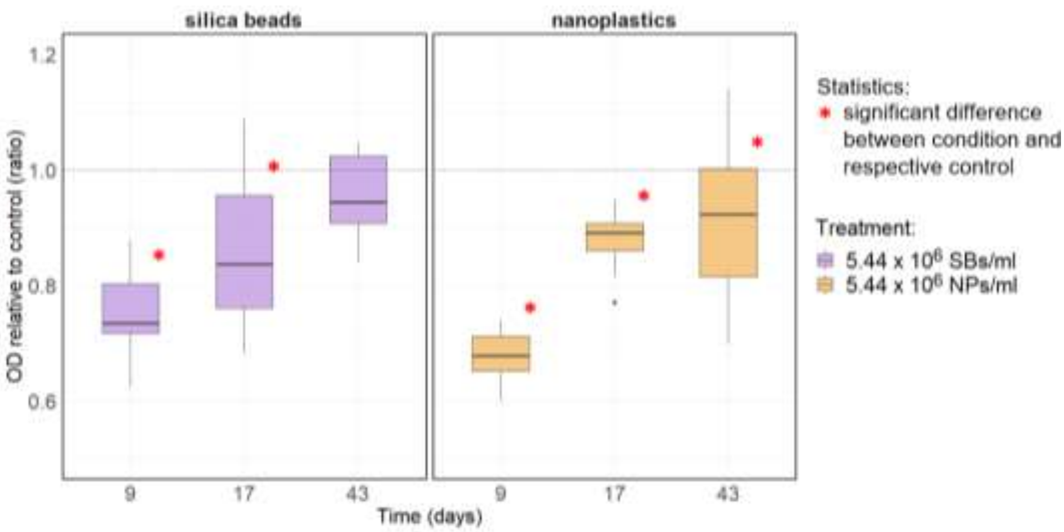

Figure 18. Ratio of the optical density (OD) of protein staining in cells treated with either SBs or NPs to the mean OD of their respective controls was monitored over time. Cells were treated in accordance with scenario 2. The values of the controls are indicated by 100%. For each condition, three biological replicates are seeded in five wells of a 96-well plates and shown together in one boxplot. When the difference between the untreated condition and the treated condition is statistically significant, a red star is placed next to the boxplot.

5.3 Lipid staining

The lipid staining was performed in two different settings, namely scenario 1 and scenario 2.

5.3.1 Test 1: Concentration-effect for NPs in scenario 1

Cells were treated with 4.55 x 10^3 NPs/mL, 4.55 x 10^6 NPs/mL, 4.55 x 10^9 NPs/mL for 9 days, and at day 9, a lipid staining was performed. Full confluence was reached in all replicates. As visible in Figure 19, all three tested conditions showed a significant increase on day 9. However, a higher concentration of NPs led to a lower increase in the relative total integrated intensity, corrected by the confluence.

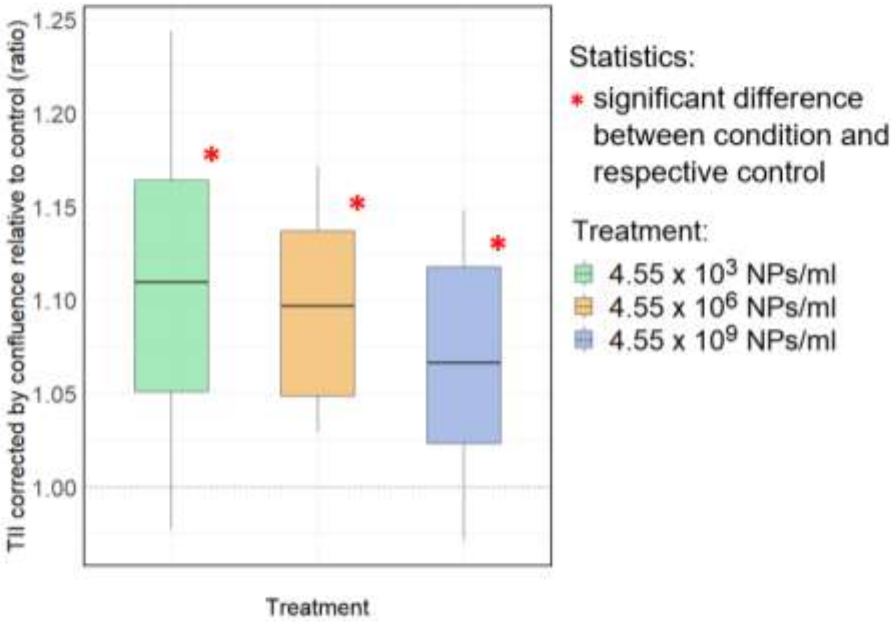

Figure 19. Ratio of the total integrated intensity (TII) corrected by the confluence of cells treated with NPs, and the mean TII corrected by the confluence of their respective controls. The values of the controls are indicated by 100%. Cells were seeded in wells of a 96-well plates (13≤n≤22) and treated for 9 days in accordance with scenario 1, whereafter lipids were stained. When the difference between the untreated condition and the treated condition is statistically significant, a red star is placed next to the boxplot.

5.3.2 Test 2: Time-effect for SBs and NPs in scenario 1

Cells treated with 4.55 x 10^3 NPs/mL, 4.55 x 10^6 NPs/mL, 4.55 x 10^3 SBs/mL or 4.55 x 10^6 SBs/mL, and lipids of respective controls were stained after 2, 5, 7, 9 and 12 days of treatment. In all conditions, cells were not confluent after 2 days of treatment. Full confluence was reached 5 days after treatment, whereupon the confluence stayed around 100% in all conditions.

First, all the solvent controls were considered, as shown in Figure 20, where the total integrated fluorescence intensity corrected by the confluence is presented. On all days except for day 7 and 9, significant differences between different groups were observed. On day two, a significant difference was noticed between the treatments with 0.1 mL ethanol/L and both the treatment with 0.1 mL ethanol/L and 0.1 µL water/L. On day 5, a significant difference was noticed between the untreated condition and the treatment with 0.1 µL ethanol/L. Lastly, on day 12, a difference was noticed between the cells treated with 0.1mL ethanol/L and all three the following conditions: untreated, 0.1 nL water/L and 0.1 µL water/L. The cells treated with the highest concentration of ethanol, which corresponds to the highest concentration of SBs, had a lower lipid content compared to the other conditions.

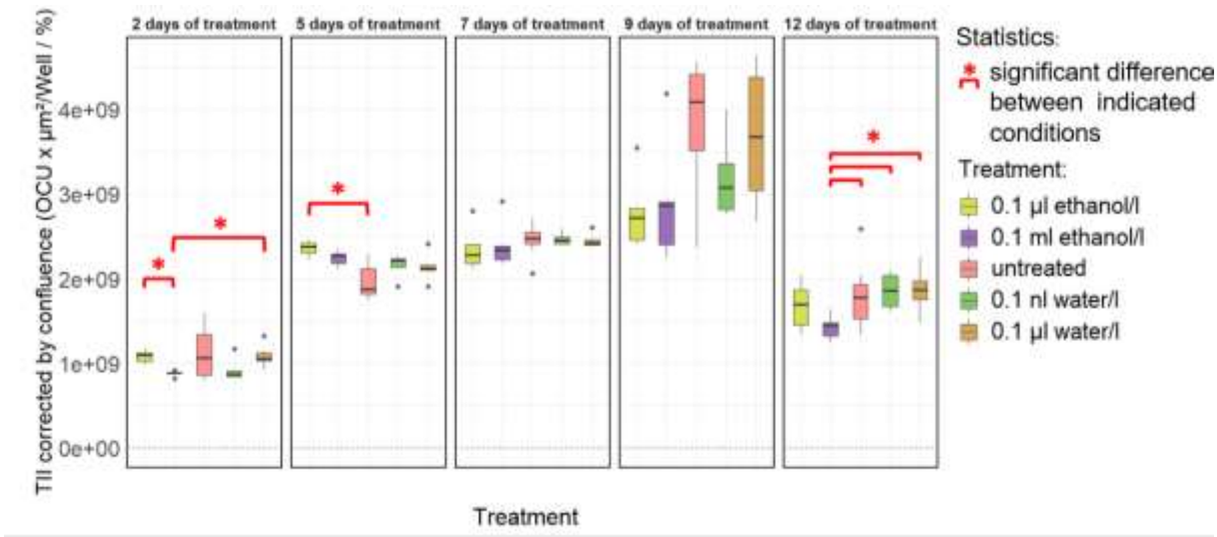

Figure 20. Total integrated intensity (TII) corrected by the confluence, expressed OCU x µm^2/well/%, of ethanol controls, water controls, and untreated conditions after lipid staining, at day 2 ,5, 7, 9 and 12 of the experiment following scenario 1. For the water and ethanol controls, six wells were used, and false results due to blurry images were removed (4≤n≤6). For the untreated condition, 12 wells were incorporated, and again, false results were removed (10≤n≤12). Statistically significant differences between two groups are indicated with a red star.

Figure 21 shows the relative total integrated intensity of the treated cells, corrected by the confluence. A significant difference compared to the control was found in the cells treated with 4.55 x 10^6 NPs/mL on day 5, and in the cells treated with 4.55 x 10^6 SBs/mL on day 12. A trend can be seen in the cells treated with 4.55 x 10^6 NPs/mL, starting with a decrease in lipid uptake at day 5, followed by an increase at days 7, 9 and 12. A similar trend can be seen in the cells treated with a lower concentration of NPs. For the SBs, no clear trend can be seen. Interestingly, in this case, the cells treated with the highest concentration (4.55 x 10^6 SBs/mL) showed a significant increase in lipid content on day twelve. Caution has to be taken, as the solvent control of the cells treated with the highest concentration of SBs influences the lipid uptake of the cells. However, since the data was normalized based on the control, this influence should be eliminated.

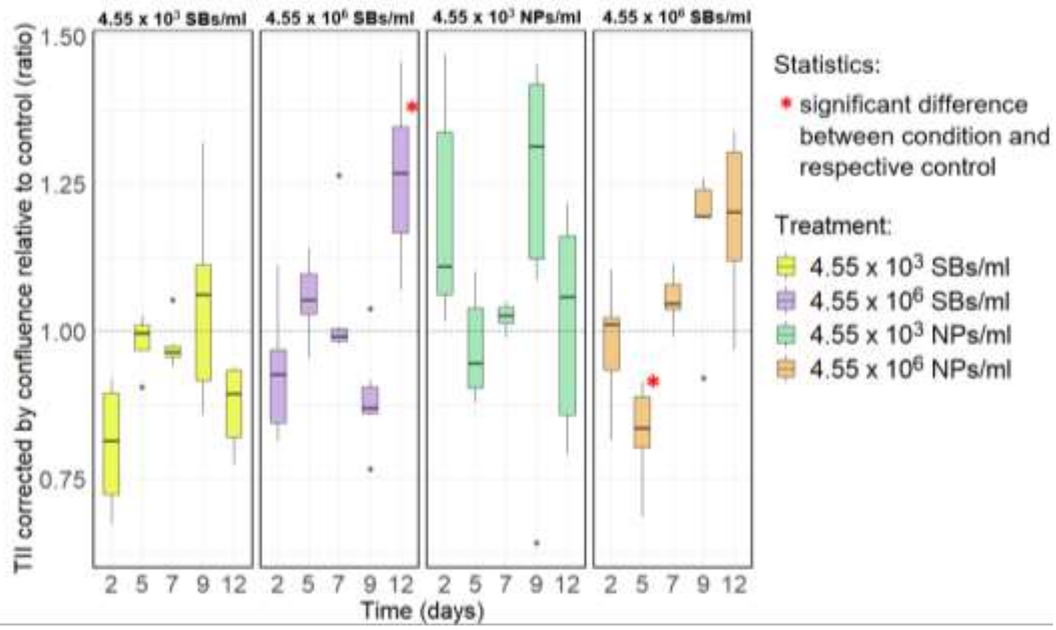

Figure 21. Ratio of the total integrated intensity (TII) corrected by the confluence of cells treated with either SBs or NPs, and the mean TII corrected by the confluence of their respective control over time. The values of the controls are indicated by 100%. Cells were seeded in six wells of a 96-well plate, and treatment was done in accordance with scenario 1. False results due to blurry images were removed (4≤n≤6). When differences between the untreated condition and the treated condition was statistically significant, a red star is placed next to the boxplot.

5.3.3 Test 3: Time-effect for SBs and NPs in Scenario 2

The total integrated intensity of the controls is given in Figure 22. At the first timepoint, after 9 days of treatment, a significant difference between the ethanol controls and the untreated biological replicates was observed. 17 days after treatment, no difference between the ethanol control and the treated condition is noticed. For the third timepoint, again, a significant difference between the two controls is noticed. However, in this case, the ethanol control contains fewer lipids than the untreated condition.

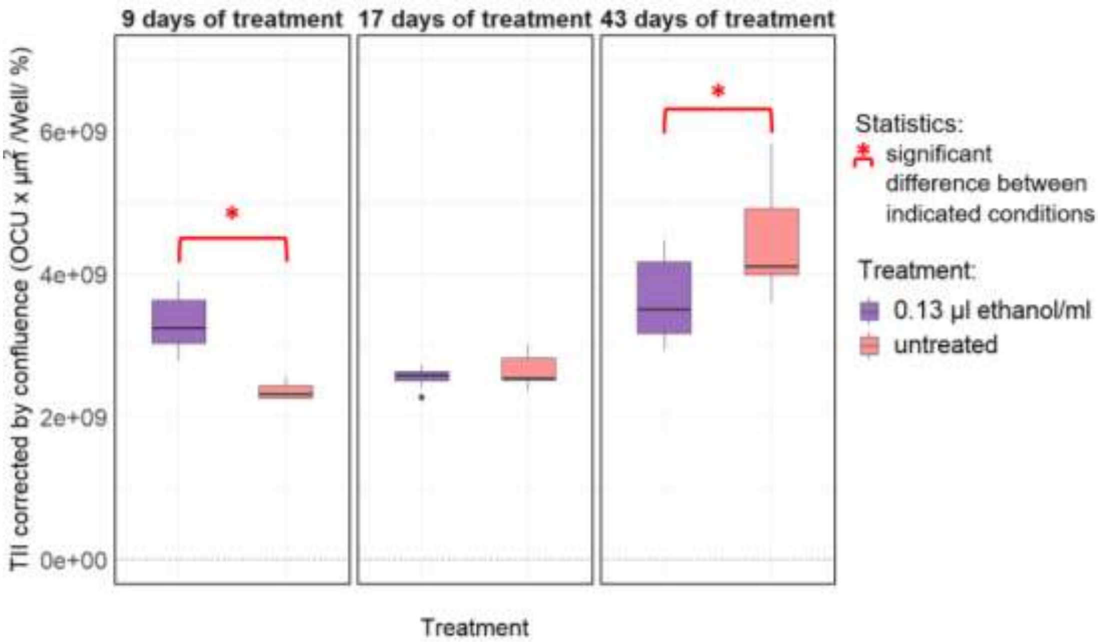

Figure 22. Total integrated intensity corrected by the confluence, expressed in OCU x µm²/well/%, of ethanol control and untreated condition after lipid staining, at day 9, 17 and 43 of the experiment following scenario 2. For each condition, three biological replicates are seeded, each in five wells of a 96-well plate, and shown together in one boxplot. Statistically significant differences between two groups are indicated with a red star.

The total integrated intensity corrected by the confluence relative to the controls is given in Figure 23. After 9 days of treatment, no significant change in lipid content was noticed when treated with SBs compared to the ethanol control. This is in line with the previous experiment, that reported no significant increase in lipid-content after 9 days of treatment with SBs. Both after 17 days and 43 days of treatment, a significant increase in lipid content after SB treatment was measured. For the NP treatment, a significantly elevated lipid content was measured at each timepoint. Additionally, the difference between the lipid content in the treated conditions and their respective controls increases for both the SBs and the NP treatment over time.

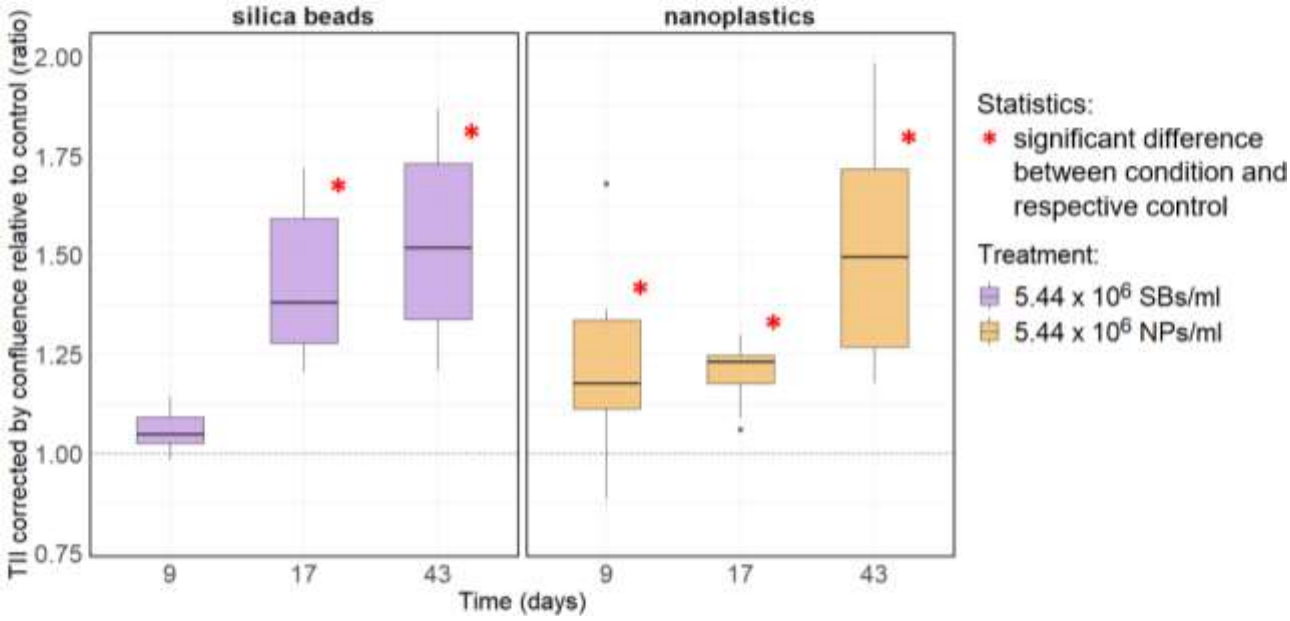

Figure 23. Ratio of total integrated intensity corrected by the confluence of the cells treated with either SBs or NPs, and the mean total integrated intensity corrected by the confluence of their respective control over time. The values of the controls are indicated by 100%. Cells were treated in accordance with scenario 2, and for each condition, three biological replicates were seeded in five wells of 96-well plates and shown together in one boxplot. When a difference between the untreated condition and the treated condition is statistically significant, a red star is placed next to the boxplot.

5.4 Respirometry

Cells were treated as described in scenario 2, and respirometry was performed. Two measurements were performed at each timepoint, one with and one without starvation conditions. The three same timepoints as previously reported are used. Since on day 9 of the experiment, the cells did not react to the inhibitors used in the respirometry without starvation, these results are not discussed in the data analysis. Three biological replicates were plated in seven to eight different wells and in one subset of the wells, the use of lipids was blocked by addition of etomoxir. In the other subset, medium was added instead of etomoxir. Wells that did not respond to the inhibitors were removed from the data analysis. For the statistical analysis, the three biological replicates were taken together, leading to $5 \leq n \leq 13$ for the analysis where etomoxir influenced the parameter (maximal respiration and spare respiratory capacity). For the parameters where etomoxir did not influence the results $15 \leq n \leq 24$. However, it must be noted that in the following conditions, there was one biological replicate for which only one well was maintained: ethanol control after 17 days of treatment in respirometry with starvation conditions, treatment with SBs after 9 days of treatment in respirometry with starvation conditions and treatment with SBs after 43 days of treatment in respirometry with starvation conditions. An overview of the kinetic graphs representing the raw data is given in Appendix 2. The respirometry data was normalized based on confluence data, acquired by the incucyte.

5.4.1 Basal respiration

When considering the controls, shown in Figure 24, it was observed that in starvation conditions, ethanol influenced basal respiration after 9 days of treatment, whereas without starvation, a slight but significant decrease was observed after 43 days of treatment.

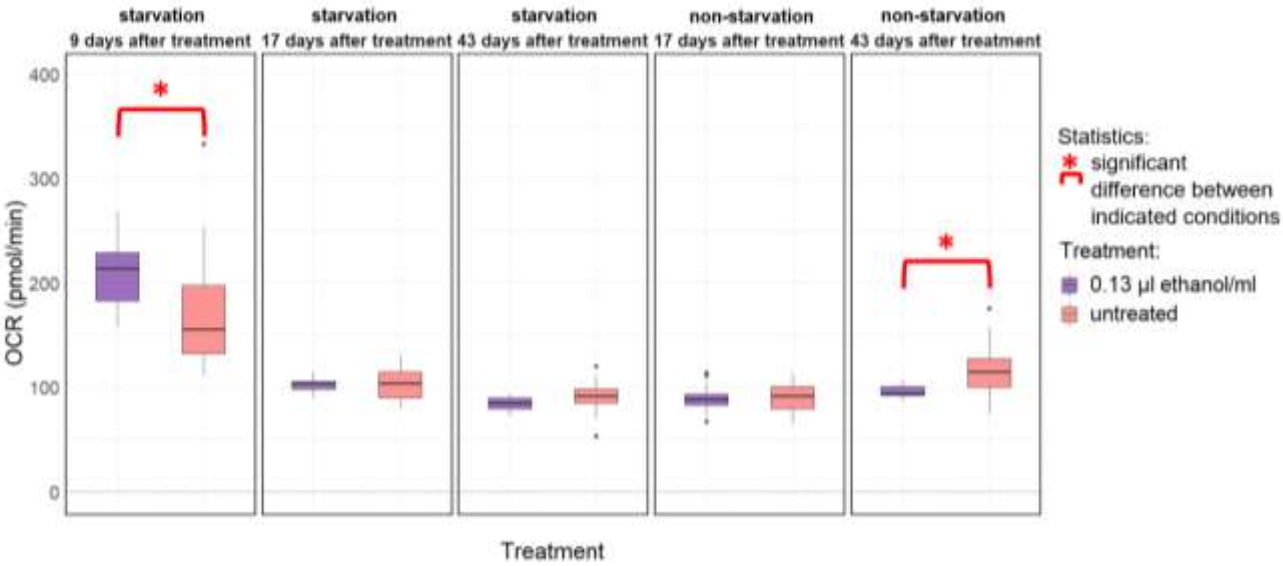

Figure 24. Basal respiration, expressed in oxygen consumption rate (OCR; pmol/min), of ethanol control and untreated condition at days 9, 17 and 43 of the experiment following scenario 2. At day 9, an efflux assay with non-starvation conditions is incorporated. At days 17 and 43, both an efflux assay with starvation and non-starvation conditions is shown. For each condition, three biological replicates are seeded in seven to eight wells and shown together in one boxplot. Statistically significant differences between two groups are indicated with a red star.

The basal respiration corrected by the confluence and relative to their respective controls is given in Figure 25. For the SB treatment, basal respiration was higher in all five efflux assays, and this increase was similar at all time-points. For the NP treatment, basal respiration was also increased. This was significant in all efflux assays, except for the assay with non-starvation conditions after 43 days of treatment. Additionally, it can be noted that the increase in basal respiration due to NPs is the most pronounced after 9 days of treatment. Thereafter, the difference between the NP treated and untreated conditions decreased.

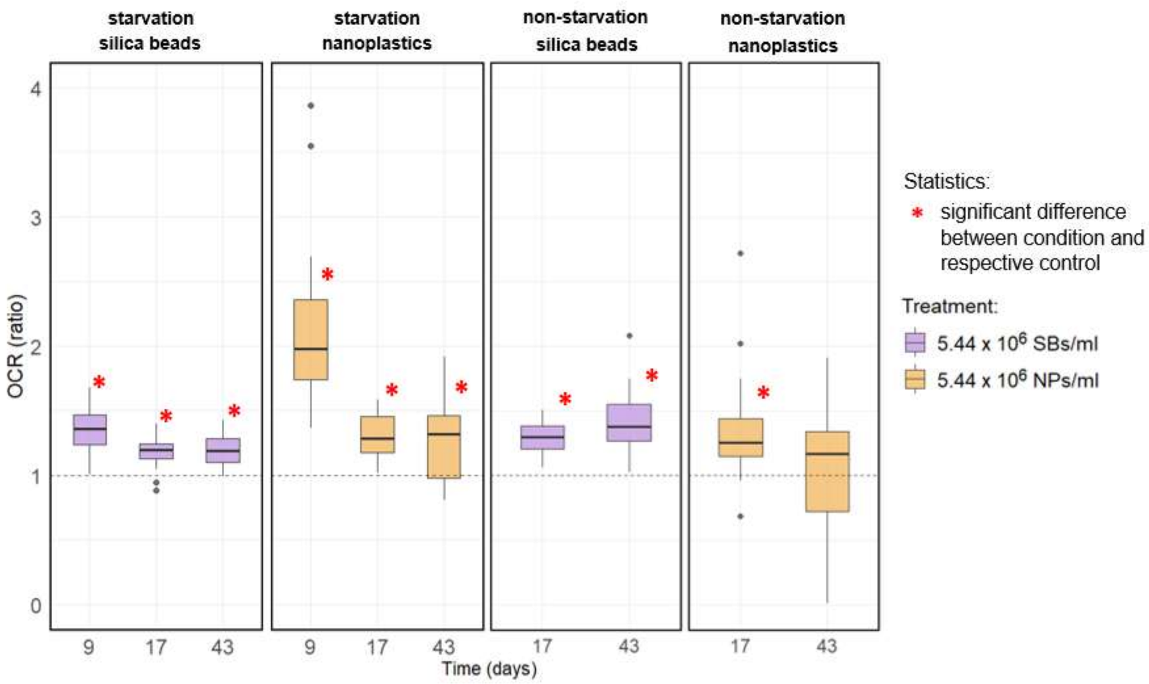

Figure 25. Ratio of basal respiration of the cells treated with either SBs or NPs, and the mean basal respiration of their respective control over time. The values of the controls are indicated by 100%. Cells were treated in accordance with scenario 2, and for each condition, three biological replicates are shown together in one boxplot. At day 9, an efflux assay with non-starvation conditions is incorporated. At day 17 and 43, both an efflux assay with starvation and non-starvation conditions is shown. When difference between the untreated condition and the treated condition was statistically significant, a red star is placed next to the boxplot.

5.4.2 Maximal respiration

When considering maximal respiration of the control samples (Figure 26), it was found that ethanol had a significant effect on the maximal respiration after 9 days and after 43 days of treatment, when using starvation. In addition, etomoxir had no significant influence on the maximal respiration of the controls.

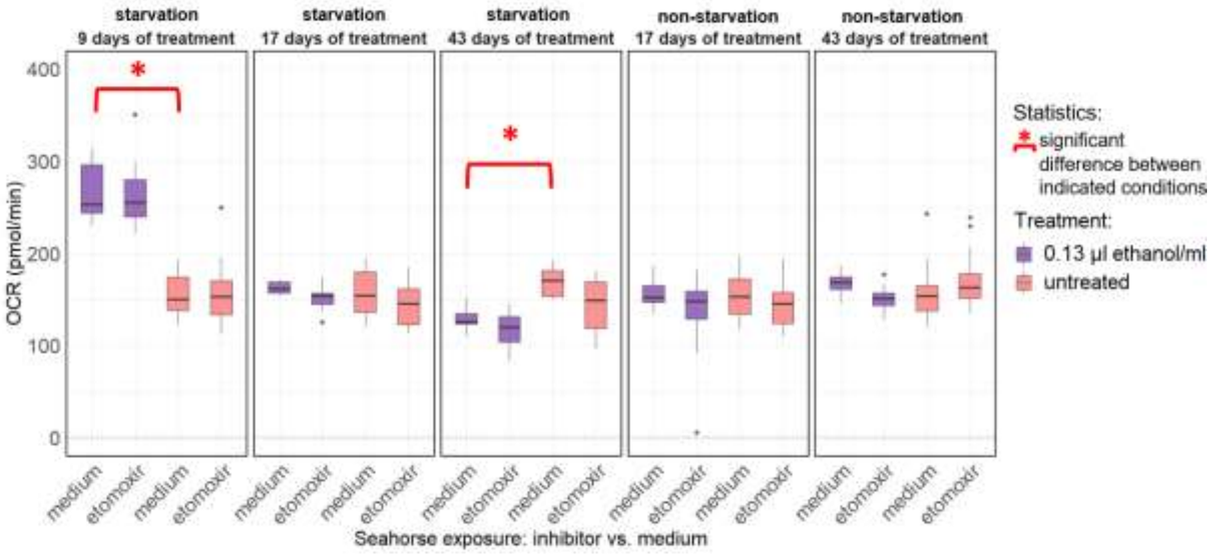

Figure 26. Maximal respiration, expressed in oxygen consumption rate (OCR; pmol/min), of ethanol control and untreated condition, either with or without addition of etomoxir during the respirometry. Cells were treated in accordance with scenario 2 and respirometry was performed at day 9, 17 and 43 of the experiment. At day 9, an efflux assay using non-starvation conditions is incorporated. At day 17 and 43, both an efflux assay with non-starvation and starvation conditions is shown. For each condition, three biological replicates are shown together in one boxplot. To test significant influence of the treatment on the maximal respiration, comparisons are made between the two controls using the data in which no etomoxir was added (medium on the x-axis). In addition, the influence of etomoxir is tested within a specific treatment by testing between the results with and without etomoxir. Significant results are indicated with a red star.

SB treatment showed similar effects at all tested timepoints, i.e. significantly higher maximal respiration compared to the control. Furthermore, maximal respiration was significantly lower when etomoxir is added to non-starvation conditions after 17 days of treatment and to starvation conditions after 43 days of treatment. However, in Figure 27, no decrease between etomoxir addition and medium addition is noticed, indicating that etomoxir influenced both the control and the treated conditions in a similar manner.

A similar result is seen for NP treatment, as the maximal respiration was higher in all conditions at all timepoints. Contrary to the stable maximal respiration after treatment with SBs, relative maximal respiration decreased over treatment time. This was clearly visible in starvation conditions. At last, for NP treatment in starvation conditions, etomoxir significantly decreased the maximal respiratory capacity after 43 days of treatment. Moreover, the relative maximal respiration, given in Figure 27, also showed a lower value when etomoxir was added, suggesting that the maximal respiration is more abundantly affected by etomoxir in the treated conditions, compared to the controls.

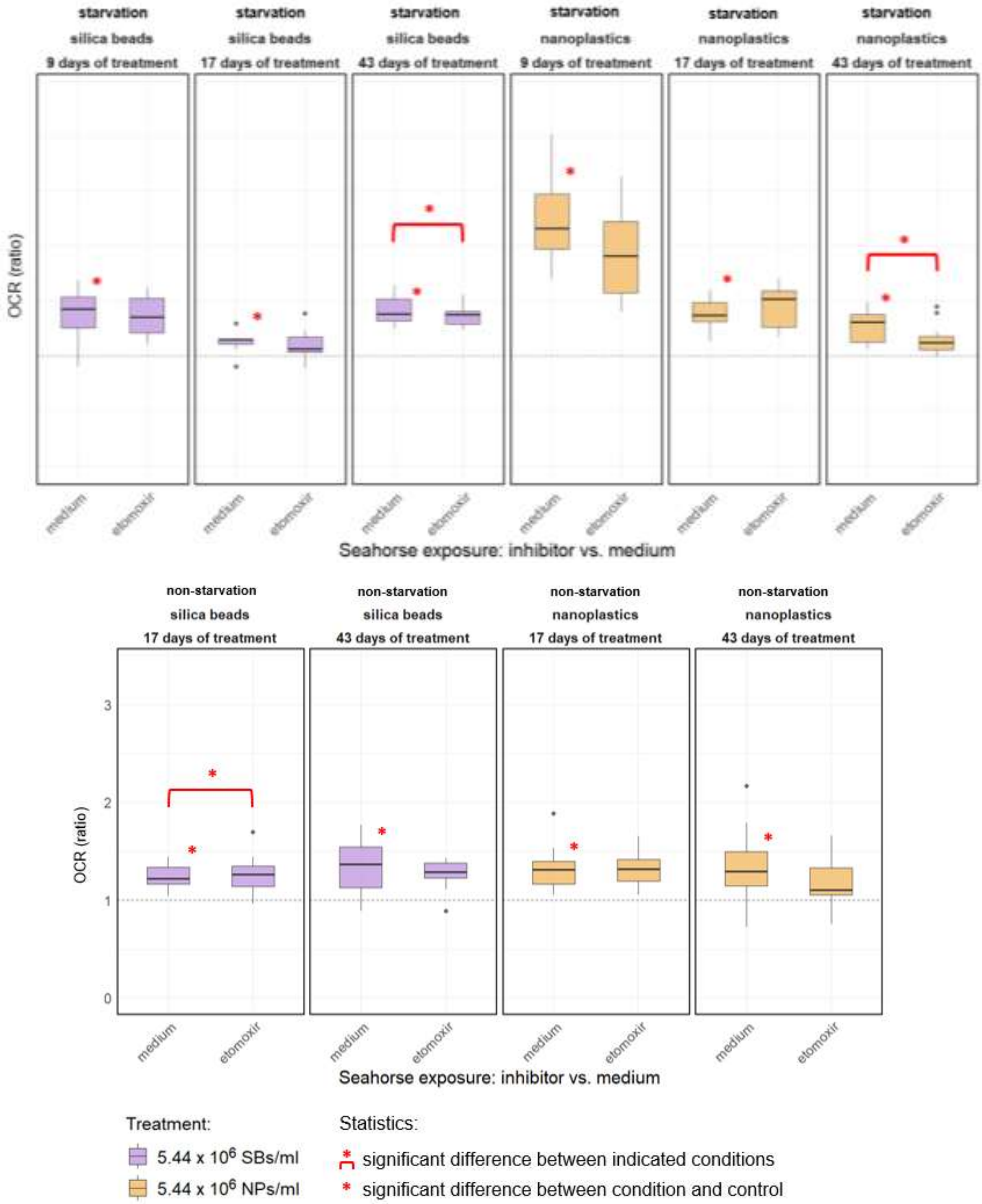

Figure 27. Ratio of maximal respiration of the cells treated with either SBs or NPs, and the mean maximal respiration of their respective controls over time. The values of the controls are indicated by 100%. Cells were treated in accordance with scenario 2, and for each condition, three biological replicates are shown together in one boxplot. At days 9, an efflux assay with non-starvation conditions is incorporated. At days 17 and 43, both an efflux assay with starvation and non-starvation conditions is shown. To test significant influence of the treatment on the maximal respiration, comparisons are made between the treated condition and their respective control. This was done using the data in which no etomoxir was added (medium on the x-axis). In addition, the influence of etomoxir is tested test between the results with and without etomoxir. Significant results are indicated with a red star.

5.4.3 Proton leak

When considering the proton leak (Figure 28), it was observed that only in the non-starvation conditions, 43 days after treatment, a significant difference between the ethanol control and the untreated condition was present. For the other conditions, ethanol had no influence on the proton leak. Furthermore, the proton leak of the controls was remarkably higher after 9 days of treatment, compared to the proton leak at other timepoints.

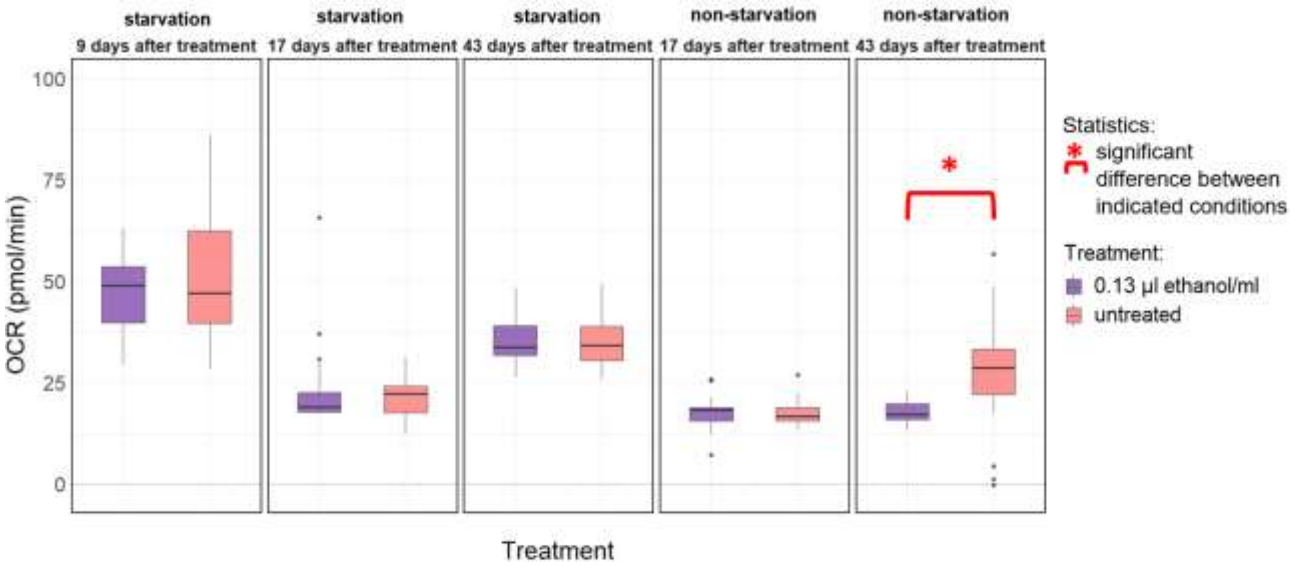

Figure 28. Proton leak, expressed in oxygen consumption rate (OCR; pmol/min), of the ethanol control and untreated condition at days 9, 17 and 43 of the experiment following scenario 2. At days 9, an efflux assay with non-starvation conditions is incorporated. At days 17 and 43, both an efflux assay with non-starvation and starvation conditions are shown. For each condition, three biological replicates are shown together in one boxplot. Statistically significant differences between two groups are indicated with a red star.

When considering particle treatments, a higher proton leak was always observed for the treated condition compared to the control, as shown in Figure 29. For SB treatment, this increase was significant for all conditions and all timepoints, with the exception of the starvation condition, 43 days after treatment. A slightly decreasing trend over time can be seen. For NP treatment, the proton leak is significantly increased at all timepoints and all conditions, except for the non-starvation condition 43 days after treatment. In the starvation conditions, the proton leak was highly affected after 9 days of NP exposure. After 17 days of treatment, the proton leak was decreased to a level closer to the untreated condition. Thereafter, the proton leak remained constant with a similar level in proton leak after 17 days of treatment and after 43 days of treatment.

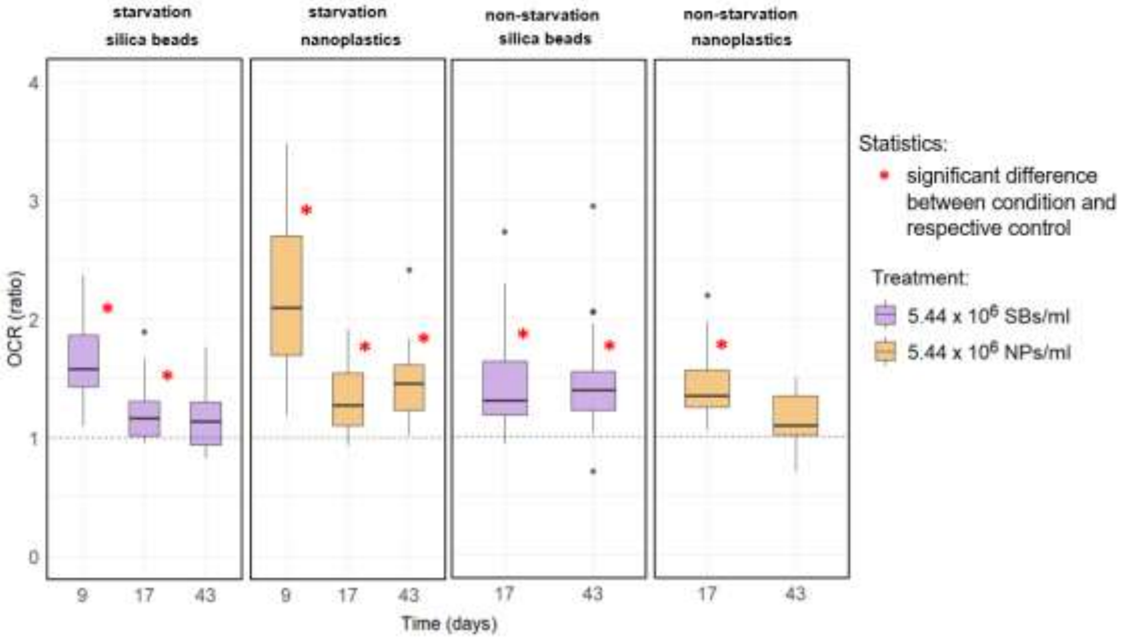

Figure 29. Ratio of proton leak of the cells treated with either SBs or NPs, and the mean proton leak of their respective control over time. The values of the controls are indicated by 100%. Cells were treated in accordance with scenario 2, and for each condition, three biological replicates are shown together in one boxplot. At days 9, an efflux assay with non-starvation conditions is incorporated. At days 17 and 43, both an efflux assay with starvation and non-starvation conditions is shown. When the difference between the untreated condition and the treated condition is statistically significant, a red star is placed next to the boxplot.

5.4.4 Spare respiratory capacity

When considering the control samples, illustrated in Figure 30, a clear difference in spare respiratory capacity between the untreated condition and the ethanol control was seen in the starvation condition after 9 days of treatment. A significant opposite effect was visible after 43 days of treatment. Etomoxir did not significantly influence the spare respiratory capacity of the controls in any condition and at any timepoint.

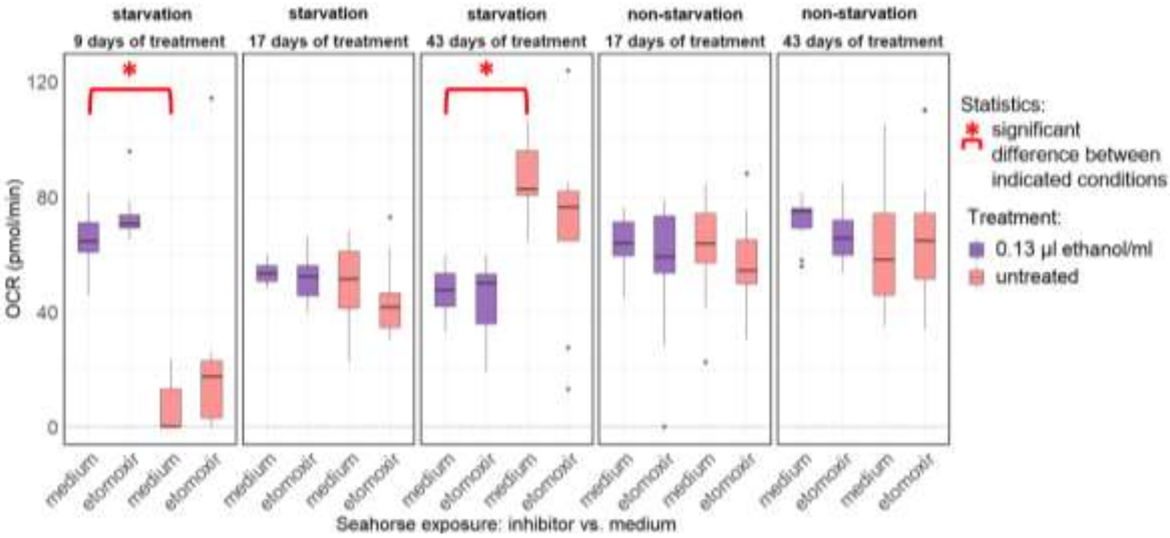

Figure 30. Spare respiratory capacity, expressed in oxygen consumption rate (OCR; pmol/min), of ethanol control and untreated condition, either with or without addition of etomoxir during the respirometry. Cells were treated in accordance with scenario 2 and respirometry was performed at days 9, 17 and 43 of the experiment. At day 9, an efflux assay with non-starvation is incorporated. At days 17 and 43, both an efflux assay with starvation and non-starvation conditions is shown. For each condition, three biological replicates are shown together in one boxplot. To test the significant influence of the treatment on the spare respiratory capacity, comparisons are made between the two controls using the data in which no etomoxir was added (medium on the x-axis). In addition, the influence of etomoxir is tested within a specific treatment by testing between the results with and without etomoxir. Significant results are indicated with a red star.

Figure 31 shows that upon 43 days of SB treatment, a significantly higher spare respiratory capacity compared to the control was observed in starvation conditions. No clear trend in the relative spare respiratory capacity over time was seen. In the respirometry with non-starvation, cells treated with SBs showed a similar spare respiratory capacity as the control. Furthermore, etomoxir addition did not affect the spare respiratory capacity.

After 17 days of NP treatment, the spare respiratory capacity was significantly increased compared to the untreated condition in both starvation and non-starvation conditions. At 43 days after treatment, a significant increase is noticed in starvation conditions. A significantly lower respiratory capacity caused by etomoxir was found in the cells treated for 43 days. Additionally, etomoxir decreased the spare respiratory capacity in a slightly higher extent than for the untreated condition.

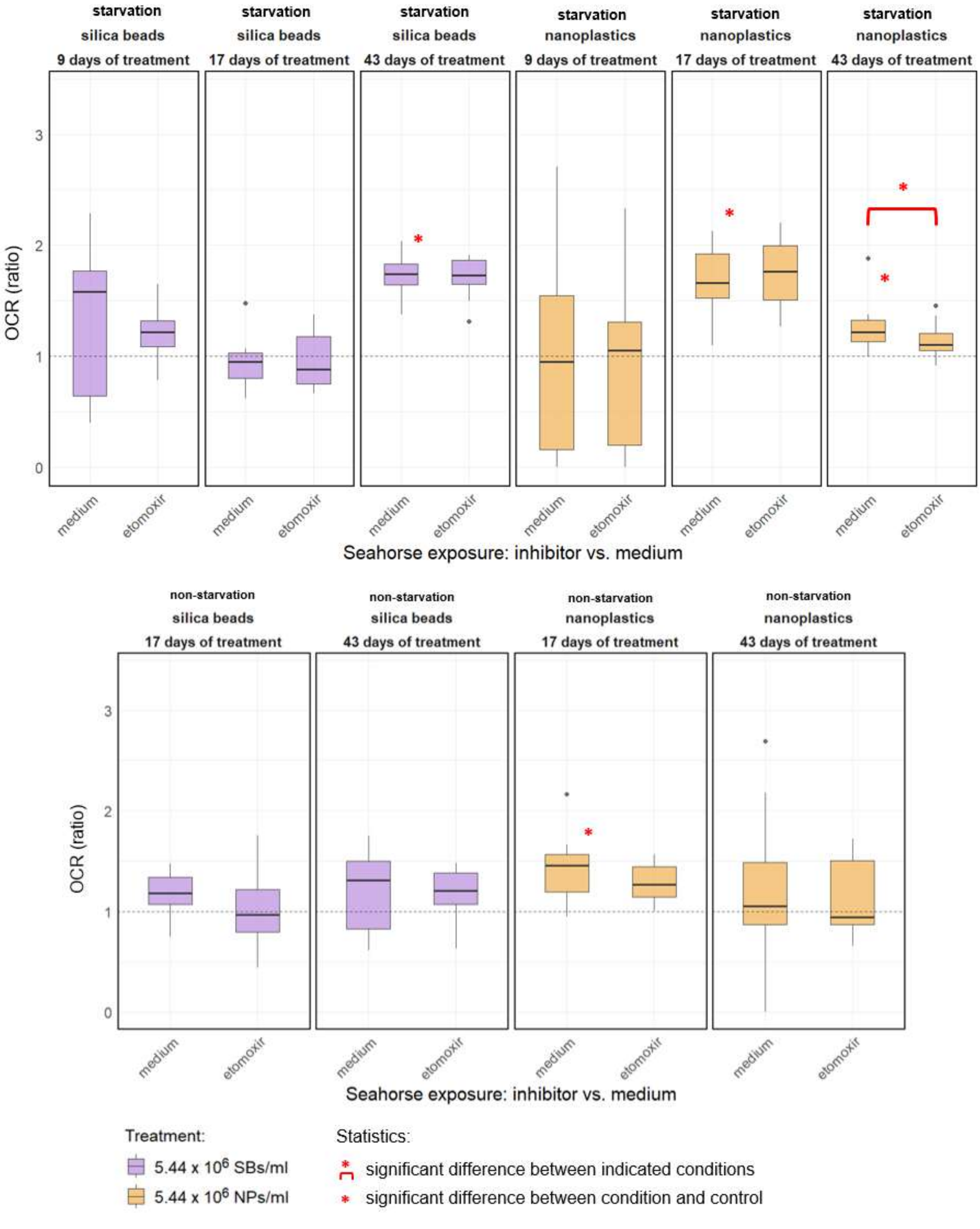

Figure 31. Ratio of spare respiratory capacity of the cells treated with either SBs or NPs, and the mean spare respiratory capacity of their respective control over time. The values of the controls are indicated by 100%. Cells were treated in accordance with scenario 2, and for each condition, three biological replicates are shown together in one boxplot. At days 9, an efflux assay with non-starvation conditions is incorporated. At days 17 and 43, both an efflux assay with starvation and non-starvation conditions is shown. To test the significant influence of the treatment on the maximal respiration, comparisons are made between the treated condition and their respective control. This was done using the data in which no etomoxir was added (medium on the x-axis). In addition, the influence of etomoxir is tested between the results with and without etomoxir. Significant results are indicated with a red star.

5.5 Transcriptomics

Transcriptomics was performed on cells treated as described in scenario 1. When considering the PCA-plot (

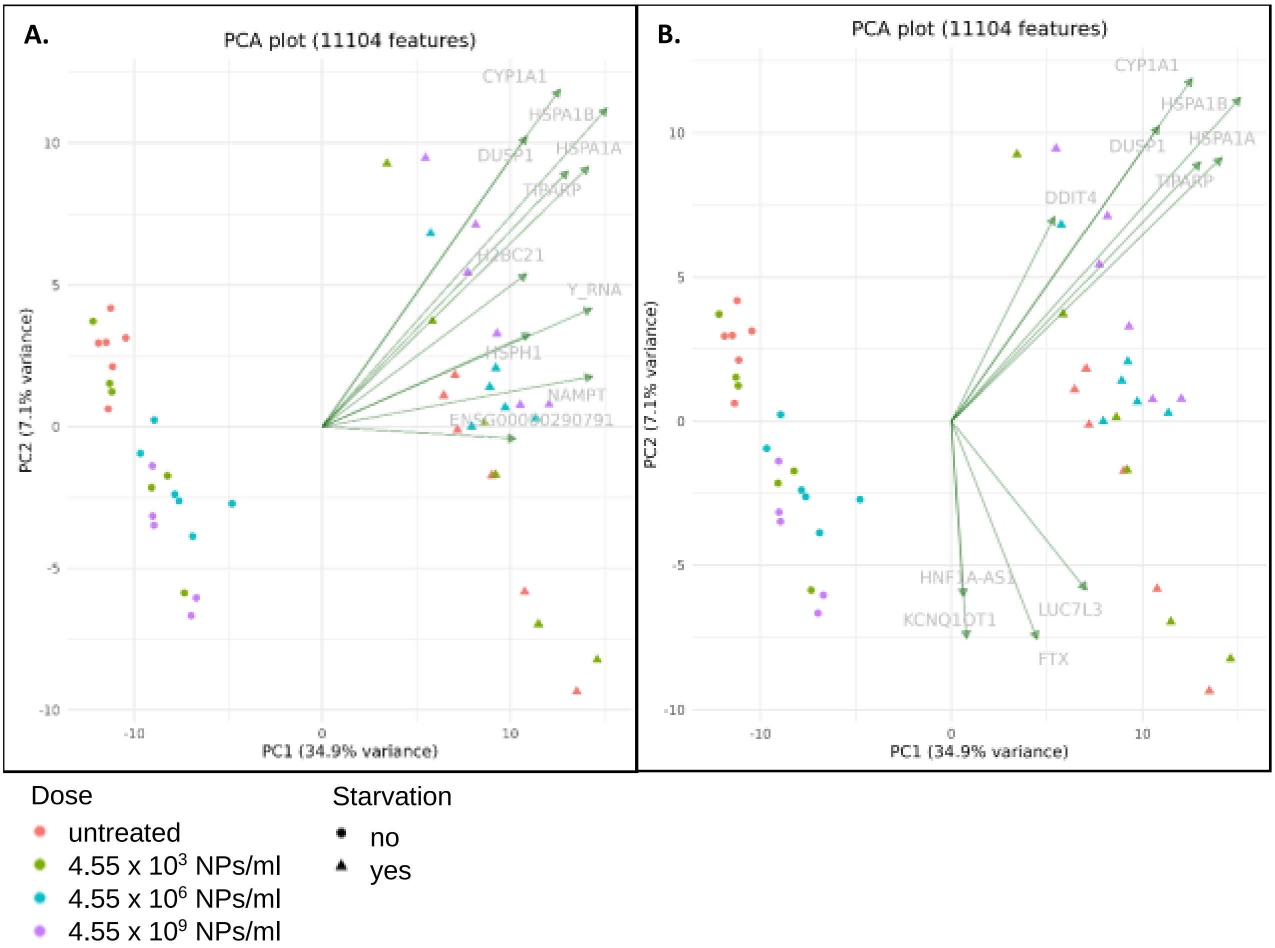

Figure 32) it can be noticed that PC1 is strongly correlated to the starvation. There is strong clustering of cells that had starvation around a value of minus 10, while cells that had no starvation cluster around a value of 10. The second principal component is more related to the dose of treatment. When considering no starvation, the untreated cells have the highest values for PC2. As the concentration of NPs increases, the PC2-values decrease. An opposite effect was visible in the starvation conditions.

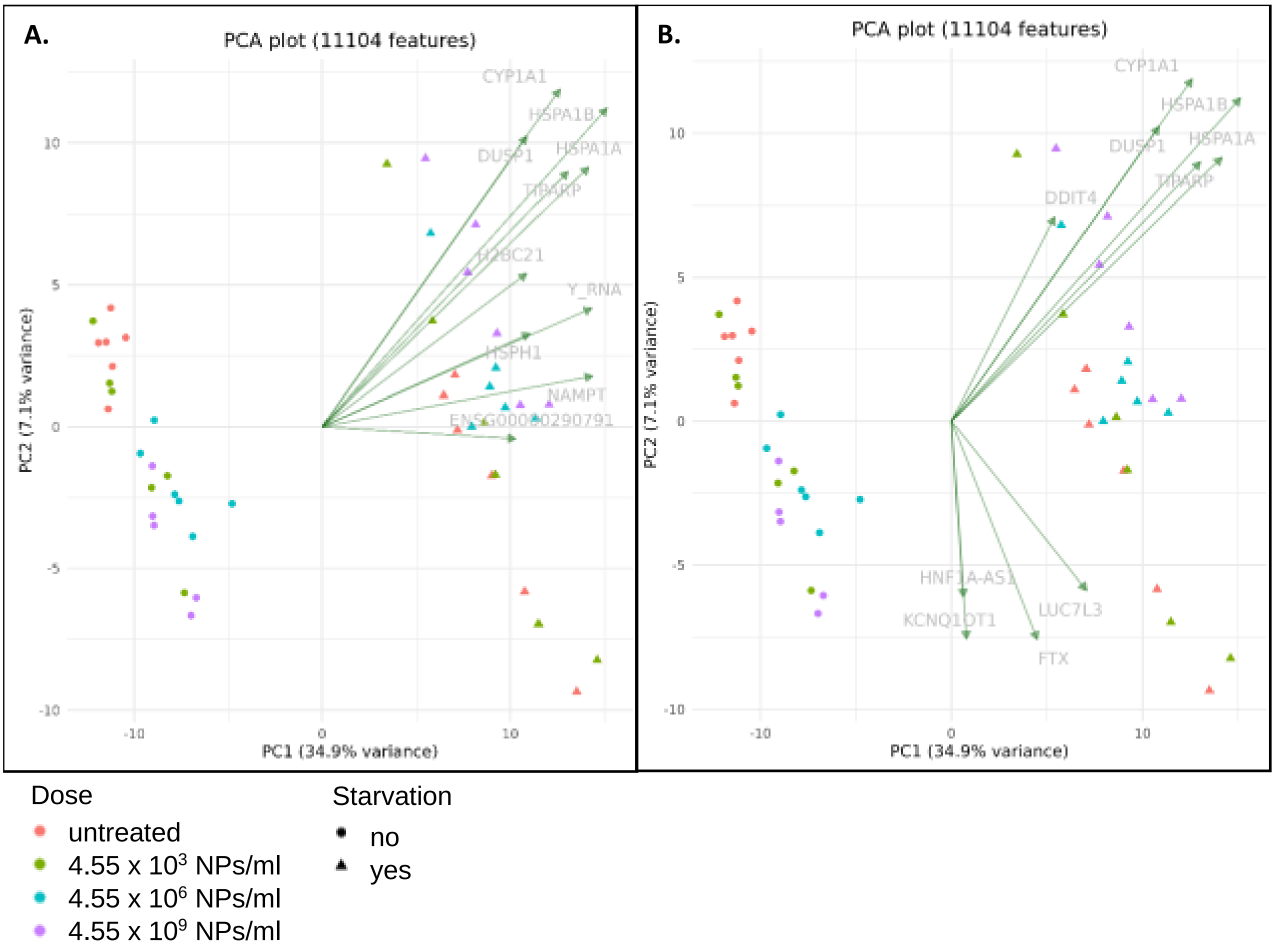

Figure 32. Principal component analysis (PCA) plot of transcriptomics with cells treated with NPs in accordance with scenario 1, and the untreated condition as control. A) Genes that are mainly correlated with PC1 are indicated with green arrows. B) Genes that are mainly correlated with PC2 are indicated with green arrows.

Dose-dependent alterations in gene expression are shown in Table 1. When comparing NP treated conditions with the untreated condition within starvation, no significantly altered gene expression was found for the treatment with 4.55 x 10^3 NPs/mL. When treated with 4.55 x 10^6 NPs/mL, six genes were found to be both statistically and biologically significantly differentially expressed, whereof two genes were downregulated and four genes were upregulated. When treated with 4.55 x 10^9 NPs/mL, 19 genes were significantly differentially expressed, of which 11 genes were downregulated and eight genes were upregulated. For the non-starvation conditions, no significantly altered genes were found when comparing the untreated condition with 4.55 x 10^3 NPs/mL and 4.55 x 10^6 NPs/mL exposure, while two genes are significantly upregulated upon exposure of 4.55 x 10^9 NPs/mL. In both starvation and non-starvation, no significantly altered genes are found between two exposure groups. Moreover, no significantly altered pathway was noted in all comparisons.

Table 1. Dose-effect of MNP exposure on the number of significantly differentially expressed genes and pathways under nutrient-rich and starvation conditions. Cells were treated in accordance with scenario 1 and comparison between each treatment group was performed. DE: differentially expressed; GO: gene ontology; NP3: cells treated with 4.55 x 10^3 NPs/mL; NP6: cells treated with 4.55 x 10^6 NPs/mL; NP9: cells treated with 4.55 x 10^9 NPs/mL.

Comparison	**NP3-blank**	**NP6-blank**	**NP9-blank**	**NP3-NP6**	**NP3-NP9**	**NP6-NP9**
	Non-starvation					
Total DE genes	**0**	**6**	**19**	**0**	**0**	**0**

Upregulated	0	4	8	0	0	0
Downregulated	0	2	11	0	0	0
GO-term enrichment	0	0	0	0	0	0
Pathway enrichment	0	0	0	0	0	0
	starvation					
Total DE genes	**0**	**0**	**2**	**0**	**0**	**0**
Upregulated	0	0	2	0	0	0
Downregulated	0	0	0	0	0	0
GO-term enrichment	0	0	0	0	0	0
Pathway enrichment	0	0	0	0	0	0

To see which genes are correlated with the different NP concentrations within one nutritional condition (either nutrient-rich or starvation medium), a PCA-plot per nutritional condition is given in Figure 33. In the conditions without starvation, untreated cells cluster together, with low values of PC1. Exposure to NPs caused an increase in the value of PC1, with higher concentrations resulting in higher PC1 values.

A similar clustering pattern is observed under starvation conditions. In the untreated condition, data points cluster in the upper-left corner of the graph, characterized by low PC1 values and high PC2 values. Exposure to NPs leads to an increase in the PC1 values and a corresponding decrease in the PC2 values, with higher concentrations resulting in clusters shifting towards the lower-right corner of the graph. The genes that affect the clustering are similar in the starvation and non-starvation conditions.

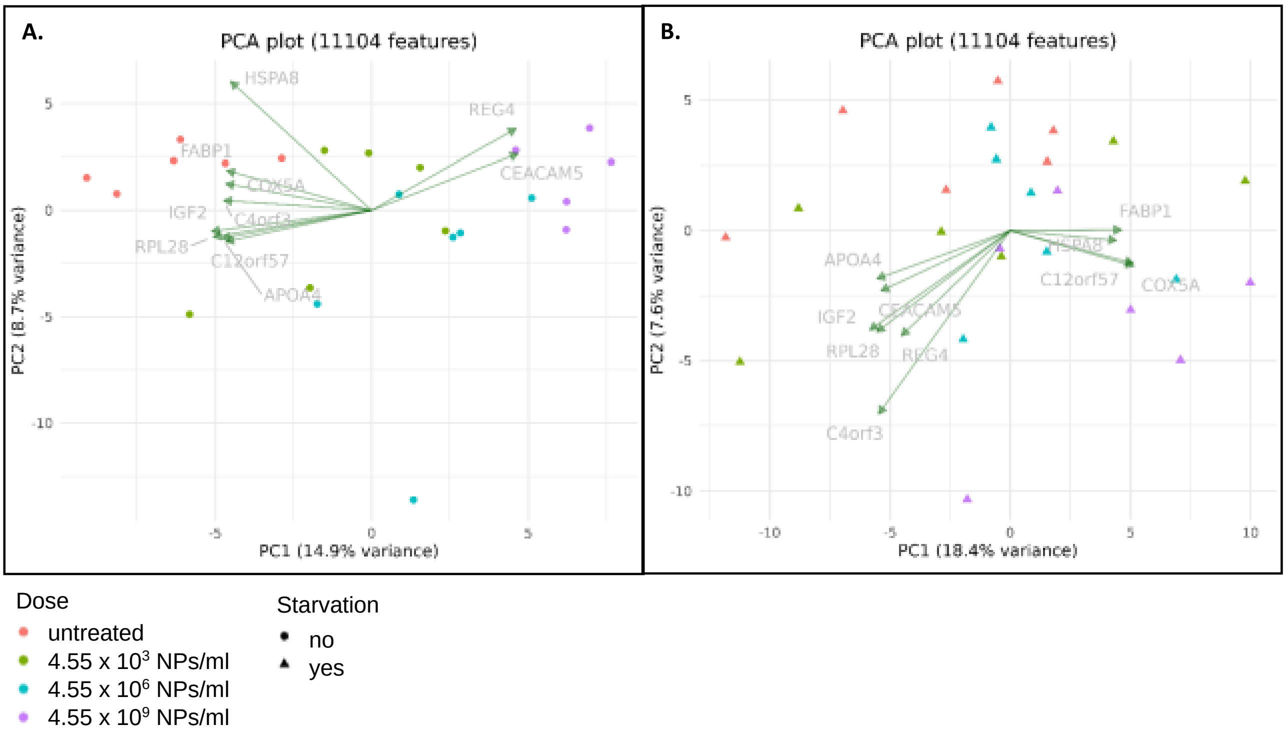

Figure 33. Principal component analysis (PCA) plot of transcriptomics with cells treated with NPs in accordance with scenario 1, and the untreated condition as control. Genes that are correlated with the PCs are indicated with green arrows. A) non-starvation conditions. B) starvation conditions.

When comparing the metabolic adaptability of the cells, i.e. the response when cells are transferred from a nutrient-rich to a starvation medium, it can be seen that this response is largely dependent on the amount of NPs to which they were exposed. Table 2 shows that starvation affected gene expression of 902 genes in the untreated condition, of which 430 were upregulated and 472 were downregulated. Treatment with 4.55 x 10^3 NPs/mL resulted in a smaller shift in gene expression, with only 594 significantly affected genes of which 290 significantly upregulated and 304 significantly downregulated genes. Treatment with 4.55 x 10^6 NPs/mL resulted in a significantly differentially expression of 430 genes of which 238 were upregulated and 192 were downregulated. When cells were treated with 4.55 x 10^9 NPs/mL, starvation led to 557 significantly differentially expressed genes, 344 of which are upregulated and 213 of which are downregulated. Additionally, no KEGG-pathway was found to be significantly altered. However, GO analysis identified 4, 11, 64 and 66 enriched GO terms in the untreated group and those treated with 4.55 x 10^3 NPs/mL, 4.55 x 10^6 NPs/mL and 4.55 x 10^9 NPs/mL, respectively.

Table 2. Starvation effect of MNP exposure on the number of significantly differentially expressed genes and pathways. Cells were treated in accordance with scenario 1 and comparisons between starvation and non-starvation were performed. DE: differentially expressed; GO: gene ontology; NP3: cells treated with 4.55 x 10^3 NPs/mL, NP6: cells treated with 4.55 x 10^6 NPs/mL, NP9: cells treated with 4.55 x 10^9 NPs/mL.

	blank	NP3	NP6	NP9
Total DE genes	**902**	**594**	**430**	**557**
Upregulated	430	290	238	344
Downregulated	472	304	192	213
GO-term enrichment	4	11	64	66
Pathway enrichment	0	0	0	0

When comparing starvation and non-starvation in the untreated condition, only four pathways were significantly altered, as shown in Figure 34. Three of these pathways relate to protein folding, and there were also changes detected in the antimicrobial humoral immune response.

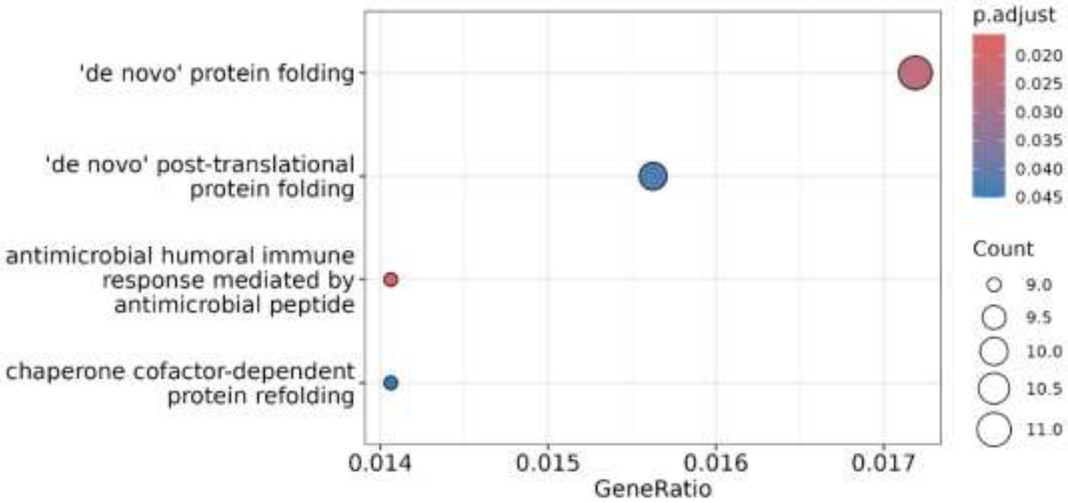

Figure 34. Statistical significantly altered pathways between starvation and non-starvation when cells were untreated in accordance with scenario 1. P.adjust indicates the statistical significance of the pathway, while count indicates the biological relevance. The GeneRatio is defined as the ratio of input genes annotated to a specific GO term relative to the total number of input genes.

Figure 35, illustrating the effects of starvation upon treatment with 4.55 x 10^3 NPs/mL, demonstrates the upregulation of pathways associated with protein folding. Furthermore, it indicates an increase in several pathways related to immune responses, as well as alterations in a pathway involved in cell development.

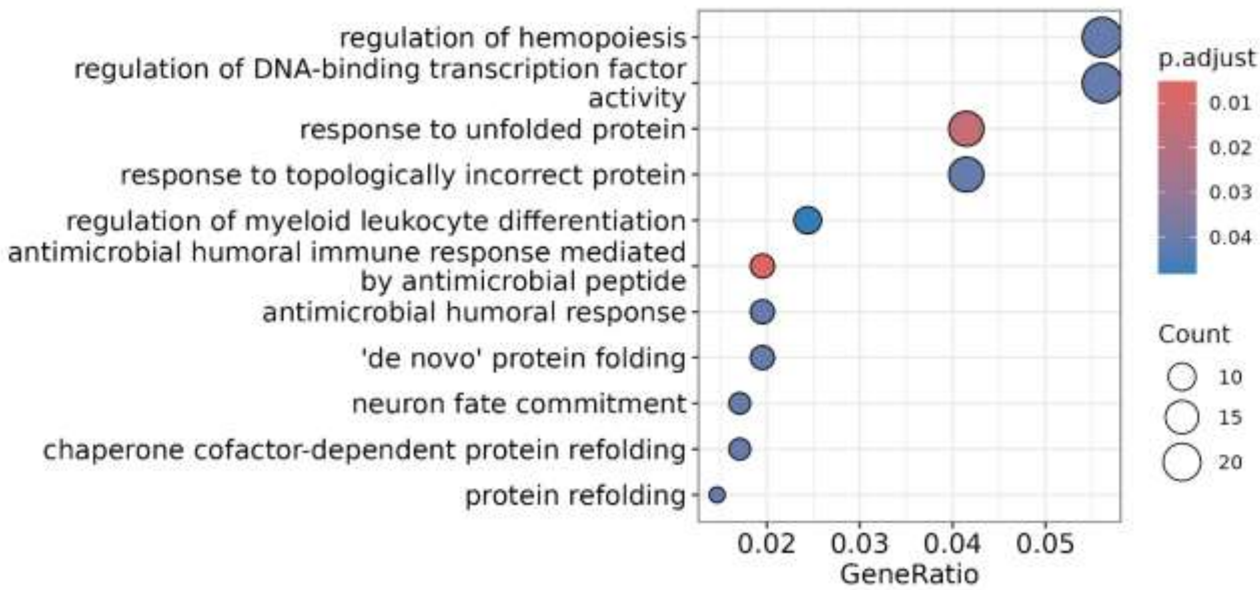

Figure 35. Statistical significantly altered pathways between starvation and non-starvation when cells were treated with 4.55 x 10^3 NPs/mL in accordance with scenario 1. P.adjust indicates the statistical significance of the pathway, while count indicates the biological relevance. The GeneRatio is defined as the ratio of input genes annotated to a specific GO term relative to the total number of input genes.

In cells, treated with 4.55 x 10^6 NPs/mL, starvation altered significantly more pathways compared to the treatment with a lower concentration. While pathways involved in protein folding were still strongly altered, as visible in Figure 36, immune responses became more important. Several inflammatory pathways, including cellular response to cytokine stimulus, reactions to chemokines and glucocorticoids were significantly upregulated. Developmental pathways and pathways involved in responses to stimuli also played a significant role.

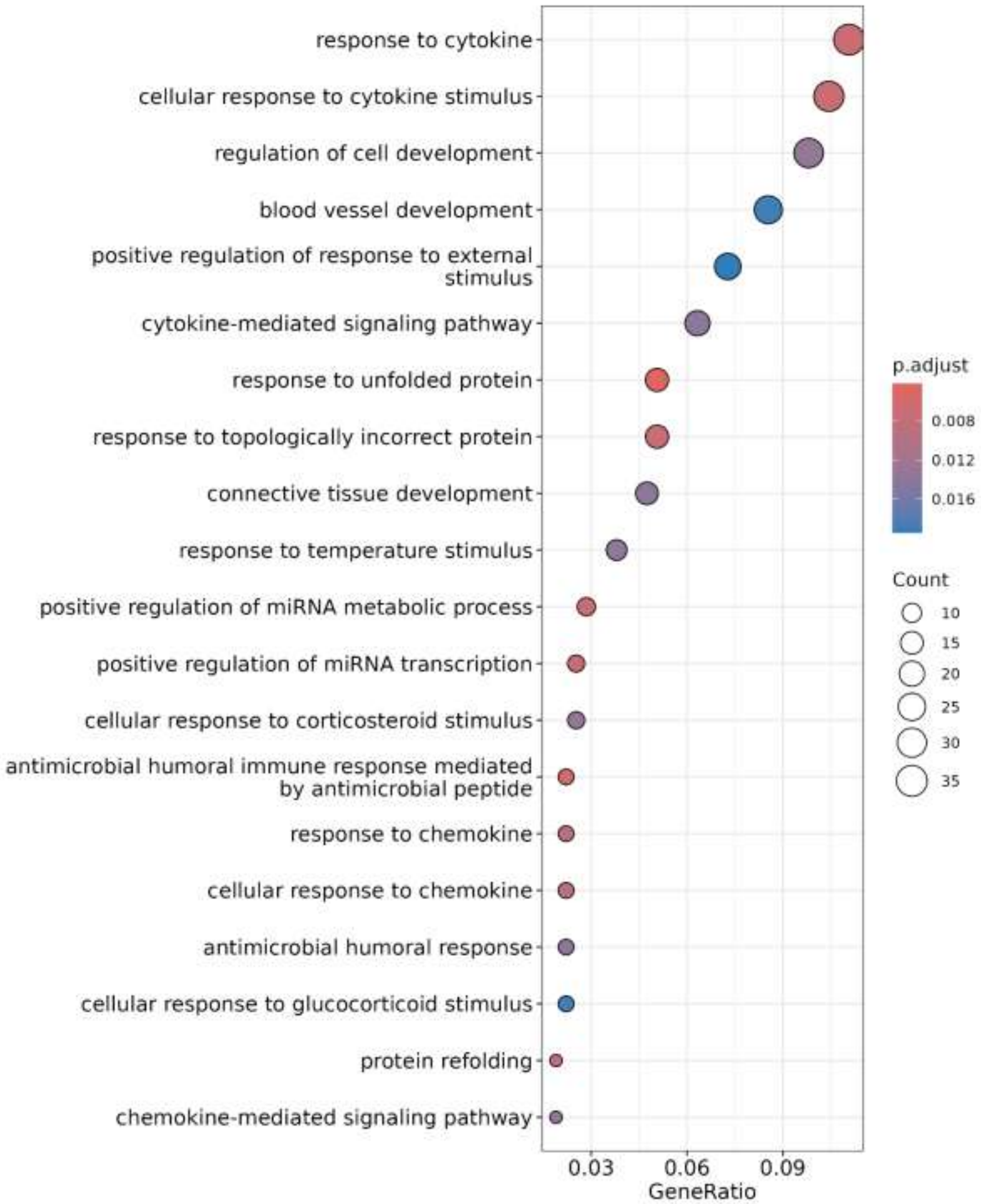

Figure 36. Statistical significantly altered pathways between starvation and non-starvation when cells were treated with 4.55 x 10^6 NPs/mL, in accordance with scenario 1. P.adjust indicates the statistical significance of the pathway, while count indicates the biological relevance. The GeneRatio is defined as the ratio of input genes annotated to a specific GO term relative to the total number of input genes.

Starvation upon treatment with 4.55 x 10^9 NPs/mL led to a similar amount of differentially expressed pathways compared to starvation upon treatment with 4.55 x 10^6 NPs/mL (Figure 37). However, the role of the pathways involved in protein folding was decreased, while altered morphogenesis played a more important role. Furthermore, immune responses, developmental pathways, responses to lipids, negative regulation of cell population proliferation, regulation of cell adhesion and branching involved in blood-vessel morphogenesis were significantly altered.

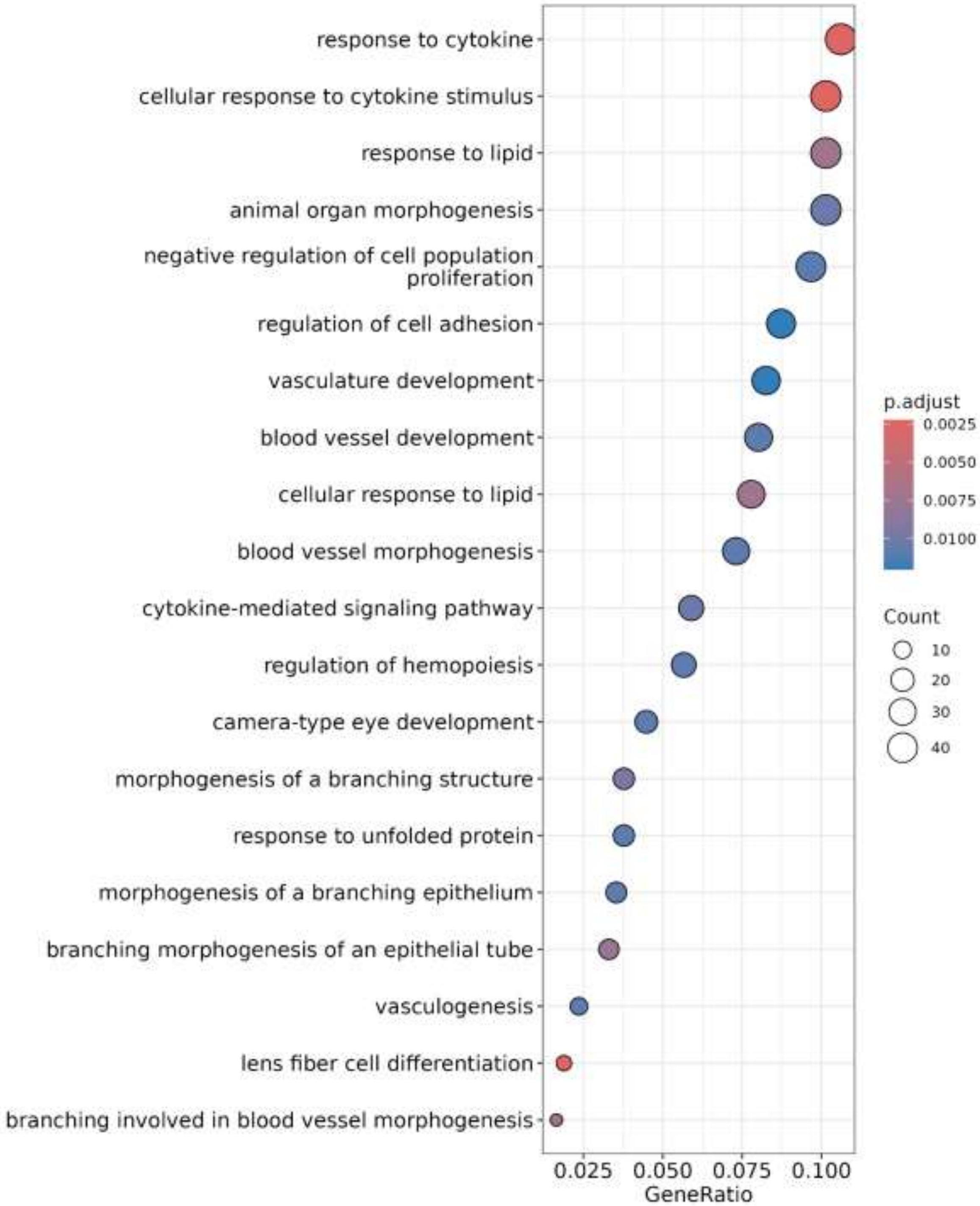

Figure 37. Statistical significant altered pathways between starvation and non-starvation when cells were treated with 4.55 x 10^9 NPs/mL in accordance with scenario 1. P.adjust indicates the statistical significance of the pathway, while count indicates the biological relevance. The GeneRatio is defined as the ratio of input genes annotated to a specific GO term relative to the total number of input genes.

6 DISCUSSION

NPs are widely present in our surrounding environment, creating concern about regular exposure and potential adverse effects on human health. In this research, Caco-2 cells were subjected to a long-term exposure to NPs and SBs. The study demonstrated that (i) both silica particles and NPs can disrupt cellular lipid metabolism. While the observed effects were not directly cytotoxic to the cells, (ii) cellular metabolism was affected. (iii) NP and SB treatment led to a lower cellular resilience as stress from either trypsinization or starvation caused different reactions in treated cells compared to the untreated cells. (iv) Higher dosages led to higher toxicity. (v) Finally, fundamental cellular functions such as respiration and growth were less affected after prolonged exposure, compared to shorter periods of treatment. This indicates that cells can adapt to the presence of SBs and NPs.

Concentrations used in this research ranged from 4.55 x 10^3 NPs/mL to 4.55 x 10^9 NPs/mL. These concentrations notably exceed the estimated ingestion range of MNPs per person, which was found to be between 11,845 and 193,200 particles/year in a study by Senathirajah et al. (2021). However, it is important to note that this study only accounted for drinking water, salt, beer and shellfish, and accurate measurement of the amount of MNPs in these items is not yet accomplished. Mortensen et al. (2021) reviewed the available information about MNP concentrations in drinking water and found a wide range of measured MNP concentrations between 11 MPs/mL (5-50 µm) and 1.1 x 10^8 MNPs/mL (1-10 µm). Additionally, a study from Oliveri Conti et al. (2020) noted concentrations up to 233,000 particle MPs/g in apples, aligning with the concentrations used in this study. Moreover, it is reported that the mean concentration of plastic particles detected in human blood was 1.6 µg/mL, which equals to approximately 7.245 × 10^4 particles/mL if 5 µm PS particles, the mean diameter of the measurement interval, was implemented in the conversion (Leslie et al., 2022). Lastly, MNPs tend to accumulate in certain organs, resulting in higher concentrations of MNPs within these tissues. Therefore, doses used in this study are thought to be as relevant as possible based on current knowledge.

To our current knowledge, no studies are available that measure the uptake rate of silica beads. However, since synthetic amorphous silica is commonly employed as a food additive to improve the taste and texture, research was performed investigating its uptake rate. Due to limited information on the absorption of nanosilica by the gastrointestinal tract, Dekkers et al. (2011) considered two scenarios in his study: one where silica is absorbed in its dissolved form, and another where nanosilica particles are absorbed directly. They examined the silica concentration in various food products, including lasagne, noodles and coffee creamers, and estimated an uptake of 7 x 10^{12} nanoparticles/day using the second uptake scenario. This concentration surpasses that of MNPs and exceeds the concentrations employed in this study. However, it is unknown how much of this silica will be dissolved, making this concentration an overestimation.

6.1 Nanoparticle exposure disrupts cellular lipid metabolism

It can be suggested that exposure to NPs decreases the lipid content after 5 days of exposure, whereafter the lipid content strongly increases, surpassing the normal lipid-content of a cell. This pattern was observed in a repeated dose treatment of Caco-2 cells with 4.55 x 10^3 NPs/mL and 4.55 x 10^6 NPs/mL without subculturing. Furthermore, a similar experiment demonstrated an increased lipid content after 9 days of treatment with 4.55 x 10^3 NPs/mL, 4.55 x 10^6 NPs/mL and 4.55 x 10^9 NPs/mL. In parallel, the results of the lipid staining after long-term repeated dose exposure with subculturing revealed an increase in lipid-content after 9, 17 and 43 days of treatment. Since most studies incorporate acute (24h) and chronic (longer than 40 days) exposure-times, there are, to our current knowledge, no other studies available that measures the effects in lipid accumulation upon NP exposure over time. Cheng et al. (2022) exposed liver organoids, generated from human pluripotent stem cells to 1 µm PS MPs for 48 hours at a dosage ranging from 4.5 x 10^5 particles/mL to 4.5 x 10^7 NPs/mL. In contrast to our results, they found lipid accumulation after these 2 days of exposure, together with increased CD36, FASN and SCD1 expression and decreased CPT-1a expression. The research by S. J. Kim et al. (2021) administered a chronic set-up, and confirms an increased lipid content. They observed a general rise in the expression of SFAs and MUFAs after 1.5 months of exposure to PS-NPs at a concentration of 1.44 x 10^9 particles/mL in Caco-2 cells. A significant advantage of their study is the use of lipidomics, allowing them to test not only the increase in lipid content but also the composition of the lipids. They found significant differences in levels of (Z)-9-hexadecenoic acid (C16:1), (E)-13-octadecenoic acid (C18:1), and (all-Z)-4,7,10,13,16,19-eicosapentaenoic acid (C20:5). However, contrary to our results, this increase in lipid content was found along with elevated expression of SREBP, indicating that SREBP was the main regulator of the lipid increase in their experiment. Future research should include a measurement of the lipid composition using the same experimental setup as in our study. This would allow for a more comprehensive comparison of lipid profiles between different studies, aiding in the identification of common patterns and potential regulatory pathways involved in lipid metabolism following nanoparticle exposure.

For the SBs, no consistent trend is visible in the results of the lipid staining upon 12-days repeated dose NP exposure without subculturing. However, the results of the lipid staining, using cells with subculturing, revealed an increase in lipid content after 17 and 43 days of treatment. Results at day 9 were also insignificant in this experiment. An increased lipid content is in accordance with the research of Duan et al. (2018) who noted lipid accumulation in animal models and liver cells exposed to SBs, in concentrations ranging from 3.8 x 10^{10} to 1.5 x 10^{11} silica particles/mL. The inconsistent results after a shorter period of exposure can be explained by the presence of ethanol in the treatment medium. Ethanol is known to influence lipid metabolism (You & Arteel, 2019). The ethanol control also shows significantly altered lipid accumulation compared to the controls and untreated condition. It is possible that, after an exposure of nine days, the ethanol affects the cellular lipid metabolism in such an extent that the effect of SBs is masked. This may also explain why there is no clear trend visible in the test without subculturing.

The respirometry in starvation conditions revealed a decrease in the maximal respiratory capacity upon introduction of etomoxir in Caco-2 cells exposed NPs for 43 days. A decrease is also noticeable in the controls, however this decrease was less pronounced. As etomoxir blocks the lipid transport to the mitochondria, the lower maximal respiration suggests that more lipids are used in ATP-linked respiration in the treated conditions, compared to their respective controls upon 43 days of exposure to NPs. This indicates that upon 43 days of treatment, cells under starvation start to use their lipid-reserve as energy source. In contrast to the lipid use, which only increases after 43 days of treatment, the lipid accumulation is already visible after 9 days of treatment. This suggests that the cell starts to accumulate lipids upon nanoparticle exposure. These lipids will accumulate and only after a longer exposure time, a shift towards the use of lipids in the cellular energy metabolism is noticed.

At last, the sequencing data showed alterations in lipid metabolism upon MNP exposure. When taking all the conditions (starvation and non-starvation in the untreated condition and upon exposure with 4.55 x 10^3 NPs/mL, 4.55 x 10^6 NPs/mL and 4.55 x 10^9 NPs/mL) into account, clustering was mainly seen between starvation conditions and non-starvation conditions. The mRNA transcripts involved in the clustering encoded for several heat shock proteins (HSPA1, HSPA2, HSPH1) and DUSP1, which were mainly involved in stress responses. Additionally, also expression of genes related to cellular metabolism, including CYP1A1 and

TIPARP played a role in the cluster formation. This indicates that starvation itself led to cellular stress and altered the cellular energy metabolism. When differences within one nutritional condition are looked into, the PCA leads to clustering of the different treatment conditions. This clustering is driven by several mRNA transcripts under which two encode for proteins that play an important role in lipid metabolism, namely FABP1 and APOA4. Next to regulation of lipid uptake, as described in 2.3, FABP1 also plays a role in basolateral lipid secretion in enterocytes (Rodriguez Sawicki et al., 2017). On the other hand, APOA4 is thought to play a role in lipid absorption and is closely tied to the production of fatty acid rich chylomicrons, which are large triglyceride-rich lipoproteins produced in enterocytes from dietary lipids (F. Wang et al., 2015). Since both APOA4 and FABP are related to lipid transport in the enterocytes, these results suggest that MNP exposure disrupts lipid transport in these cells. Previous findings which highlights the disruptions of the ER and lysozymes, as discussed in section 2.2, supports these findings, since ER and lysosymes are known to play crucial roles in lipid trafficking pathways (Henne, 2019). In conclusion, the results of the gene expression indicate that lipid metabolism is indeed affected by NP exposure. However, the data is not indicative for which regulators might be involved in the cellular lipid accumulation.

Similar as in obesity, MNP exposure affected cellular pathways involved in lipid metabolism and lipid accumulation, and these pathways might be closely linked to inflammation as described before (see section 2.4.). In parallel, PPAR and SREBP, which may regulate this lipid accumulation and inflammation, are associated with obesity pathophysiology (Shimano, 2009; Stienstra et al., 2007). Specific outcomes of altered lipid metabolism and lipid accumulation are dependent on the affected cell type. Therefore, it is of major importance that future research investigates similar effects, using different cell-types. A shift in intestinal epithelial lipid metabolism is indicative for inflammatory bowel disease (Boldyreva et al., 2021). Hepatic lipid accumulation is the key factor in the development of non-alcoholic fatty liver disease, while lipid accumulation in muscle cells plays a crucial role in insulin resistance (Morales et al., 2017). All these phenotypes can be linked to obesity. This all together leads us back to the obesogen hypothesis, which posits that MNPs may contribute to increasing rates of obesity (Kannan & Vimalkumar, 2021). However, they stated that it are mainly the chemical factors that induce the obesogenic effect. In contrast, our result show similar increased lipid content upon SB and NP treatment, suggesting that the obesogen effect is not only induced by the leaches, but also by the physical presence of the particles.

6.2 Nanoparticle exposure leads to metabolic shift

In long-term exposure with subculturing, cell mortality stayed low throughout the full experiment, indicating no direct cytotoxic effect of MNPs. Additionally, no effect of the treatment on the cumulative cell production was noticed. Negligible decrease in cell viability is also noticed by S. J. Kim et al. (2021). However, this is contradicted by the research of Visalli et al. (2021), who noticed an increased mortality of up to 25% after 48 days of exposure to a similar concentration of NPs as used in our research. Moreover, Cheng et al. (2022) exposed liver organoids, generated from human pluripotent stem cells to 1 µm PS MPs for 48 hours at a dosage ranging from 4.5 x 10^5 particles/mL to 4.5 x 10^7 NPs/mL and found a decreased size in organoids, indicating a cytotoxic effect. In conclusion, low mortality in our research indicate that no acute effect was induced by MNPs, however, different researchers have reported varying and sometimes contradictory results, highlighting the ambivalence in the findings.

Despites the limited cytotoxicity of the MNPs, the results of the respirometry show elevated OCR upon exposure of both the SBs and NPs, indicating an elevated cellular metabolism due to nanoparticle exposure. Similar reactions due to SBs exposure and NP exposure were found. Increased basal respiration, proton leak and spare respiratory capacity is also found by Halimu et al. (2022), who treated A549 cells with 20 nm and

50 nm PS-NPs for 24 hours with relatively high dosage (40 µg/mL). Contrary, Bonanomi et al. (2022) exposed fibroblasts to 0.5 µm and 2 µm PS MNPs at low dose in both acute (48 hour) and subchronic (28 days) setups. They observed a decrease in basal respiration, along with an increased glycolysis, indicating a shift from mitochondrial respiration towards glycolysis. This effect was present in both acute and chronic treatments, but was more pronounced after longer exposure.

6.3 Nanoparticle exposure lowers resilience of cells

A discrepancy in the results describing the cell growth is noticed. Growth was influenced 48 hours after trypsinization, while a full week after trypsinization, no differences in cell count between the treated and untreated conditions could be noticed. This discrepancy is not stated by other researchers that performed similar experiments (S. J. Kim et al., 2021; Visalli et al., 2021). A possible explanation is that trypsinization caused a certain stress on the treated cells, which induced a slower growth. The treated cells might subsequently produce an elevated level of growth factors, resulting in a faster growth compared to the controls. After a full week of growth, the treated cells catch up with the controls.

Indications for lower resilience were also found in the transcriptomics data. After long-term exposure without subculturing, cells were put under starvation, whereafter gene expression was measured. In the untreated cells, almost 1,000 genes were differentially expressed between starvation and non-starvation. However, cells that were treated with NPs only showed half the amount of significantly differentially expressed genes when comparing non-starvation and starvation. Contrary, in the untreated conditions, starvation led to only four altered GO-pathways, and 11 differentially expressed pathways were found when stress was induced upon treatment with 4.55×10^3 NPs/mL. When treated with 4.55×10^6 NPs/mL and 4.55×10^9 NPs/mL, the number of differentially expressed GO-pathways between starvation and non-starvation increased up to 64 and 66 respectively. This all together indicated that stress, under the form of starvation, in untreated cells led to a shift in gene expression, and these genes were not specific to certain pathways but more random. Contrary, stress in cells treated with NPs shifted the gene expression to a lesser extent, but the genes that were differentially expressed were mostly involved in specific pathways. Exposure with 4.55×10^3 NPs/mL led to an intermediate stage with both a low number of statistically differentially expressed genes and GO-pathways.

Stress, in the form of starvation, triggered an increase in protein-folding pathways in untreated cells, thereby restoring the cellular health. However, in cells exposed to the lowest dose of NPs, starvation also upregulated pathways involved in inflammation. This initially appears beneficial for dealing with cellular stress. However, chronic inflammation can lead to tissue damage and contribute to various diseases. Higher NP concentrations led to upregulation of diverse pathways associated with not only protein folding and inflammation, but also with cell development, adhesion, morphogenesis and proliferation, indicating a more severe disruption of normal cellular processes. The exposure to NPs may have induced changes in genetic regulation, placing certain genes in a poised state. Stress in the form of starvation subsequently activated these pathways. For example, starvation in cells treated for 12 days with 4.55×10^9 NPs/mL altered the cellular response to lipids. Differentially expressed genes involved in this altered lipid response included NF-κB2, MAPK3, and PPARα. Interestingly, these factors may also play a role in regulating lipid accumulation upon MNP exposure itself, as described in section 2.4. It is conceivable that MNP exposure primed these genes for activation, with additional stress from starvation triggering their activation. Moreover, NPs may be recognized as extracellular matrix (ECM) components, leading to a poised state of genes involved in cell morphogenesis. Once again, starvation triggered these pathways, followed by the upregulation of pathways mainly involved in the special organisation of these cells.

6.4 Cells adapt to the presence of nanoparticles

In the results using long-term treatment without subculturing, decreased cellular growth after trypsinization is visible in both cells treated with SBs and NPs. However, over time, the difference between the treated cells and their respective controls diminishes. This indicates that cells treated with nanoparticles can adapt to their environment, leading to diminished effects over time. A similar effect is observed in respirometry experiments upon NP exposure. Initially, cells treated with NPs show significant increases in basal respiration, maximal respiration, proton leak, and spare respiratory capacity, compared to controls. However, these differences decrease as time progresses. In contrast, cellular metabolism after SBs exposure was more stable over time with a consistent elevation in basal respiration, maximal respiration and spare respiratory capacity. Only the relative OCR of the proton leak decreases over time. Visalli et al. (2021) also showed adaptation of cells to the presence of MNPs. This was done by exposing epithelial cells to a low-dose of MNPs, leading to an initial increased ROS formation after 7 days of exposure. Subsequently, ROS formation decreased to reach a level lower than the control. A minimum ROS level occurs between 14 and 28 days of exposure, whereafter ROS increased again. This indicates that cells may indeed adapt upon MNP exposure, however eventually these adaptations were annulled.

Cells might try to adapt to NP exposure in a similar manner to cancer cells i.e. via alterations in the lipid metabolism. Petan et al. (2018) noted that cancer cells adapt through enhanced mechanisms of lipid synthesis, mobilization and recycling. Lipid droplets play a crucial role in regulating lipid metabolism, trafficking and signalling under stress. These droplets form in response to nutrient and oxidative stress and help cells manage energy production and protect against oxidative damage. Additionally, lipid droplets may sequester toxic particles to prevent cell damage and interact with autophagy processes (Petan et al., 2018).

6.5 Exposure to high dosages of nanoparticles results in elevated toxicity

The results of the lipid staining upon long-term exposure without subculturing indicates the importance of the use of low dosages. In this test, a significant increase of lipid content was noticed in all three the tested NP concentrations after 9 days of treatment. However, the increase in lipid accumulation was inversely proposal to the concentration of NPs. It is possible that NPs clump together, leading to lower influences of the NPs when they are present in a higher concentration. However, no clumping is found in the research of Cortés et al. (2020) who noticed an increase in particle uptake by the cells when higher NP concentrations were used. On the other hand, H. Wang et al. (2022) stated that human liver cells showed inhibited lipid biosynthesis upon acute NP exposure, which contradicts our results. However, unlike our study, high dosages were used by Wang et al., which appear to be toxic and damages lipid metabolism. Also Y. Li et al. (2024) noted a decrease in FASN and ACC activities when the pacific whiteleg shrimp (*Litopenaeus vannamei*) was treated with increasing levels of NPs, indicating a lower 'de novo' lipid formation upon higher exposure levels. Therefore, our results support their hypothesis that higher dosages are toxic towards the lipid metabolism while lower doses increase lipid metabolism. Substantial differences in cellular reactions upon acute exposure with high doses and chronic exposure with low doses highlights the importance of studying low-dose chronic exposure to mimic reality.

When analyzing the gene expression data, higher doses resulted in a greater number of significantly differentially expressed genes, suggesting a modest dose-effect relationship. However, the overall number of significantly differentially expressed genes remained low, with a maximum observed difference of 19 genes. This difference was observed when comparing cells treated with 4.55×10^9 NPs/mL to the untreated condition under non-starvation conditions. J. Deng et al. (2023) exposed zebrafish to PS-NPs and found between 73 and 278 differentially expressed genes, depending on the studied cell-type. Their threshold for significant upregulation was lower than in our research, which may partially declare the higher amount of differentially expressed genes compared to our results. Additionally, the difference in experimental set-up may play a crucial role. It is important to note that mRNA levels do not directly correlate with protein levels. Post-transcriptional regulation also plays an important role, and is not taken into account by transcriptomics. Therefore, future research should include proteomics to examine the dose-effect of MNP exposure at different concentrations.

6.6 SBs and NPs exhibit similar effects on cell metabolism

Even though there were a lot of differences found between cells exposed to SBs and NPs, the overall results of lipid accumulation, cell proliferation and cellular energy metabolism were comparable. This indicates that the reaction of the cells after MNP exposure is due to the physical presence of a particle, rather than a chemical reaction towards the particle or its leaches. In contrast, other studies indicate different cellular reactions upon treatment with different types of MNPs (Stock et al., 2021; D. Xu et al., 2021). Interestingly, the study of Domenech et al. (2021) indicated no ROS elevation and effects upon chronic NP exposure. They hypothesized that the induction of ROS and genotoxicity after MNP exposure is induced by environmental contaminants on the surface of these MNPs, and not due to the MNPs itself. As the PS-NPs used in our research were spherical and had similar properties as the SBs, they react with environmental compounds in a similar way. This could declare the difference between previous findings and our findings. Future research could include a ROS-assay to confirm this.

Toxicity of the particles might still be influenced by alterations in size and shape of the MNPs, and by interactions of the MNPs with environmental compounds. However, as main reactions upon NPs and SBs exposure are similar, the question arises whether MNPs should be seen as a separated, new type of nanoparticles, or if they can be considered similar to other nanoparticles. Similarly to MNPs, humans are highly exposed to synthetic amorphous silica, since it has been used for many years in food applications, such as for clearing of beers and wines, as anticaking agent to maintain flow properties in powder products and to thicken pastes (Dekkers et al., 2011). These silica particles, both in the amorphous and crystalline form, can interact either directly with human cells (physical toxicity) but also with the environment by forming a corona (chemical toxicity) (Docter et al., 2014; Mortensen et al., 2013). While much research focuses on the potential risks associated with MNPs, little attention has been paid to the presence of these silica nanoparticles in our food, and its potential effects on health.

7 CONCLUSION

In this research, two experimental setups, involving repeated doses long-term treatment of Caco-2 cells with 100 nm PS-NPs at environmentally relevant concentrations were employed. In the first setup, cells were continuously cultured, while in the second setup, cells were subcultured during treatment. The results showed that chronic exposure to an environmentally relevant dose of MNPs is not directly cytotoxic but influences cellular metabolism. Similar results upon treatment with SBs and NPs raise questions about the toxicity of silica nanoparticles and other nanoparticles as well. Lipid accumulation was one of the most important findings of the study and goes together with altered gene expression and increased lipid usage for energy metabolism in starvation conditions. Since regulatory pathways between lipid accumulation and inflammation are crosslinked, lipid accumulation could be linked to inflammatory processes. Respirometry showed that cellular energy metabolism is overactivated upon MNP exposure, with elevated basal respiration, maximal respiration and proton leak. Longer treatment led to lower overreactions, indicating that cells adapt to this environment, and this adaptation may be linked to the lipid accumulation. At last, cellular resilience is found to be decreased. Trypsinization caused a decreased cell growth and starvation led to a different cellular reaction compared to the control. This different reaction included a shift towards inflammatory pathways. Therefore, exposure to MNPs is shown to induce a shift towards a more stressed cellular phenotype. In a broader context, this could be linked to obesity, one of the major players in the development of non-communicable diseases. Therefore, MNPs should be considered a crucial component of the exposome, necessitating further research to elucidate their full impact on human health and disease progression. Future research is needed to elucidate the impact of different NP concentrations and sizes on different cellular types. In addition, measuring lipodomics and proteomics could clarify which pathways are involved in the cellular reactions upon MNP-exposure.

REFERENCES

Abumradsb, N. A., Raafat El-Maghrabis, M., Amrill, E.-Z., Lopezs, E., & Grimaldill, P. A. (1993). *THE JOURNAL OF BIOLOGICAL CHEMISTRY Cloning of a Rat Adipocyte Membrane Protein Implicated in Binding or Transport of Long-chain Fatty Acids That Is Induced during Preadipocyte Differentiation* (Vol. 268, Issue 24).

Agilent Technologies. (2020). Agilent XF Substrate Oxidation Stress Test Kits: User Manual. In *Retrieved from https://www.agilent.com/cs/library/usermanuals/public/user-manual-substrate-oxidation-stress-test-kits-cell-analysis-5994-1164en-agilent.pdf*.

Alberts, B. , J. A. , L. J. , R. M. , R. K. , & W. P. (2002). How cells obtain energy from food. In Molecular biology of the cell. *(4th Ed.). New York, NY: Garland Science. Available from Https://Www.Ncbi.Nlm.Nih.Gov/Books/NBK26882/*.

Alvarez-Román, R., Naik, A., Kalia, Y. N., Guy, R. H., & Fessi, H. (2004). Skin penetration and distribution of polymeric nanoparticles. *Journal of Controlled Release*, *99*(1), 53–62. https://doi.org/10.1016/j.jconrel.2004.06.015

Amato-Lourenço, L. F., Carvalho-Oliveira, R., Júnior, G. R., dos Santos Galvão, L., Ando, R. A., & Mauad, T. (2021). Presence of airborne microplastics in human lung tissue. *Journal of Hazardous Materials*, *416*. https://doi.org/10.1016/j.jhazmat.2021.126124

Antunes, J., Sobral, P., Martins, M., & Branco, V. (2023). Nanoplastics activate a TLR4/p38-mediated pro-inflammatory response in human intestinal and mouse microglia cells. *Environmental Toxicology and Pharmacology*, *104*. https://doi.org/10.1016/j.etap.2023.104298

Avio, C. G., Gorbi, S., Milan, M., Benedetti, M., Fattorini, D., D'Errico, G., Pauletto, M., Bargelloni, L., & Regoli, F. (2015). Pollutants bioavailability and toxicological risk from microplastics to marine mussels. *Environmental Pollution*, *198*, 211–222. https://doi.org/10.1016/j.envpol.2014.12.021

Babaei, A. A., Rafiee, M., Khodagholi, F., Ahmadpour, E., & Amereh, F. (2022). *Nanoplastics-induced oxidative stress, antioxidant defense, and physiological response in exposed Wistar albino rats*. https://doi.org/10.1007/s11356-021-15920-0/Published

Barguilla, I., Domenech, J., Ballesteros, S., Rubio, L., Marcos, R., & Hernández, A. (2022). Long-term exposure to nanoplastics alters molecular and functional traits related to the carcinogenic process. *Journal of Hazardous Materials*, *438*. https://doi.org/10.1016/j.jhazmat.2022.129470

Bender, T., & Martinou, J. C. (2016). The mitochondrial pyruvate carrier in health and disease: To carry or not to carry? In *Biochimica et Biophysica Acta - Molecular Cell Research* (Vol. 1863, Issue 10, pp. 2436–2442). Elsevier B.V. https://doi.org/10.1016/j.bbamcr.2016.01.017

Bergami, E., Krupinski Emerenciano, A., González-Aravena, M., Cárdenas, C. A., Hernández, P., Silva, J. R. M. C., & Corsi, I. (2019). Polystyrene nanoparticles affect the innate immune system of the Antarctic sea urchin Sterechinus neumayeri. *Polar Biology*, *42*(4), 743–757. https://doi.org/10.1007/s00300-019-02468-6

Bernatsky, S., Fournier, M., Pineau, C. A., Clarke, A. E., Vinet, E., & Smargiassi, A. (2011). Associations between ambient fine particulate levels and disease activity in patients with systemic lupus erythematosus (SLE). *Environmental Health Perspectives*, *119*(1), 45–49. https://doi.org/10.1289/ehp.1002123

Boldyreva, L. V., Morozova, M. V., Saydakova, S. S., & Kozhevnikova, E. N. (2021). Fat of the gut: Epithelial phospholipids in inflammatory bowel diseases. In *International Journal of Molecular Sciences* (Vol. 22, Issue 21). MDPI. https://doi.org/10.3390/ijms222111682

Bolsoni-Lopes, A., & Alonso-Vale, M. I. C. (2015). Lipolysis and lipases in white adipose tissue – An update. In *Archives of Endocrinology and Metabolism* (Vol. 59, Issue 4, pp. 335–342). Sociedade Brasileira de Endocrinologia e Metabologia. https://doi.org/10.1590/2359-3997000000067

Bonanomi, M., Salmistraro, N., Porro, D., Pinsino, A., Colangelo, A. M., & Gaglio, D. (2022). Polystyrene micro and nano-particles induce metabolic rewiring in normal human colon cells: A risk factor for human health. *Chemosphere*, *303*. https://doi.org/10.1016/j.chemosphere.2022.134947

Boucher, J., & Billard, G. (2019). *The challenges of measuring plastic pollution.* http://journals.openedition.org/factsreports/5319

Brown, R. E., Sharma, A. M., Ardern, C. I., Mirdamadi, P., Mirdamadi, P., & Kuk, J. L. (2016). Secular differences in the association between caloric intake, macronutrient intake, and physical activity with obesity. *Obesity Research and Clinical Practice*, *10*(3), 243–255. https://doi.org/10.1016/j.orcp.2015.08.007

Calcaterra, V., & Zuccotti, G. (2022). Non-Communicable Diseases and Rare Diseases: A Current and Future Public Health Challenge within Pediatrics. In *Children* (Vol. 9, Issue 10). Multidisciplinary Digital Publishing Institute (MDPI). https://doi.org/10.3390/children9101491

Cao, J., Xu, R., Geng, Y., Xu, S., & Guo, M. (2023). Exposure to polystyrene microplastics triggers lung injury via targeting toll-like receptor 2 and activation of the NF-κB signal in mice. *Environmental Pollution*, *320*. https://doi.org/10.1016/j.envpol.2023.121068

Chamorro-Garcia, R., Diaz-Castillo, C., Shoucri, B. M., Käch, H., Leavitt, R., Shioda, T., & Blumberg, B. (2017). Ancestral perinatal obesogen exposure results in a transgenerational thrifty phenotype in mice. *Nature Communications*, *8*(1). https://doi.org/10.1038/s41467-017-01944-z

Chang, K. H., Hsu, C. C., Muo, C. H., Hsu, C. Y., Liu, H. C., Kao, C. H., Chen, C. Y., Chang, M. Y., & Hsu, Y. C. (2016). Air pollution exposure increases the risk of rheumatoid arthritis: A longitudinal and nationwide study. *Environment International*, *94*, 495–499. https://doi.org/10.1016/j.envint.2016.06.008

Chaudhry R, & Varacallo M. (2023). *Biochemistry, Glycolysis*. StatPearls - NCBI Bookshelf. https://www.ncbi.nlm.nih.gov/books/NBK482303/

Chen, Q., Gundlach, M., Yang, S., Jiang, J., Velki, M., Yin, D., & Hollert, H. (2017). Quantitative investigation of the mechanisms of microplastics and nanoplastics toward zebrafish larvae locomotor activity. *Science of the Total Environment*, *584–585*, 1022–1031. https://doi.org/10.1016/j.scitotenv.2017.01.156

Chen, T., Jiang, H., He, Y., Shen, Y., Huang, Z., Gu, Y., Wei, Q., Zhao, J., & Chen, X. (2024). Nanoplastics and chrysene pollution: Potential new triggers for nonalcoholic fatty liver disease and hepatitis, insights from juvenile Siniperca chuatsi. *Science of the Total Environment*, *922*. https://doi.org/10.1016/j.scitotenv.2024.171125

Cheng, W., Li, X., Zhou, Y., Yu, H., Xie, Y., Guo, H., Wang, H., Li, Y., Feng, Y., & Wang, Y. (2022). Polystyrene microplastics induce hepatotoxicity and disrupt lipid metabolism in the liver organoids. *Science of the Total Environment*, *806*. https://doi.org/10.1016/j.scitotenv.2021.150328

Cortés, C., Domenech, J., Salazar, M., Pastor, S., Marcos, R., & Hernández, A. (2020). Nanoplastics as a potential environmental health factor: effects of polystyrene nanoparticles on human intestinal epithelial Caco-2 cells. *Environ. Sci.: Nano*, *7*(1), 272–285. https://doi.org/10.1039/C9EN00523D

Daynes, R. A., & Jones, D. C. (2002). Emerging roles of PPARs in inflammation and immunity. In *Nature Reviews Immunology* (Vol. 2, Issue 10, pp. 748–759). https://doi.org/10.1038/nri912

Dekkers, S., Krystek, P., Peters, R. J. B., Lankveld, D. P. K., Bokkers, B. G. H., Van Hoeven-Arentzen, P. H., Bouwmeester, H., & Oomen, A. G. (2011). Presence and risks of nanosilica in food products. *Nanotoxicology*, *5*(3), 393–405. https://doi.org/10.3109/17435390.2010.519836

Del Piano, F., Lama, A., Piccolo, G., Addeo, N. F., Iaccarino, D., Fusco, G., Riccio, L., De Biase, D., Mattace Raso, G., Meli, R., & Ferrante, M. C. (2023). Impact of polystyrene microplastic exposure on gilthead seabream (Sparus aurata Linnaeus, 1758): Differential inflammatory and immune response between anterior and posterior intestine. *Science of the Total Environment*, *879*. https://doi.org/10.1016/j.scitotenv.2023.163201

Deloid, G. M., Cao, X., Coreas, R., Bitounis, D., Singh, D., Zhong, W., & Demokritou, P. (2022). Incineration-Generated Polyethylene Micro-Nanoplastics Increase Triglyceride Lipolysis and Absorption in an in Vitro Small Intestinal Epithelium Model. *Environmental Science and Technology*, *56*(17), 12288–12297. https://doi.org/10.1021/acs.est.2c03195

Deloid, G. M., Sohal, I. S., Lorente, L. R., Molina, R. M., Pyrgiotakis, G., Stevanovic, A., Zhang, R., McClements, D. J., Geitner, N. K., Bousfield, D. W., Ng, K. W., Loo, S. C. J., Bell, D. C., Brain, J., & Demokritou, P. (2018). Reducing Intestinal Digestion and Absorption of Fat Using a Nature-Derived Biopolymer: Interference of Triglyceride Hydrolysis by Nanocellulose. *ACS Nano*, *12*(7), 6469–6479. https://doi.org/10.1021/acsnano.8b03074

Delon, L., Gibson, R. J., Prestidge, C. A., & Thierry, B. (2022). Mechanisms of uptake and transport of particulate formulations in the small intestine. In *Journal of Controlled Release* (Vol. 343, pp. 584–599). Elsevier B.V. https://doi.org/10.1016/j.jconrel.2022.02.006

Deng, J., Zeng, X., Li, J., Luo, L., Yang, Y., & Luan, T. (2023). Single-cell transcriptomic analysis reveals heterogeneity of the patterns of responsive genes and cell communications in liver cell populations of zebrafish exposed to polystyrene nanoplastics. *Science of the Total Environment*, *889*. https://doi.org/10.1016/j.scitotenv.2023.164082

Deng, Y., Chen, H., Huang, Y., Wang, Q., Chen, W., & Chen, D. (2022). Polystyrene Microplastics Affect the Reproductive Performance of Male Mice and Lipid Homeostasis in Their Offspring. *Environmental Science & Technology Letters*, *9*(9), 752–757. https://doi.org/10.1021/acs.estlett.2c00262

Deng, Y., Zhang, Y., Lemos, B., & Ren, H. (2017). Tissue accumulation of microplastics in mice and biomarker responses suggest widespread health risks of exposure. *Scientific Reports*, *7*. https://doi.org/10.1038/srep46687

Docter, D., Bantz, C., Westmeier, D., Galla, H. J., Wang, Q., Kirkpatrick, J. C., Nielsen, P., Maskos, M., & Stauber, R. H. (2014). The protein corona protects against size- and dose-dependent toxicity of amorphous silica nanoparticles. *Beilstein Journal of Nanotechnology*, *5*(1), 1380–1392. https://doi.org/10.3762/bjnano.5.151

Domenech, J., de Britto, M., Velázquez, A., Pastor, S., Hernández, A., Marcos, R., & Cortés, C. (2021). Long-term effects of polystyrene nanoplastics in human intestinal Caco-2 cells. *Biomolecules*, *11*(10). https://doi.org/10.3390/biom11101442

Dong, C. Di, Chen, C. W., Chen, Y. C., Chen, H. H., Lee, J. S., & Lin, C. H. (2020). Polystyrene microplastic particles: In vitro pulmonary toxicity assessment. *Journal of Hazardous Materials*, *385*. https://doi.org/10.1016/j.jhazmat.2019.121575

Du, F., Cai, H., Zhang, Q., Chen, Q., & Shi, H. (2020). Microplastics in take-out food containers. *Journal of Hazardous Materials*, *399*. https://doi.org/10.1016/j.jhazmat.2020.122969

Duan, J., Li, Y., Gao, J., Cao, R., Shang, E., & Zhang, W. (2022). ROS-mediated photoaging pathways of nano- and micro-plastic particles under UV irradiation. *Water Research*, *216*. https://doi.org/10.1016/j.watres.2022.118320

Duan, J., Liang, S., Feng, L., Yu, Y., & Sun, Z. (2018). Silica nanoparticles trigger hepatic lipid-metabolism disorder in vivo and in vitro. *International Journal of Nanomedicine*, *13*, 7303–7318. https://doi.org/10.2147/IJN.S185348

Edelblum, K. L., & Turner, J. R. (2015). Epithelial Cells: Structure, Transport, and Barrier Function. Structure, Transport, and Barrier Function. In *Mucosal Immunology: Fourth Edition* (Vols. 1–2, pp. 187–210). Elsevier Inc. https://doi.org/10.1016/B978-0-12-415847-4.00012-4

Egusquiza, R. J., & Blumberg, B. (2020). Environmental obesogens and their impact on susceptibility to obesity: New mechanisms and chemicals. In *Endocrinology (United States)* (Vol. 161, Issue 3). Endocrine Society. https://doi.org/10.1210/endocr/bqaa024

Fang, D. L., Wan, Y., Shen, W., Cao, J., Sun, Z. X., Yu, H. H., Zhang, Q., Cheng, W. H., Chen, J., & Ning, B. (2013). Endoplasmic reticulum stress leads to lipid accumulation through upregulation of SREBP-1c in normal hepatic and hepatoma cells. *Molecular and Cellular Biochemistry*, *381*(1–2), 127–137. https://doi.org/10.1007/s11010-013-1694-7

Feingold, K. R., Shigenaga, J. K., Kazemi, M. R., McDonald, C. M., Patzek, S. M., Cross, A. S., Moser, A., & Grunfeld, C. (2012). Mechanisms of triglyceride accumulation in activated macrophages. *Journal of Leukocyte Biology*, *92*(4), 829–839. https://doi.org/10.1189/jlb.1111537

Feng, Y., Tu, C., Li, R., Wu, D., Yang, J., Xia, Y., Peijnenburg, W. J. G. M., & Luo, Y. (2023). A systematic review of the impacts of exposure to micro- and nano-plastics on human tissue accumulation and health. In

Eco-Environment and Health (Vol. 2, Issue 4, pp. 195–207). Elsevier B.V. https://doi.org/10.1016/j.eehl.2023.08.002

Frank, D. N., St Amand, A. L., Feldman, R. A., Boedeker, E. C., Harpaz, N., & Pace, N. R. (2007). *Molecular-phylogenetic characterization of microbial community imbalances in human inflammatory bowel diseases*. www.pnas.org/cgi/content/full/

Geyer, R., Jambeck, J. R., & Law, K. L. (2017). *Production, use, and fate of all plastics ever made*. https://www.science.org

Goodman, K. E., Hua, T., & Sang, Q. X. A. (2022). Effects of Polystyrene Microplastics on Human Kidney and Liver Cell Morphology, Cellular Proliferation, and Metabolism. *ACS Omega*, *7*(38), 34136–34153. https://doi.org/10.1021/acsomega.2c03453

Greven, A.-C., Merk, T., Karagöz, F., Mohr, K., Klapper, M., Jovanović, B., & Palić, D. (2016). Polycarbonate and polystyrene nanoplastic particles act as stressors to the innate immune system of fathead minnow (Pimephales promelas). *Environmental Toxicology and Chemistry*, *35*(12), 3093–3100. https://doi.org/https://doi.org/10.1002/etc.3501

Guedes-Alonso, R., Sosa-Ferrera, Z., & Santana-Rodríguez, J. J. (2021). Analysis of microplastics-sorbed endocrine-disrupting compounds in pellets and microplastic fragments from beaches. *Microchemical Journal*, *171*. https://doi.org/10.1016/j.microc.2021.106834

Halimu, G., Zhang, Q., Liu, L., Zhang, Z., Wang, X., Gu, W., Zhang, B., Dai, Y., Zhang, H., Zhang, C., & Xu, M. (2022). Toxic effects of nanoplastics with different sizes and surface charges on epithelial-to-mesenchymal transition in A549 cells and the potential toxicological mechanism. *Journal of Hazardous Materials*, *430*. https://doi.org/10.1016/j.jhazmat.2022.128485

Hall, K. (2000). *Impacts of marine debris and oil: economic and social costs to coastal communities*. Kommunenes Internasjonale Miljøorganisasjon.

Han, M., Bushong, E. A., Segawa, M., Tiard, A., Wong, A., Brady, M. R., Momcilovic, M., Wolf, D. M., Zhang, R., Petcherski, A., Madany, M., Xu, S., Lee, J. T., Poyurovsky, M. V., Olszewski, K., Holloway, T., Gomez, A., John, M. S., Dubinett, S. M., … Shackelford, D. B. (2023). Spatial mapping of mitochondrial networks and bioenergetics in lung cancer. *Nature*, *615*(7953), 712–719. https://doi.org/10.1038/s41586-023-05793-3

He, Y. J., Qin, Y., Zhang, T. L., Zhu, Y. Y., Wang, Z. J., Zhou, Z. S., Xie, T. Z., & Luo, X. D. (2021). Migration of (non-) intentionally added substances and microplastics from microwavable plastic food containers. *Journal of Hazardous Materials*, *417*. https://doi.org/10.1016/j.jhazmat.2021.126074

Henne, M. (2019). And three's a party: lysosomes, lipid droplets, and the ER in lipid trafficking and cell homeostasis. In *Current Opinion in Cell Biology* (Vol. 59, pp. 40–49). Elsevier Ltd. https://doi.org/10.1016/j.ceb.2019.02.011

Hernandez, L. M., Yousefi, N., & Tufenkji, N. (2017). Are there nanoplastics in your personal care products? *Environmental Science and Technology Letters*, *4*(7), 280–285. https://doi.org/10.1021/acs.estlett.7b00187

Hillyer, J. F., & Albrecht, R. M. (2001). Gastrointestinal persorption and tissue distribution of differently sized colloidal gold nanoparticles. *Journal of Pharmaceutical Sciences*, *90*(12), 1927–1936. https://doi.org/https://doi.org/10.1002/jps.1143

Hollóczki, O., & Gehrke, S. (2020). Can Nanoplastics Alter Cell Membranes? *Chemphyschem : A European Journal of Chemical Physics and Physical Chemistry*, *21*(1), 9–12. https://doi.org/10.1002/cphc.201900481

Hu, M., & Palić, D. (2020). Micro- and nano-plastics activation of oxidative and inflammatory adverse outcome pathways. In *Redox Biology* (Vol. 37). Elsevier B.V. https://doi.org/10.1016/j.redox.2020.101620

Huang, Y. L., Morales-Rosado, J., Ray, J., Myers, T. G., Kho, T., Lu, M., & Munford, R. S. (2014). Toll-like receptor agonists promote prolonged triglyceride storage in macrophages. *Journal of Biological Chemistry*, *289*(5), 3001–3012. https://doi.org/10.1074/jbc.M113.524587

Hurst, C. H., & Waxman, D. J. (2003). Activation of PPARα and PPARγ by environmental phthalate monoesters. In *Toxicological Sciences* (Vol. 74, Issue 2, pp. 297–308). https://doi.org/10.1093/toxsci/kfg145

Im, S. S., Yousef, L., Blaschitz, C., Liu, J. Z., Edwards, R. A., Young, S. G., Raffatellu, M., & Osborne, T. F. (2011). Linking lipid metabolism to the innate immune response in macrophages through sterol regulatory element binding protein-1a. *Cell Metabolism*, *13*(5), 540–549. https://doi.org/10.1016/j.cmet.2011.04.001

Jia, R., Han, J., Liu, X., Li, K., Lai, W., Bian, L., Yan, J., & Xi, Z. (2023). Exposure to Polypropylene Microplastics via Oral Ingestion Induces Colonic Apoptosis and Intestinal Barrier Damage through Oxidative Stress and Inflammation in Mice. *Toxics*, *11*(2). https://doi.org/10.3390/toxics11020127

Jiang, M., Wang, B., Ye, R., Yu, N., Xie, Z., Hua, Y., Zhou, R., Tian, B., & Dai, S. (2022). Evidence and Impacts of Nanoplastic Accumulation on Crop Grains. *Advanced Science*, *9*(33). https://doi.org/10.1002/advs.202202336

Jin, H., Ma, T., Sha, X., Liu, Z., Zhou, Y., Meng, X., Chen, Y., Han, X., & Ding, J. (2021). Polystyrene microplastics induced male reproductive toxicity in mice. *Journal of Hazardous Materials*, *401*. https://doi.org/10.1016/j.jhazmat.2020.123430

Jin, Y., Lu, L., Tu, W., Luo, T., & Fu, Z. (2019). Impacts of polystyrene microplastic on the gut barrier, microbiota and metabolism of mice. *Science of the Total Environment*, *649*, 308–317. https://doi.org/10.1016/j.scitotenv.2018.08.353

Jin, Y., Xia, J., Pan, Z., Yang, J., Wang, W., & Fu, Z. (2018). Polystyrene microplastics induce microbiota dysbiosis and inflammation in the gut of adult zebrafish. *Environmental Pollution*, *235*, 322–329. https://doi.org/10.1016/j.envpol.2017.12.088

Kannan, K., & Vimalkumar, K. (2021). A Review of Human Exposure to Microplastics and Insights Into Microplastics as Obesogens. In *Frontiers in Endocrinology* (Vol. 12). Frontiers Media S.A. https://doi.org/10.3389/fendo.2021.724989

Kazemi, M., Faisal Kabir, S., & Fini, E. H. (2021). State of the art in recycling waste thermoplastics and thermosets and their applications in construction. In *Resources, Conservation and Recycling* (Vol. 174). Elsevier B.V. https://doi.org/10.1016/j.resconrec.2021.105776

Kim, E. H., Choi, S., Kim, D., Park, H. J., Bian, Y., Choi, S. H., Chung, H. Y., & Bae, O. N. (2022). Amine-modified nanoplastics promote the procoagulant activation of isolated human red blood cells and thrombus formation in rats. *Particle and Fibre Toxicology*, *19*(1). https://doi.org/10.1186/s12989-022-00500-y

Kim, S. J., Long, N. P., Jung, C. W., Anh, N. H., Min, J. E., Kim, H. M., & Kwon, S. W. (2021). Exposure to nano-polystyrene induces metabolic alteration in lipid homeostasis in Caco-2. *Environmental Science: Nano*, *8*(5), 1408–1424. https://doi.org/10.1039/D1EN00145K

Koelmans, B. , Pahl, S., Backhaus, T., Bessa, F., Van Calster, G., Contzen, N., Cronin, R., Galloway, T., Hart, A., Henderson, L. , Kalcikova, G., Kelly, F., Kolodziejczyk, B., Marku, E., Poortinga, W., Rillig, M., Van Sebille, E., Steg, L., Steinhorst, J., … Wright, S. (2019). *A scientific perspective on microplastics in nature and society: Evidence review report.* https://doi.org/https://doi.org/10.26356/microplastics

Kreyling, W. G., Hirn, S., Möller, W., Schleh, C., Wenk, A., Celik, G., Lipka, J., Schäffler, M., Haberl, N., Johnston, B. D., Sperling, R., Schmid, G., Simon, U., Parak, W. J., & Semmler-Behnke, M. (2014). Air-blood barrier translocation of tracheally instilled gold nanoparticles inversely depends on particle size. *ACS Nano*, *8*(1), 222–233. https://doi.org/10.1021/nn403256v

Lai, H., Liu, X., & Qu, M. (2022). Nanoplastics and Human Health: Hazard Identification and Biointerface. In *Nanomaterials* (Vol. 12, Issue 8). MDPI. https://doi.org/10.3390/nano12081298

Laplante, M., & Sabatini, D. M. (2009). An Emerging Role of mTOR in Lipid Biosynthesis. In *Current Biology* (Vol. 19, Issue 22). https://doi.org/10.1016/j.cub.2009.09.058

Lechthaler, S., Waldschläger, K., Stauch, G., & Schüttrumpf, H. (2020). The way of macroplastic through the environment. In *Environments - MDPI* (Vol. 7, Issue 10, pp. 1–30). MDPI AG. https://doi.org/10.3390/environments7100073

Lee, C. W., Hsu, L. F., Wu, I. L., Wang, Y. L., Chen, W. C., Liu, Y. J., Yang, L. T., Tan, C. L., Luo, Y. H., Wang, C. C., Chiu, H. W., Yang, T. C. K., Lin, Y. Y., Chang, H. A., Chiang, Y. C., Chen, C. H., Lee, M. H., Peng, K. T., & Huang, C. C. Y. (2022). Exposure to polystyrene microplastics impairs hippocampus-dependent learning and memory in mice. *Journal of Hazardous Materials*, *430*. https://doi.org/10.1016/j.jhazmat.2022.128431

Lee, H. S., Amarakoon, D., Wei, C. i., Choi, K. Y., Smolensky, D., & Lee, S. H. (2021). Adverse effect of polystyrene microplastics (PS-MPs) on tube formation and viability of human umbilical vein endothelial cells. *Food and Chemical Toxicology*, *154*. https://doi.org/10.1016/j.fct.2021.112356

Leslie, H. A., van Velzen, M. J. M., Brandsma, S. H., Vethaak, A. D., Garcia-Vallejo, J. J., & Lamoree, M. H. (2022). Discovery and quantification of plastic particle pollution in human blood. *Environment International*, *163*. https://doi.org/10.1016/j.envint.2022.107199

Ley, R. E., Turnbaugh, P. J., Klein, S., & Gordon, J. I. (2006). Human gut microbes associated with obesity. *Nature*, *444*(7122), 1022–1023. https://doi.org/10.1038/4441022a

Li, B., Ding, Y., Cheng, X., Sheng, D., Xu, Z., Rong, Q., Wu, Y., Zhao, H., Ji, X., & Zhang, Y. (2020). Polyethylene microplastics affect the distribution of gut microbiota and inflammation development in mice. *Chemosphere*, *244*. https://doi.org/10.1016/j.chemosphere.2019.125492

Li, L.-C., Varghese, Z., Moorhead, J. F., Lee, C.-T., Chen, J.-B., & Ruan, X. Z. (2013). Cross-talk between TLR4-MyD88-NF-B and SCAP-SREBP2 pathways mediates macrophage foam cell formation. *Am J Physiol Heart Circ Physiol*, *304*, 874–884. https://doi.org/10.1152/ajpheart.00096.2012.-Myeloid

Li, Y., Ye, Y., Rihan, N., Zhu, B., Jiang, Q., Liu, X., Zhao, Y., & Che, X. (2024). Polystyrene nanoplastics induce lipid metabolism disorder and alter fatty acid composition in the hepatopancreas of Pacific whiteleg shrimp (Litopenaeus vannamei). *Science of the Total Environment*, *906*. https://doi.org/10.1016/j.scitotenv.2023.167616

Liao, Y. liang, & Yang, J. yan. (2020). Microplastic serves as a potential vector for Cr in an in-vitro human digestive model. *Science of the Total Environment*, *703*. https://doi.org/10.1016/j.scitotenv.2019.134805

Lim, S. L., Ng, C. T., Zou, L., Lu, Y., Chen, J., Bay, B. H., Shen, H. M., & Ong, C. N. (2019). Targeted metabolomics reveals differential biological effects of nanoplastics and nanoZnO in human lung cells. *Nanotoxicology*, *13*(8), 1117–1132. https://doi.org/10.1080/17435390.2019.1640913

Liu, L., Xu, K., Zhang, B., Ye, Y., Zhang, Q., & Jiang, W. (2021). Cellular internalization and release of polystyrene microplastics and nanoplastics. *Science of the Total Environment*, *779*. https://doi.org/10.1016/j.scitotenv.2021.146523

Liu, L., Zheng, H., Luan, L., Luo, X., Wang, X., Lu, H., Li, Y., Wen, L., Li, F., & Zhao, J. (2021). Functionalized polystyrene nanoplastic-induced energy homeostasis imbalance and the immunomodulation dysfunction of marine clams (Meretrix meretrix) at environmentally relevant concentrations. *Environmental Science: Nano*, *8*(7), 2030–2048. https://doi.org/10.1039/d1en00212k

Liu, Z., Zhuan, Q., Zhang, L., Meng, L., Fu, X., & Hou, Y. (2022). Polystyrene microplastics induced female reproductive toxicity in mice. *Journal of Hazardous Materials*, *424*. https://doi.org/10.1016/j.jhazmat.2021.127629

Llorca, M., & Farré, M. (2021). Current Insights into Potential Effects of Micro-Nanoplastics on Human Health by in-vitro Tests. In *Frontiers in Toxicology* (Vol. 3). Frontiers Media S.A. https://doi.org/10.3389/ftox.2021.752140

Luo, Y., Li, L., Feng, Y., Li, R., Yang, J., Peijnenburg, W. J. G. M., & Tu, C. (2022). Quantitative tracing of uptake and transport of submicrometre plastics in crop plants using lanthanide chelates as a dual-functional tracer. *Nature Nanotechnology*, *17*(4), 424–431. https://doi.org/10.1038/s41565-021-01063-3

Ma, Y., Nenkov, M., Chen, Y., Press, A. T., Kaemmerer, E., & Gassler, N. (2021). Fatty acid metabolism and acyl-CoA synthetases in the liver-gut axis. *World Journal of Hepatology*, *13*(11), 1512–1533. https://doi.org/10.4254/wjh.v13.i11.1512

Maradonna, F., & Carnevali, O. (2018). Lipid metabolism alteration by endocrine disruptors in animal models: An overview. In *Frontiers in Endocrinology* (Vol. 9). Frontiers Media S.A. https://doi.org/10.3389/fendo.2018.00654

Marana, M. H., Poulsen, R., Thormar, E. A., Clausen, C. G., Thit, A., Mathiessen, H., Jaafar, R., Korbut, R., Hansen, A. M. B., Hansen, M., Limborg, M. T., Syberg, K., & von Gersdorff Jørgensen, L. (2022). Plastic nanoparticles cause mild inflammation, disrupt metabolic pathways, change the gut microbiota and affect reproduction in zebrafish: A full generation multi-omics study. *Journal of Hazardous Materials*, *424*. https://doi.org/10.1016/j.jhazmat.2021.127705

Massey, J. B., Bick, D. H., & Pownall, H. J. (1997). Spontaneous transfer of monoacyl amphiphiles between lipid and protein surfaces. *Biophysical Journal*, *72*(4), 1732–1743. https://doi.org/10.1016/S0006-3495(97)78819-2

Matsumoto, M., Hirata-Koizumi, M., & Ema, M. (2008). Potential adverse effects of phthalic acid esters on human health: A review of recent studies on reproduction. *Regulatory Toxicology and Pharmacology*, *50*(1), 37–49. https://doi.org/10.1016/j.yrtph.2007.09.004

McCubrey, J. A., LaHair, M. M., & Franklin, R. A. (2006). Reactive Oxygen Species-Induced Activation of the MAP Kinase Signaling Pathways. *Antioxidants & Redox Signaling*, *8*(9–10), 1775–1789. https://doi.org/10.1089/ars.2006.8.1775

McMahon, C. R., Holley, D., & Robinson, S. (1999). The diet of itinerant male Hooker’s sea lions, Phocarctos hookeri, at sub-Antarctic Macquarie Island. *Wildlife Research*, *26*(6), 839–846. https://doi.org/10.1071/WR98079

Meng, X., Zhang, J., Wang, W., Gonzalez-Gil, G., Vrouwenvelder, J. S., & Li, Z. (2022). Effects of nano- and microplastics on kidney: Physicochemical properties, bioaccumulation, oxidative stress and immunoreaction. *Chemosphere*, *288*. https://doi.org/10.1016/j.chemosphere.2021.132631

Mitrano, D. M., Wick, P., & Nowack, B. (2021). Placing nanoplastics in the context of global plastic pollution. In *Nature Nanotechnology* (Vol. 16, Issue 5, pp. 491–500). Nature Research. https://doi.org/10.1038/s41565-021-00888-2

Mohamed Nor, N. H., Kooi, M., Diepens, N. J., & Koelmans, A. A. (2021). Lifetime Accumulation of Microplastic in Children and Adults. *Environmental Science and Technology*, *55*(8), 5084–5096. https://doi.org/10.1021/acs.est.0c07384

Morales, P. E., Bucarey, J. L., & Espinosa, A. (2017). Muscle lipid metabolism: Role of lipid droplets and perilipins. In *Journal of Diabetes Research* (Vol. 2017). Hindawi Limited. https://doi.org/10.1155/2017/1789395

Mortensen, N. P., Fennell, T. R., & Johnson, L. M. (2021). Unintended human ingestion of nanoplastics and small microplastics through drinking water, beverages, and food sources. In *NanoImpact* (Vol. 21). Elsevier B.V. https://doi.org/10.1016/j.impact.2021.100302

Mortensen, N. P., Hurst, G. B., Wang, W., Foster, C. M., Nallathamby, P. D., & Retterer, S. T. (2013). Dynamic development of the protein corona on silica nanoparticles: Composition and role in toxicity. *Nanoscale*, *5*(14), 6372–6380. https://doi.org/10.1039/c3nr33280b

Nicholls, D. G. (2021). Mitochondrial proton leaks and uncoupling proteins. In *Biochimica et Biophysica Acta - Bioenergetics* (Vol. 1862, Issue 7). Elsevier B.V. https://doi.org/10.1016/j.bbabio.2021.148428

OECD. (2022). *Global Plastics Outlook: Policy Scenarios to 2060* . OECD Publications. https://www.oecd.org/newsroom/global-plastic-waste-set-to-almost-triple-by-2060.htm

Oishi, Y., Spann, N. J., Link, V. M., Muse, E. D., Strid, T., Edillor, C., Kolar, M. J., Matsuzaka, T., Hayakawa, S., Tao, J., Kaikkonen, M. U., Carlin, A. F., Lam, M. T., Manabe, I., Shimano, H., Saghatelian, A., & Glass, C. K. (2017). SREBP1 Contributes to Resolution of Pro-inflammatory TLR4 Signaling by Reprogramming Fatty Acid Metabolism. *Cell Metabolism*, *25*(2), 412–427. https://doi.org/10.1016/j.cmet.2016.11.009

Oliveri Conti, G., Ferrante, M., Banni, M., Favara, C., Nicolosi, I., Cristaldi, A., Fiore, M., & Zuccarello, P. (2020). Micro- and nano-plastics in edible fruit and vegetables. The first diet risks assessment for the general population. *Environmental Research*, *187*. https://doi.org/10.1016/j.envres.2020.109677

Park, E. J., Han, J. S., Park, E. J., Seong, E., Lee, G. H., Kim, D. W., Son, H. Y., Han, H. Y., & Lee, B. S. (2020). Repeated-oral dose toxicity of polyethylene microplastics and the possible implications on reproduction and development of the next generation. *Toxicology Letters*, *324*, 75–85. https://doi.org/10.1016/j.toxlet.2020.01.008

Peng, M., Vercauteren, M., Grootaert, C., Rajkovic, A., Boon, N., Janssen, C., & Asselman, J. (2023). Cellular and bioenergetic effects of polystyrene microplastic in function of cell type, differentiation status and post-exposure time. *Environmental Pollution*, *337*. https://doi.org/10.1016/j.envpol.2023.122550

Petan, T., Jarc, E., & Jusović, M. (2018). Lipid droplets in cancer: Guardians of fat in a stressful world. In *Molecules* (Vol. 23, Issue 8). MDPI AG. https://doi.org/10.3390/molecules23081941

Pironti, C., Notarstefano, V., Ricciardi, M., Motta, O., Giorgini, E., & Montano, L. (2023). First Evidence of Microplastics in Human Urine, a Preliminary Study of Intake in the Human Body. *Toxics*, *11*(1). https://doi.org/10.3390/toxics11010040

Prata, J. C., da Costa, J. P., Lopes, I., Duarte, A. C., & Rocha-Santos, T. (2020). Environmental exposure to microplastics: An overview on possible human health effects. In *Science of the Total Environment* (Vol. 702). Elsevier B.V. https://doi.org/10.1016/j.scitotenv.2019.134455

Qu, M., Liu, Y., Xu, K., & Wang, D. (2019). Activation of p38 MAPK Signaling-Mediated Endoplasmic Reticulum Unfolded Protein Response by Nanopolystyrene Particles. *Advanced Biosystems*, *3*(4), 1800325. https://doi.org/https://doi.org/10.1002/adbi.201800325

Ragusa, A., Svelato, A., Santacroce, C., Catalano, P., Notarstefano, V., Carnevali, O., Papa, F., Rongioletti, M. C. A., Baiocco, F., Draghi, S., D'Amore, E., Rinaldo, D., Matta, M., & Giorgini, E. (2021). Plasticenta: First evidence of microplastics in human placenta. In *Environment International* (Vol. 146). Elsevier Ltd. https://doi.org/10.1016/j.envint.2020.106274

Ramsperger, A. F. R. M., Narayana, V. K. B., Gross, W., Mohanraj, J., Thelakkat, M., Greiner, A., Schmalz, H., Kress, H., & Laforsch, C. (2020). *Environmental exposure enhances the internalization of microplastic particles into cells*. https://www.science.org

Regoli, F., & Winston, G. W. (1999). Quantification of Total Oxidant Scavenging Capacity of Antioxidants for Peroxynitrite, Peroxyl Radicals, and Hydroxyl Radicals Quantification of Total Oxidant Scavenging Capacity of Anti-oxidants for Peroxynitrite, Peroxyl Radicals, and Hydroxyl Radi-cals. In *Toxicol. Appl. Phar-macol* (Vol. 156). http://www.idealibrary.com

Reth, M. (2002). Hydrogen peroxide as second messenger in lymphocyte activation. *Nature Immunology*, *3*(12), 1129–1134. https://doi.org/10.1038/ni1202-1129

Ribeiro, F., Garcia, A. R., Pereira, B. P., Fonseca, M., Mestre, N. C., Fonseca, T. G., Ilharco, L. M., & Bebianno, M. J. (2017). Microplastics effects in Scrobicularia plana. *Marine Pollution Bulletin*, *122*(1–2), 379–391. https://doi.org/10.1016/j.marpolbul.2017.06.078

Rieux, A. Des, Ragnarsson, E. G. E., Gullberg, E., Préat, V., Schneider, Y. J., & Artursson, P. (2005). Transport of nanoparticles across an in vitro model of the human intestinal follicle associated epithelium. *European Journal of Pharmaceutical Sciences*, *25*(4–5), 455–465. https://doi.org/10.1016/j.ejps.2005.04.015

Rochester, J. R. (2013). Bisphenol A and human health: A review of the literature. In *Reproductive Toxicology* (Vol. 42, pp. 132–155). https://doi.org/10.1016/j.reprotox.2013.08.008

Rodriguez Sawicki, L., Bottasso Arias, N. M., Scaglia, N., Falomir Lockhart, L. J., Franchini, G. R., Storch, J., & Córsico, B. (2017). FABP1 knockdown in human enterocytes impairs proliferation and alters lipid metabolism. *Biochimica et Biophysica Acta - Molecular and Cell Biology of Lipids*, *1862*(12), 1587–1594. https://doi.org/10.1016/j.bbalip.2017.09.006

Rose, S., Frye, R. E., Slattery, J., Wynne, R., Tippett, M., Pavliv, O., Melnyk, S., & James, S. J. (2014). Oxidative stress induces mitochondrial dysfunction in a subset of autism lymphoblastoid cell lines in a well-matched case control cohort. *PLoS ONE*, *9*(1). https://doi.org/10.1371/journal.pone.0085436

Santana, M. F. M., Moreira, F. T., & Turra, A. (2017). Trophic transference of microplastics under a low exposure scenario: Insights on the likelihood of particle cascading along marine food-webs. *Marine Pollution Bulletin*, *121*(1–2), 154–159. https://doi.org/10.1016/j.marpolbul.2017.05.061

Santillo, D., Miller, K., & Johnston, P. (2017). Microplastics as contaminants in commercially important seafood species. In *Integrated Environmental Assessment and Management* (Vol. 13, Issue 3, pp. 516–521). Wiley-Blackwell. https://doi.org/10.1002/ieam.1909

Schaffer', J. E., & Lodisht, H. F. (1994). Expression Cloning and Characterization of a Novel Adipocyte Long Chain Fatty Acid Transport Protein. In *Cell* (Vol. 79).

Schneider, M., Stracke, F., Hansen, S., & Schaefer, U. F. (2009). Nanoparticles and their interactions with the dermal barrier. *Dermato-Endocrinology*, *1*(4), 197–206. https://doi.org/10.4161/derm.1.4.9501

Schwabl, P., Köppel, S., Königshofer, P., Bucsics, T., Trauner, M., Reiberger, T., & Liebmann, B. (2019). Detection of Various Microplastics in Human Stool. *Annals of Internal Medicine*, *171*(7), 453–457. https://doi.org/10.7326/M19-0618

Schwarz, D. S., & Blower, M. D. (2016). The endoplasmic reticulum: Structure, function and response to cellular signaling. In *Cellular and Molecular Life Sciences* (Vol. 73, Issue 1, pp. 79–94). Birkhauser Verlag AG. https://doi.org/10.1007/s00018-015-2052-6

Senathirajah, K., Attwood, S., Bhagwat, G., Carbery, M., Wilson, S., & Palanisami, T. (2021). Estimation of the mass of microplastics ingested – A pivotal first step towards human health risk assessment. *Journal of Hazardous Materials*, *404*. https://doi.org/10.1016/j.jhazmat.2020.124004

Serra, N. D., & Sundaram, M. V. (2021). Transcytosis in the development and morphogenesis of epithelial tissues. *The EMBO Journal*, *40*(9). https://doi.org/10.15252/embj.2020106163

Shen, R., Yang, K., Cheng, X., Guo, C., Xing, X., Sun, H., Liu, D., Liu, X., & Wang, D. (2022). Accumulation of polystyrene microplastics induces liver fibrosis by activating cGAS/STING pathway. *Environmental Pollution*, *300*. https://doi.org/10.1016/j.envpol.2022.118986

Shi, W., Cao, Y., Chai, X., Zhao, Q., Geng, Y., Liu, D., & Tian, S. (2022). Potential health risks of the interaction of microplastics and lung surfactant. *Journal of Hazardous Materials*, *429*. https://doi.org/10.1016/j.jhazmat.2021.128109

Shimano, H. (2009). SREBPs: Physiology and pathophysiology of the SREBP family. In *FEBS Journal* (Vol. 276, Issue 3, pp. 616–621). https://doi.org/10.1111/j.1742-4658.2008.06806.x

Smyth, S. H., Feldhaus, S., Schumacher, U., & Carr, K. E. (2008). Uptake of inert microparticles in normal and immune deficient mice. *International Journal of Pharmaceutics*, *346*(1–2), 109–118. https://doi.org/10.1016/j.ijpharm.2007.06.049

Song, W., Popp, L., Yang, J., Kumar, A., Gangoli, V. S., & Segatori, L. (2015). The autophagic response to polystyrene nanoparticles is mediated by transcription factor EB and depends on surface charge. *Journal of Nanobiotechnology*, *13*(1). https://doi.org/10.1186/s12951-015-0149-6

Song, Z., Xiaoli, A. M., & Yang, F. (2018). Regulation and metabolic significance of De Novo lipogenesis in adipose tissues. In *Nutrients* (Vol. 10, Issue 10). MDPI AG. https://doi.org/10.3390/nu10101383

Sternschuss, G., Ostergard, D. R., & Patel, H. (2012). Post-implantation alterations of polypropylene in the human. In *Journal of Urology* (Vol. 188, Issue 1, pp. 27–32). https://doi.org/10.1016/j.juro.2012.02.2559

Stienstra, R., Duval, C., Müller, M., & Kersten, S. (2007). PPARs, obesity, and inflammation. In *PPAR Research*. https://doi.org/10.1155/2007/95974

Stock, V., Laurisch, C., Franke, J., Dönmez, M. H., Voss, L., Böhmert, L., Braeuning, A., & Sieg, H. (2021). Uptake and cellular effects of PE, PP, PET and PVC microplastic particles. *Toxicology in Vitro*, *70*. https://doi.org/10.1016/j.tiv.2020.105021

Sui, A., Yao, C., Chen, Y., Li, Y., Yu, S., Qu, J., Wei, H., Tang, J., & Chen, G. (2023). Polystyrene nanoplastics inhibit StAR expression by activating HIF-1α via ERK1/2 MAPK and AKT pathways in TM3 Leydig cells and testicular tissues of mice. *Food and Chemical Toxicology*, *173*. https://doi.org/10.1016/j.fct.2023.113634

Takeuchi, K., & Reue, K. (2009). AGPAT, and lipin enzymes in triglyceride synthesis. *Am J Physiol Endocrinol Metab*, *296*, 1195–1209. https://doi.org/10.1152/ajpendo.90958.2008.-Triacylglyc

Tang, Y., Rong, J., Guan, X., Zha, S., Shi, W., Han, Y., Du, X., Wu, F., Huang, W., & Liu, G. (2020). Immunotoxicity of microplastics and two persistent organic pollutants alone or in combination to a bivalve species. *Environmental Pollution*, *258*. https://doi.org/10.1016/j.envpol.2019.113845

Tanvir, A., Faruq, M., & Yusof, N. A. (2014). *Polystyrene: synthesis, characteristics and applications* (C. Lynwood, Ed.). Nova publisher.

Topete, M. V., Andrade, S., Bernardino, R. L., Guimarães, M., Pereira, A. M., Oliveira, S. B., Costa, M. M., Nora, M., Monteiro, M. P., & Pereira, S. S. (2023). Visceral Adipose Tissue Bioenergetics Varies According to Individuals' Obesity Class. *International Journal of Molecular Sciences*, *24*(2). https://doi.org/10.3390/ijms24021679

Varga, T., Czimmerer, Z., & Nagy, L. (2011). PPARs are a unique set of fatty acid regulated transcription factors controlling both lipid metabolism and inflammation. In *Biochimica et Biophysica Acta - Molecular Basis of Disease* (Vol. 1812, Issue 8, pp. 1007–1022). https://doi.org/10.1016/j.bbadis.2011.02.014

Vianello, A., Jensen, R. L., Liu, L., & Vollertsen, J. (2019). Simulating human exposure to indoor airborne microplastics using a Breathing Thermal Manikin. *Scientific Reports*, *9*(1). https://doi.org/10.1038/s41598-019-45054-w

Vineis, P., Robinson, O., Chadeau-Hyam, M., Dehghan, A., Mudway, I., & Dagnino, S. (2020). What is new in the exposome? In *Environment International* (Vol. 143). Elsevier Ltd. https://doi.org/10.1016/j.envint.2020.105887

Visalli, G., Facciolà, A., Ciarello, M. P., De Marco, G., Maisano, M., & Di Pietro, A. (2021). Acute and sub-chronic effects of microplastics (3 and 10 µm) on the human intestinal cells ht-29. *International Journal of Environmental Research and Public Health*, *18*(11). https://doi.org/10.3390/ijerph18115833

Vogt, A., Combadiere, B., Hadam, S., Stieler, K. M., Lademann, J., Schaefer, H., Autran, B., Sterry, W., & Blume-Peytavi, U. (2006). 40 nm, but not 750 or 1,500 nm, nanoparticles enter epidermal CD1a+ cells after transcutaneous application on human skin. *Journal of Investigative Dermatology*, *126*(6), 1316–1322. https://doi.org/10.1038/sj.jid.5700226

Völker, J., Ashcroft, F., Vedøy, Å., Zimmermann, L., & Wagner, M. (2022). Adipogenic Activity of Chemicals Used in Plastic Consumer Products. *Environmental Science and Technology*, *56*(4), 2487–2496. https://doi.org/10.1021/acs.est.1c06316

Walczak, A. P., Kramer, E., Hendriksen, P. J. M., Tromp, P., Helsper, J. P. F. G., Van Der Zande, M., Rietjens, I. M. C. M., & Bouwmeester, H. (2015). Translocation of differently sized and charged polystyrene nanoparticles in in vitro intestinal cell models of increasing complexity. *Nanotoxicology*, *9*(4), 453–461. https://doi.org/10.3109/17435390.2014.944599

Wang, F., Kohan, A. B., Lo, C. M., Liu, M., Howles, P., & Tso, P. (2015). Apolipoprotein A-IV: A protein intimately involved in metabolism. In *Journal of Lipid Research* (Vol. 56, Issue 8, pp. 1403–1418). American Society for Biochemistry and Molecular Biology Inc. https://doi.org/10.1194/jlr.R052753

Wang, F., Yu, L., Monopoli, M. P., Sandin, P., Mahon, E., Salvati, A., & Dawson, K. A. (2013). The biomolecular corona is retained during nanoparticle uptake and protects the cells from the damage induced by cationic nanoparticles until degraded in the lysosomes. *Nanomedicine: Nanotechnology, Biology, and Medicine*, *9*(8), 1159–1168. https://doi.org/10.1016/j.nano.2013.04.010

Wang, H., Shi, X., Gao, Y., Zhang, X., Zhao, H., Wang, L., Zhang, X., & Chen, R. (2022). Polystyrene nanoplastics induce profound metabolic shift in human cells as revealed by integrated proteomic and metabolomic analysis. *Environment International*, *166*. https://doi.org/10.1016/j.envint.2022.107349

Wang, S., Han, Q., Wei, Z., Wang, Y., Xie, J., & Chen, M. (2022). Polystyrene microplastics affect learning and memory in mice by inducing oxidative stress and decreasing the level of acetylcholine. *Food and Chemical Toxicology*, *162*. https://doi.org/10.1016/j.fct.2022.112904

Wang, Y. L., Lee, Y. H., Hsu, Y. H., Chiu, I. J., Huang, C. C. Y., Huang, C. C., Chia, Z. C., Lee, C. P., Lin, Y. F., & Chiu, H. W. (2021). The kidney-related effects of polystyrene microplastics on human kidney proximal tubular epithelial cells hk-2 and male c57bl/6 mice. *Environmental Health Perspectives*, *129*(5). https://doi.org/10.1289/EHP7612

Wang, Y., Wang, S., Xu, T., Cui, W., Shi, X., & Xu, S. (2022). A new discovery of polystyrene microplastics toxicity: The injury difference on bladder epithelium of mice is correlated with the size of exposed particles. *Science of the Total Environment*, *821*. https://doi.org/10.1016/j.scitotenv.2022.153413

Woldemar D'ambrières. (2019). *Field Actions Science Reports Plastics recycling worldwide: current overview and desirable changes PLASTICS RECYCLING WORLDWIDE: CURRENT OVERVIEW AND DESIRABLE CHANGES • PLASTICS ECONOMY • RECYCLING • REGULATION • ECO-DESIGN*. : http://journals.openedition.org/factsreports/5102

Woo, J. H., Seo, H. J., Lee, J. Y., Lee, I., Jeon, K., Kim, B., & Lee, K. (2023). Polypropylene nanoplastic exposure leads to lung inflammation through p38-mediated NF-κB pathway due to mitochondrial damage. *Particle and Fibre Toxicology*, *20*(1). https://doi.org/10.1186/s12989-022-00512-8

Wu, S., Wu, M., Tian, D., Qiu, L., & Li, T. (2020). Effects of polystyrene microbeads on cytotoxicity and transcriptomic profiles in human Caco-2 cells. *Environmental Toxicology*, *35*(4), 495–506. https://doi.org/10.1002/tox.22885

Xu, D., Ma, Y., Han, X., & Chen, Y. (2021). Systematic toxicity evaluation of polystyrene nanoplastics on mice and molecular mechanism investigation about their internalization into Caco-2 cells. *Journal of Hazardous Materials*, *417*. https://doi.org/10.1016/j.jhazmat.2021.126092

Xu, M., Halimu, G., Zhang, Q., Song, Y., Fu, X., Li, Y., Li, Y., & Zhang, H. (2019). Internalization and toxicity: A preliminary study of effects of nanoplastic particles on human lung epithelial cell. *Science of the Total Environment*, *694*. https://doi.org/10.1016/j.scitotenv.2019.133794

Yang, W., Jannatun, N., Zeng, Y., Liu, T., Zhang, G., Chen, C., & Li, Y. (2022). Impacts of microplastics on immunity. In *Frontiers in Toxicology* (Vol. 4). Frontiers Media S.A. https://doi.org/10.3389/ftox.2022.956885

Yang, Y., Bazhin, A. V., Werner, J., & Karakhanova, S. (2013). Reactive oxygen species in the immune system. *International Reviews of Immunology*, *32*(3), 249–270. https://doi.org/10.3109/08830185.2012.755176

Yang, Y., Shao, H., Wu, Q., & Wang, D. (2020). Lipid metabolic response to polystyrene particles in nematode Caenorhabditis elegans. *Environmental Pollution*, *256*. https://doi.org/10.1016/j.envpol.2019.113439

Yang, Y., Wu, Q., & Wang, D. (2021). Dysregulation of G protein-coupled receptors in the intestine by nanoplastic exposure in Caenorhabditis elegans. *Environmental Science: Nano*, *8*(4), 1019–1028. https://doi.org/10.1039/D0EN00991A

Yin, M., & O'Neill, L. A. J. (2021). The role of the electron transport chain in immunity. In *FASEB Journal* (Vol. 35, Issue 12). John Wiley and Sons Inc. https://doi.org/10.1096/fj.202101161R

Yoon, H., Shaw, J. L., Haigis, M. C., & Greka, A. (2021). Lipid metabolism in sickness and in health: Emerging regulators of lipotoxicity. In *Molecular Cell* (Vol. 81, Issue 18, pp. 3708–3730). Cell Press. https://doi.org/10.1016/j.molcel.2021.08.027

You, M., & Arteel, G. E. (2019). *Effect of ethanol on lipid metabolism*. *70*(2), 237–248. https://doi.org/https://doi.org/10.1016/j.jhep.2018.10.037

Zhang, G., Cao, G., Luo, R.-H., Song, Q., Zeng, Y., Liu, K., Qu, J., Lin, X., Liu, F.-L., Wang, G., Li, H., Li, L., Zheng, Y.-T., Boraschi, D., Wu, L., Chang, Y.-Z., & Li, Y. (2022). Microplastics interact with SARS-CoV-2 and facilitate host cell infection. *Environmental Science: Nano*, *9*(8), 2653–2664. https://doi.org/10.1039/D2EN00019A

Zhang, W., Li, J. ya, Wei, X. chen, Wang, Q., Yang, J. yang, Hou, H., Du, Z. wei, & Wu, X. an. (2021). Effects of dibutyl phthalate on lipid metabolism in liver and hepatocytes based on PPARα/SREBP-1c/FAS/GPAT/AMPK signal pathway. *Food and Chemical Toxicology*, *149*. https://doi.org/10.1016/j.fct.2021.112029

Zhang, Z., Xu, M., Wang, L., Gu, W., Li, X., Han, Z., Fu, X., Wang, X., Li, X., & Su, Z. (2023). Continuous oral exposure to micro- and nanoplastics induced gut microbiota dysbiosis, intestinal barrier and immune dysfunction in adult mice. *Environment International*, *182*. https://doi.org/10.1016/j.envint.2023.108353

Zhao, Y., Bao, Z., Wan, Z., Fu, Z., & Jin, Y. (2020). Polystyrene microplastic exposure disturbs hepatic glycolipid metabolism at the physiological, biochemical, and transcriptomic levels in adult zebrafish. *Science of the Total Environment*, *710*. https://doi.org/10.1016/j.scitotenv.2019.136279

Zorov, D. B., Juhaszova, M., & Sollott, S. J. (2006). Mitochondrial ROS-induced ROS release: An update and review. In *Biochimica et Biophysica Acta - Bioenergetics* (Vol. 1757, Issues 5–6, pp. 509–517). https://doi.org/10.1016/j.bbabio.2006.04.029

APPENDIX 1

1. RNA extraction and DNase treatment (Ugent)

RNA extraction was performed with the RNeasy® Mini Kit (Qiagen), following the instruction handbook. In short, 350 µL lysis Buffer RLT was used to lyse the cells. A Qiagen shredder column was used to improve the RNA release. 350 µL 70% ethanol was added, and the total volume was transferred to an RNeasy Mini spin column placed in a collection tube to be centrifuged at 8000 g for 15 s. The flow through was discarded, and the column is washed with Buffer RW1 and Buffer RPE, before eluting the RNA in 40 µL RNase-free water. RNA-content was measured using a Biodrop device. Although an on-column DNA removal step was already included in this kit, an additional DNase treatment (Thermo Scientific) was applied to a standardized quantity of 0.5 µg RNA. For each µg of RNA in the sample, 1 µL 10X reaction buffer with $MgCl_2$, 1 U DNase I, RNase-free, and 8 µL DEPC-treated Water were added. After incubation at 37°C for 30 min, 1 µL 50 mM EDTA was added to avoid RNA hydrolysis and the samples were incubated at 65°C for 10 min and stored at -80°C for further analysis.

2. RNA processing and sequencing (NXTGNT)

For each sample, a sequencing library was constructed using the QuantSeq 3' mRNA-Seq Library Prep Kit FWD for Illumina (Lexogen) and the UMI Second Strand Synthesis Module for QuantSeq FWD (Illumina, Read 1). This incorporates a unique molecular identifier (UMI) in the first 6 nucleotides of each read, allowing to identify polymerase chain reaction (PCR) duplicates and eliminate amplification bias. The libraries were sequenced as single-end 75nt reads on an Aviti sequencer (Element Biosciences). The tool FastQC was used to assess the quality and length of raw sequencing reads. Additionally, putative contamination was checked using FastQ Screen with a set of genomes of common lab organisms.

Adapter and quality trimming was performed using Cutadapt (v4.8). Filtering options were applied to remove reads containing ambiguities or failing to meet a Phred score threshold of 20. Additionally, adapter sequences and poly-A tails were removed where detected. The quality of the remaining reads was checked using FastQC as before.

3. Read mapping and statistics (NXTGNT)

For each sample, trimmed reads were mapped on the latest human genome (GRCh38, ENSEMBL release 111) using the splice-aware STAR mapper. UMI-based removal of PCR duplicates from the mapped reads was done with UMI-tools. Feature counting was done using the featureCounts program. To check if the sequencing depth reflects the sample's active gene diversity, a rarefaction (a.k.a. saturation or complexity) plot was generated. The data was generated using preseq and plotted with Python.
All statistical analyses were executed in R using the DESeq2 package. Prior to the differential gene expression analysis, the samples were filtered for low counts. A PCA plot was generated to check if the count data groups according to their expected biological differences. Prior to differential expression analysis, it is beneficial to omit genes that have little or no chance of being detected as differentially expressed. By default, this filtering will be performed by DESeq2.

Feature counts were normalized using DESeq2's size factor normalization method. P-values for each gene based on a negative binomial distribution were calculated and adjusted (= padj) using the Benjamini-Hochberg procedure. Genes were considered significantly differentially expressed if they both had a false discovery rate (FDR) < 0.05 and if the absolute value of the log2-transformed fold change was at least 1.5. Gene set enrichment analysis (GSEA) was performed using the R Package clusterProfiler. Utilizing the same package, a Gene Ontology (GO) analysis identified significantly differential pathways using the same criteria as in the GSEA.

APPENDIX 2

Kinetic graphs

9 days of treatment

starvation

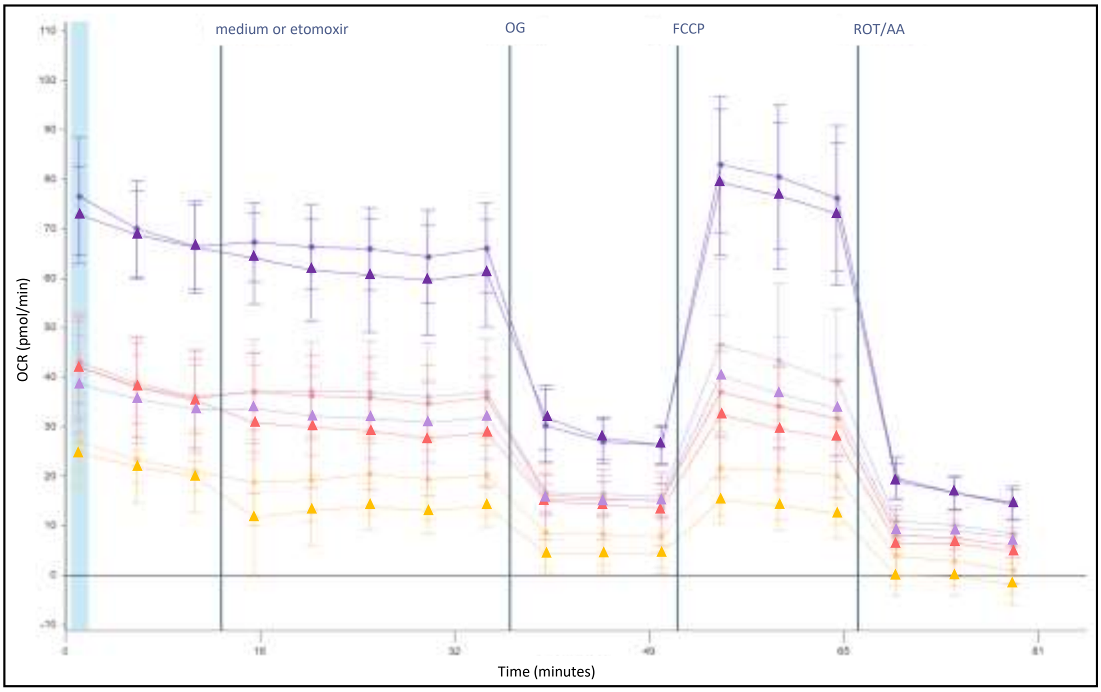

17 days of treatment

starvation

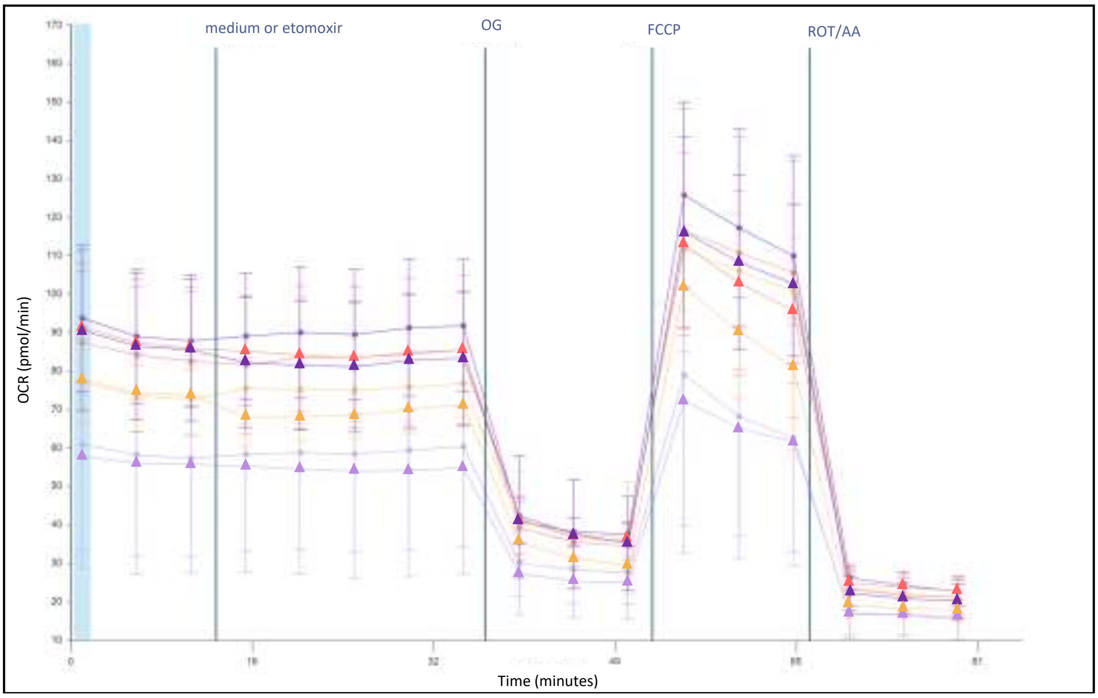

Treatment: 5.44 x 10^6 SB/ml 5.44 x 10^6 NPs/ml ethanol control untreated

First injection port: medium etomoxir

43 days of treatment

starvation

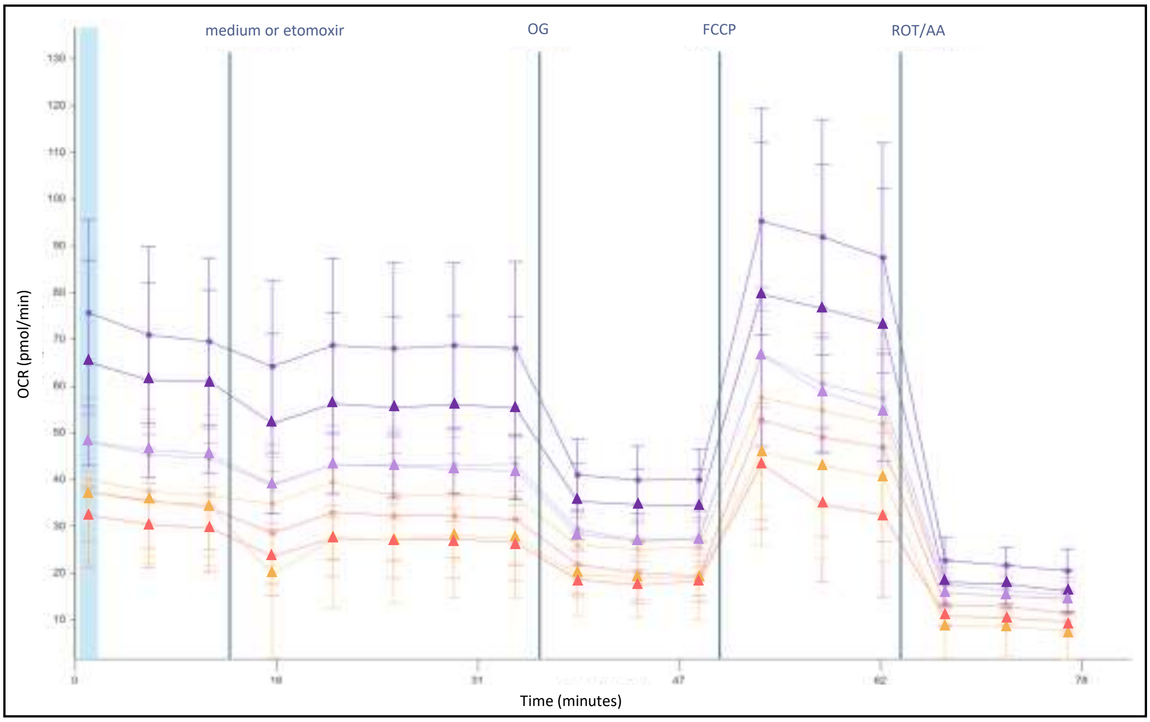

17 days of treatment

non-starvation

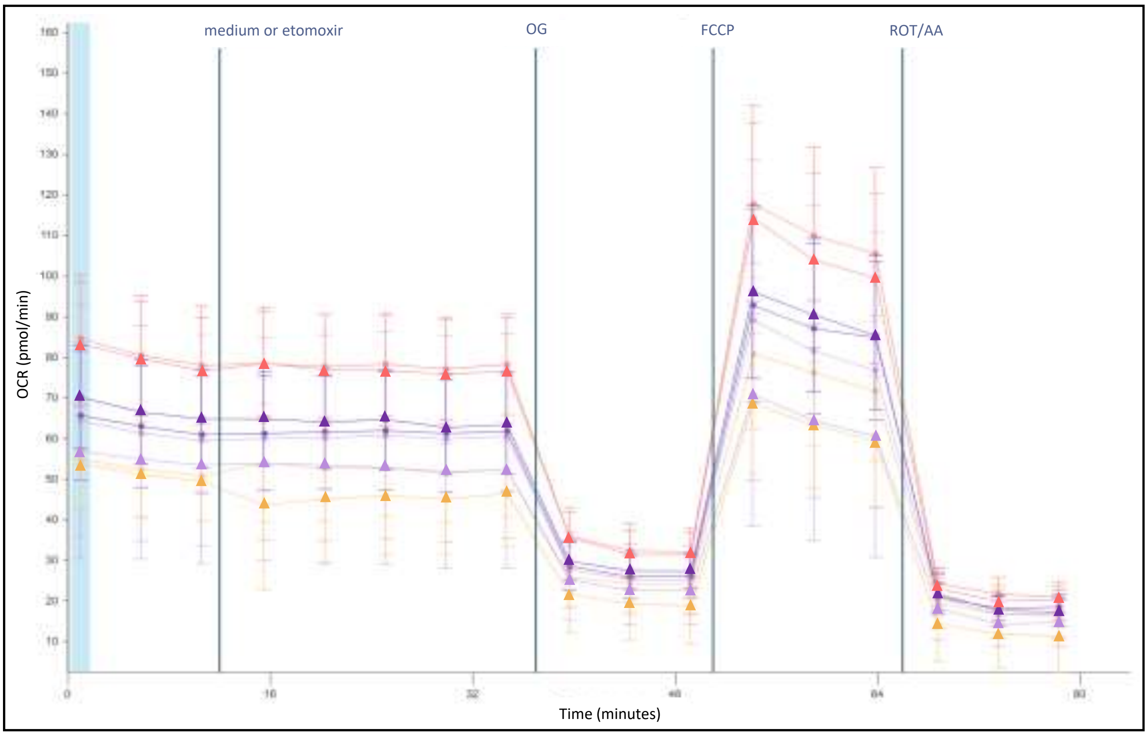

43 days of treatment

non-starvation